

1-1-2009

Thin wafer dicing using a high repetition rate femtosecond laser

Nitinkumar Sudani
Ryerson University

Follow this and additional works at: <http://digitalcommons.ryerson.ca/dissertations>



Part of the [Mechanical Engineering Commons](#)

Recommended Citation

Sudani, Nitinkumar, "Thin wafer dicing using a high repetition rate femtosecond laser" (2009). *Theses and dissertations*. Paper 1025.

This Thesis is brought to you for free and open access by Digital Commons @ Ryerson. It has been accepted for inclusion in Theses and dissertations by an authorized administrator of Digital Commons @ Ryerson. For more information, please contact bcameron@ryerson.ca.

THIN WAFER DICING USING A HIGH REPETITION RATE FEMTOSECOND LASER

by

Nitinkumar Sudani

Bachelor of Engineering (Mechanical)

The Maharaja Sayajirao University of Baroda (India), 1995

A Thesis

presented to Ryerson University

in partial fulfillment of the requirement for the degree of

Master of Applied Science

in the program of

Mechanical Engineering


Toronto, Ontario, Canada, 2009

© Nitinkumar Sudani 2009

AUTHOR'S DECLARATION


I hereby declare that I am the sole author of this thesis report.

I authorize Ryerson University to lend this thesis to other institutions or individuals for the purpose of scholarly research.



Nitinkumar Sudani
Department of Mechanical Engineering
Ryerson University

I further authorize Ryerson University to reproduce this project by photocopying or by other means, in total or in part, at the request of other institutions or individuals for the purpose of scholarly research.



Nitinkumar Sudani
Department of Mechanical Engineering
Ryerson University

ABSTRACT

THIN WAFER DICING USING A HIGH REPETITION RATE FEMTOSECOND LASER

Nitinkumar Sudani, Master of Applied Science, 2009

Department of Mechanical Engineering, Ryerson University

The demand for more compact and more efficient stackable devices is driving the semiconductor industry towards the use of thin wafers with thickness less than 100 μ m. The stackable devices made with these thin wafers offer a greater advantage for the IC manufacturing industry in terms of circuit density, higher clock speeds and heat dissipation. Dicing, being the first step of the assembly process, plays an important role in the success of the application of thin wafers. Currently used mechanical saw dicing and conventional dicing do not satisfy the need for quality and throughput. The mechanical and thermal damage, low die strength and low throughput, push towards seeking of a new dicing technique.

This thesis proposes a femtosecond laser dicing technique to overcome the limitation of the currently used techniques. A high repetition rate, high power femtosecond laser is investigated for meeting the quality and throughput requirement. A feasibility study of the proposed laser system and the analysis of control parameters, such as the number of pulses, scan speed and pulse energy, are also presented. The influence of pulsewidth and repetition rate on parameters such as the ablation threshold, kerf width, ablation depth, fluence and debris are analyzed in detail. Results of die strength and surface analysis of the dies cut using the proposed laser system show the capability of meeting the current quality and throughput requirement and hence can be considered a significant step towards commercial application of the proposed dicing technique.

ACKNOWLEDGMENTS

I would like to thank my research supervisors Dr. K. Venkatakrishnan and Dr. Bo Tan, for their outstanding supervision and guidance. Their unconditional support, advice and constructive criticism throughout my research study have been invaluable.

I would like to thank Dr. Greg Kawall, Director of Mechanical Engineering Graduate program, all the faculty members, technical officers and administrative staff members for their kind support and cooperation all the time during my stay at Ryerson University.

I am also grateful to my family for their continued support, prayers and love. Deepest gratitude to my wife and kids, who had to sacrifice their time and needs to support me to finish my studies successfully.

Finally, I am grateful to the Grace of God for the countless blessings I have received.

DEDICATION

The author hereby would like to dedicate this thesis to his parents, wife Mily and his kids, Ansh and Aarav, as a token of humble and sincere appreciation for their invaluable love and support.

TABLE OF CONTENTS

Author's Declaration	ii
Abstract.....	iii
Acknowledgments	iv
Dedication	iv
Table of Contents	vi
List of Tables	ix
List of Figures.....	x
Nomenclature.....	xiii

Chapter 1 : Introduction

1.1	Introduction to Dicing Techniques	1
1.2	Wafer Dicing process	4
1.3	Dicing Techniques.....	6
1.3.1	Diamond Scribing.....	6
1.3.2	Mechanical Saw or Blade Dicing	7
1.3.3	Dicing Before grinding.....	8
1.3.4	Conventional Laser Dicing.....	10
1.3.5	Laser Water-Jet Cutting Technique	13
1.3.6	Femtosecond laser Dicing.....	15
1.3.7	Summary of dicing techniques	17
1.4	Research Objectives.....	18
1.5	Overview of thesis	19

Chapter 2 : Laser Ablation mechanism

2.1	Introduction	21
2.2	Mechanisms in Laser Ablation Process.....	22
2.2.1	Absorbtion and Ionization	23
2.2.1.1	Linear Absorbtion.....	24
2.2.1.2	Nonlinear Absorbtion	24
2.2.2	Energy Relaxation	27
2.2.3	Heat Transport	27

2.2.4	The Laser Generated Plasma	28
2.2.5	The Melt Flows in Laser Ablation.....	28
2.2.6	Shock Wave	29
2.3	Nanosecond Laser Ablation.....	30
2.4	Femtosecond Laser Ablation	32
2.5	Theory for ns and fs laser ablation	36
2.5.1	Nanosecond pulses.....	38
2.5.2	Femtosecond pulses.....	39
2.6	Summary	41

Chapter 3 : Experimental Details and Parameters

3.1	Introduction	43
3.2	Experimental Setup.....	43
3.3	Parameters	46
3.3.1	Spot Size.....	47
3.3.2	Spot Overlap	48
3.3.3	Polarization.....	50
3.3.4	Focusing and Aberration.....	52
3.3.5	Pulsewidth and Dispersion	53
3.4	Summary	54

Chapter 4 : Effect of pulsewidth

4.1	Introduction	56
4.2	Effect of pulsewidth on Ablation Threshold Fluence.....	59
4.3	Influence of pulsewidth on Kerf Width.....	61
4.4	Effect of pulsewidth on Ablation Depth.....	63
4.5	Debris & contamination.....	68
4.6	Summary	71

Chapter 5 : Effect of Repetition rate

5.1	Introduction	73
5.2	Effect of scan speed and effective number of pulses.....	75

5.3	Effect of pulse energy	80
5.4	Summary	83

Chapter 6 : Analysis of Die strength and Surface Roughness of sidewalls

6.1	Introduction	85
6.2	Methodology.....	86
6.2.1	Surface Roughness.....	87
6.3	Results and discussion	88
6.3.1	Surface roughness of sidewalls.....	88
6.4	Die Strength.....	91
6.5	Effect of assist gas	93
6.6	Summary	95

Chapter 7 : Summary, Conclusions and future work

7.1	Summary	97
7.2	Conclusions	99
7.3	Future Work.....	100

References	101
-------------------------	-----

LIST OF TABLES

Table 1: Thin wafer usage market trend	3
Table 2: Laser parameters	55
Table 3: Dicing parameters	55
Table 4: Die strength at different repetition rate and pulsewidth.....	92

LIST OF FIGURES

Figure 1-1: Wafer parameters.....	5
Figure 1-2: Diamond Scribing Technique	6
Figure 1-3: Mechanical Blade dicing	7
Figure 1-4: Dicing Before Grinding process	9
Figure 1-5: Setup for laser micromachining.....	11
Figure 1-6: long pulse ablation process, which includes plasma, shock wave, vaporization and melting	12
Figure 1-7: Principle of the LMJ, coupling of a laser beam into a water jet	14
Figure 1-8: Femtosecond laser pulse ablation process	16
Figure 2-1: Laser Ablation of material	23
Figure 2-2: (a) Schematics of electron avalanche by collisional impact ionization (b) The multiphoton ionization process	25
Figure 2-3: Formation of plasma during laser ablation	28
Figure 3-1: Experimental Setup.....	44
Figure 3-2: Laser spot size and depth of focus for converging laser beam using a convex lens.....	47
Figure 3-3: Effect of spot overlap on the quality of sidewall	49
Figure 3-4: Defination of S and P polarization.....	51
Figure 3-5: Unequal kerf widths in X and Y axis with a linearly polarized beam	51
Figure 4-1: Influence of pulsewidth on threshold fluence at repetition rate of 2 - 13 MHz.....	60
Figure 4-2: Kerf width cut at repetition rate of 2 MHz at scan speed of 3000 mm/s at pulsewidth of (a)214 fs, (b)429 fs, (c)714 fs, (d)1429 fs and (e) 3571fs.....	62
Figure 4-3: Influence of pulsewidth on kerf width at repetition rates of 2–13 MHz.....	63
Figure 4-4: Ablation depth cut at repetition rate of 2 MHz and scan speed of 3000 mm/s at pulsewidth of (a)214 fs, (b)429 fs, (c)714 fs, (d)1429 fs and (e) 3571fs and for	

repetition rate of 13 MHz at scan speed of 3000 mm/s at pulsewidth of (f)214 fs, (g)429 fs, (h)714 fs, (i)1429 fs and (j) 3571fs	64
Figure 4-5: Influence of pulsewidth on Ablation depth at different repetition rate (2MHz – 13 MHz) having the same total energy deposited (30.34 J cm ⁻² , number of pulses x laser fluence)	65
Figure 4-6: Influence of pulsewidth on Ablation Rate at different repetition rate having the same total energy deposited (30.34 J cm ⁻² , number of pulses x laser fluence)	66
Figure 4-7: Plot of laser fluence and threshold fluence for pulsewidth of 214 fs and 3.5 ps at repetition rate from 2 MHz to 13 MHz.....	67
Figure 4-8: Zoomed image of the surface area on either side of grooves cut with repetition rate of 2 MHz at scan speed of 3000 mm s ⁻¹ at (a)214 fs and (b) 3.5 ps.....	68
Figure 4-9: Grooves cut at repetition rate of 13 MHz and scan speed of 3000 mm s ⁻¹ at pulsewidth of (a) 214 fs, (b) 429 fs, (c) 714 fs, (d) 1429 fs.....	69
Figure 4-10: Grooves cut at repetition rate of 13 MHz and pulsewidth of 214 fs at scan speed of (a) 1000 mm s ⁻¹ , (b) 2000 mm s ⁻¹ , (c) 3000 mm s ⁻¹ and at pulsewidth of 1429 fs at scan speed of (d) 1000 mm s ⁻¹ , (e) 2000 mm s ⁻¹ , (f) 3000 mm s ⁻¹	70
Figure 5-1: Influence of Scan speed on the depth of cut at repetition rate of 2 MHz, 4.33 MHz, 8.67 MHz & 13 MHz.....	76
Figure 5-2: Cross section of grooves cut on a thin Si wafer at 13MHz, scan speed of (a) 500 mm s ⁻¹ , (b) 3000 mm s ⁻¹ and top surface view for 13 MHz at scan speed of (c) 500 mm s ⁻¹ (d) 3000 mm s ⁻¹	77
Figure 5-3: Influence of Scan speed on the kerf width at repetition rate of 2 MHz, 4.33 MHz, 8.67 MHz & 13 MHz.....	78
Figure 5-4: Cross-section view of a groove cut on the Si wafer at 1000 mm s ⁻¹ for repetition rate of (a) 2 MHz, (b) 13 MHz.....	79
Figure 5-5: Influence of pulse energy on the depth of cut at scan speed ranging from 500 mm s ⁻¹ to 3000 mm s ⁻¹	81
Figure 5-6: Influence of pulse energy on the kerf width at scan speed ranging from 500 mm s ⁻¹ to 3000 mm s ⁻¹	82
Figure 6-1: 3-Point bending test configuration.....	87

Figure 6-2: Plot of surface average surface roughness value at different pulsewidth for 4.33 MHz and 8.67 MHz.....89

Figure 6-3: Sidewalls of si dice cut at repetition rate of 4.33 MHz and pulsewidth of (a)214fs, (b)1.4ps, (c)3.5 ps89

Figure 6-4: Sidewalls of si dice cut at repetition rate of 8.67 MHz and pulsewidth of (a)214fs, (b)1.4ps, (c)3.5 ps90

Figure 6-5: Backside surface finish of si dice cut at 4.33 MHz and (a) 214fs, (b) 728fs (d) 3.5ps.....93

Figure 6-6: Sidewall quality in (a) Air and (b) Nitrogen (c) Helium gas assist.....95

NOMENCLATURE

ns	nanosecond (10^{-9} s)
ps	picosecond (10^{-12} s)
fs	femtosecond (10^{-15} s)
μm	micrometer (10^{-6} m)
MHz	megahertz (10^6 Hz)
nm	nanometer (10^{-9} m)
W	watt
GW	gigawatt (10^9 s)
μJ	micro-Joule (10^{-6} J)
C_e	heat capacity (per unit volume) of the electron lattice
T_e	electron temperature
z	direction perpendicular to target surface
Q	heat flux
T_i	lattice temperature
S	laser heating source term
C_i	heat capacity (per unit volume) of the lattice
γ	parameter characterizing electron-lattice coupl
$I(t)$	laser intensity at time t
A	absorptivity
α	surface transmissivity
k_e	electron thermal conductivity
k_0	conventional equilibrium thermal conductivity
I_0	Intensity
I_α	Intensity
t	time
τ_L	pulsewidth
τ_e	Electron cooling time
τ_i	Lattice heating time
F_a	ablation fluence
F_{th}, \varnothing_{th}	threshold fluence

δ	skin depth
l	heat penetration depth
D	heat diffusion coefficient
E	energy deposited inside target per unit mass
ρ	density
Ω	specific heat of evaporation
I	laser intensity
I_{th}	threshold intensity
F	laser fluence
F_a	absorbed laser fluence
F_{th}	threshold laser fluence
D_e	Electron thermal diffusivity
T_0	temperature at time $t = 0$
T_i	initial temperature
$2\omega_0$	spot diameter
λ_0	wavelength of the laser beam
f_l	effective focal length of the scan lens
D	diameter of the laser beam at the input of the galvo-scanner
N_{eff}	number of effective pulses at a given spot
f	repetition rate
v	scanning speed
D	feature size
ϕ_0	maximum laser fluence
E_{pulse}	laser pulse energy
τ	pulsewidth
E_0	pulse energy
E_{th}	threshold pulse energy
σ	stress at breaking
F_b	breaking load
L	support length

CHAPTER 1

INTRODUCTION

1.1 INTRODUCTION TO DICING TECHNIQUES

Over recent years, there is a rapid advancement seen in modern Integrated Circuit (IC) technology, which is driven by the continuous demand for smaller and more functional microelectronic circuits. In 1965, Gordon Moore, a visionary and co-founder of Intel, predicted that the number of transistors on a chip will double about every two years. This prediction, more commonly known as *Moore's Law*, has kept that pace for nearly the last four decades and will continue to help move the industry forward. An uninterrupted continuation of this trend is due to the constant adoption of technological innovation by the semiconductor industry. The trend of microelectronics devices is moving towards higher I/O density, more functional devices and higher clock speed.

Microelectronic devices are individual packages, singulated from a larger array. In order to create an array of these devices, a number of processing steps, including deposition, lithography, etching and developing, are performed on a silicon wafer. The singulation of these arrays into individual packages, also known as “dicing”, is the first step in electronics packaging. The silicon wafers, after going through numerous lithography and development processes of making micro-circuits, are at its highest value. Hence dicing, which is the next step in the process, becomes very crucial and has a significant effect on the cost and reliability of the chips produced. The process of dicing needs to be optimized to minimize the overall cost of package and to maximize its reliability for a life cycle. The continuous reduction in package size, along

with the uncompromising demand for increased throughput without sacrificing machining quality, has resulted in a shift from shearing/punching techniques to dicing processes for many matrix array packages. The trends in package singulation are expected to have a significant impact on the semiconductor industry.

Of the many recent developments adopted by the industry, there are a few that have had a significant impact on the dicing process in semiconductor fabrication. The first of these developments is the ongoing trend to reduce wafer thickness. One of the main reasons for this trend is the limit on the maximum number of features that can be packed into a two-dimensional layout. By employing the third dimension, silicon dice can be vertically stacked, enabling increased density and higher levels of integration [1]. Furthermore, reducing wafer thickness reduces overall package size while improving its clock cycle speed [2]. In addition, a specific need for very thin wafers has been created by the introduction of smart cards, where dice need to be thin enough to be laminated as part of a plastic card. The other driving force for the reduction of silicon wafer thickness is the relatively poor thermal conductivity of thick silicon wafers [3]. Heat is generated on the active topside of silicon dice and is removed by a heat sink that contacts the backside of the dice. For high-power devices, the rate of heat transfer through the thickness of the silicon may become too slow for optimal performance. Thin wafers in this case provide an advantage in dissipating the heat generated more efficiently than thicker wafers [4]

The standard 200 mm wafers are usually 625 μm thick, with 300 mm wafers reaching a typical thickness of 720-750 μm . Although wafers thinner than 150 μm currently account for only a small percentage of the total silicon wafer market, their use is growing significantly. In

recent years, the volume of thinned silicon wafers has increased dramatically [5]. Table 1 shows the market trend of thin wafer usage.

Year	2004	2006	2008
Total Number of wafers (millions eq. 8 inch)	140	146	155
Thin Wafers < 150 micron thickness	< 5%	20%	30%

Table 1: Thin wafer usage market trend [5]

The starting point for microelectronic packaging is the wafer, which contains a (very large) number of circuits and devices, separated by small gaps, and electrically isolated from each other as part of the processing. Starting with a blank wafer of extremely pure silicon, then building up layers by deposition techniques, etching patterns, and implanting dopants into the silicon structure using high energy particles, the semiconductor ‘fab’ produces a wafer which is partially probe-tested, but needs terminations in order to communicate with the outside world. These ‘front end’ processes attract the headlines, but the back end of the pantomime horse is just as important.

The ‘back end’ process consists of dicing the wafer into individual dice (the terms ‘chip’ and ‘die’ are equivalent), mounting the die on a lead-frame or other mount using conductive adhesive, and finally making fine wire connections to the top surface – this ‘wire bonding’ process uses gold and aluminum wires typically 25-33 μm in diameter. As wires are relatively fragile and easy to contaminate, the dies are sometimes protected using a casing. In this chapter, different dicing techniques will be discussed and evaluated in reference to their advantages and limitations.

1.2 WAFER DICING PROCESS

Wafer singulation or dicing is the process by which individual silicon chips or integrated circuits on a silicon wafer are separated following the lithography processing of the wafer. The dicing process can be accomplished by principally two major categories: contact dicing or non contact dicing, or in some instances using a combination of these techniques.

In wafer dicing process, silicon wafer of required thickness is typically mounted on dicing tape or DAF (Die Attach Film), which has a sticky backing that holds the wafer on a vacuum chuck. Once a wafer has been diced, the remaining components that are left on the dicing tape are referred to as die, dice or dies; these are the small integrated circuits that will be integrated into a lead-frame package or placed directly on a power circuit board substrate as a "bare die". The area that has been cut away is called die street or kerf width. Once a wafer has been diced, the die will stay on the dicing tape until they are extracted by die handling equipment, such as die bonder or die sorter, further in the electronics assembly process. Figure 1-1 shows the details of wafer parameters.

The size of the dice left on the tape may range from 35 mm^2 (very large) to 0.5 mm^2 (very small). The die created may be of any shape generated by straight lines, but it is typically rectangular or square shaped. Wafers are designed to hold as many dies as possible, because of the fixed cost associated to produce a wafer. The more dies that can be fit onto a wafer, the lower is the die production cost. Each die is segregated by a narrow "street" that is the cut line for die singulation. Some wafers also have extra monitoring circuits built onto the wafers that take the place of a few dies. These circuits are used to measure process controls during wafer fabrication.

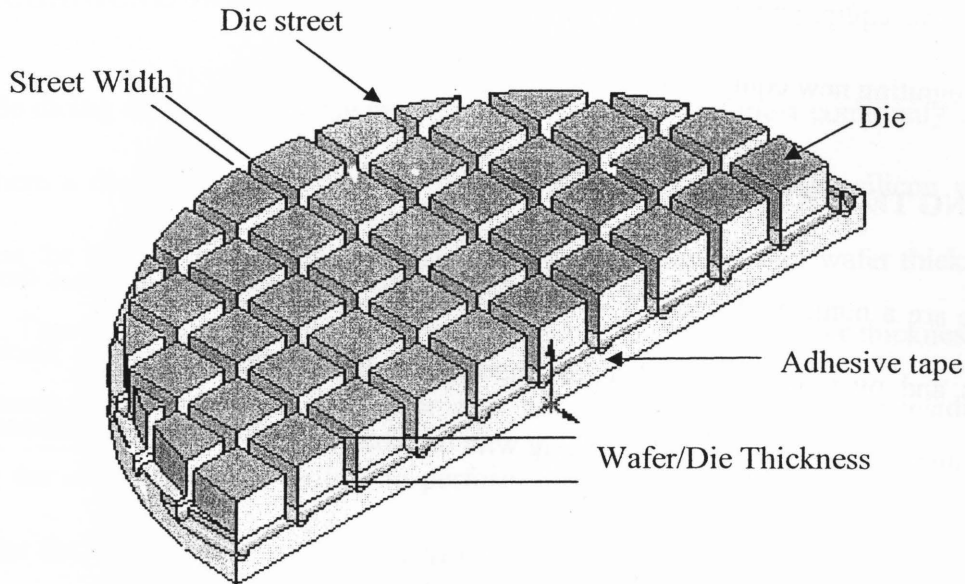


Figure 1-1: Wafer parameters

The goal in silicon wafer dicing applications is to maximize throughput and yield while minimizing cost of ownership. The challenge, however, is that increasing throughput often reduces yield and vice versa. The rate at which the wafer substrate is fed into the cutting blade determines throughput. As the feed rate increases, it becomes more difficult to maintain the cut quality within acceptable process windows. The narrow street widths require the dicing equipment to place each and every cut within several micrometers of the street center. This dictates the use of equipment with high indexing axis accuracy.

Two major forces are driving the development of dicing technology today: the trend toward automation and the need for technological sophistication, resulting from wafer and production evolution. Some factors that typify this evolution include thin wafers with larger diameter, narrower die streets, larger variety of die sizes and shapes, die strength and reliability of the product. Maximum-reliability equipment design and consistent, flexible image/pattern processing capabilities represent the newest challenges to dicing system manufacturers. At the

same time, dicing equipment users are reexamining older concepts and must now participate actively in integrating new equipment into their facilities.

1.3 DICING TECHNIQUES

There are a number of dicing techniques that have been suggested to meet the stringent requirements and overcome the challenges imposed by thin wafer singulation. Each of these techniques interweaves some advantages along with drawbacks. In the following sections, some of these proposed techniques are studied.

1.3.1 DIAMOND SCRIBING

This is the oldest separating method, mainly used for silicon & GaAs wafers before 1970 [6]. Figure 1-2 shows a model of diamond scribed silicon wafer.

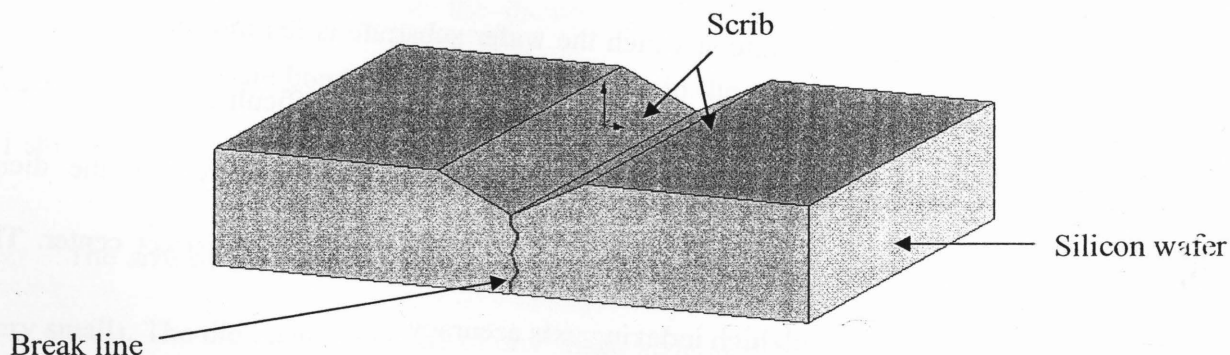


Figure 1-2: Diamond Scribing Technique

In this technique, a diamond tip scribes a shallow scratch on the wafer and dice are then separated by the application of a mechanical force. However, the edge quality of a scribed and broken die is poor. Breaking produces dies that are irregular in size and shape. The strength of such dies is also poor due to the mechanical stress produced while breaking. This technique is not used for mass production but only for some specialty applications.

1.3.2 MECHANICAL SAW OR BLADE DICING

Blade dicing or mechanical sawing / abrasive sawing is the most commonly used dicing process, where a diamond coated blade is used to mechanically saw the silicon wafer. This technique has the highest throughput compared to any other processes for wafer thickness above $150\text{ }\mu\text{m}$ [7]. There are many variables involved in sawing the wafers. Wafer thickness, width of the saw streets, composition of the wafer and die size, all have to be considered when formulating the saw parameters. Failure to perform the process correctly can cause mechanical damage to the die [8,9]. Figure 1-3 shows a typical mechanical blade dicing arrangement.

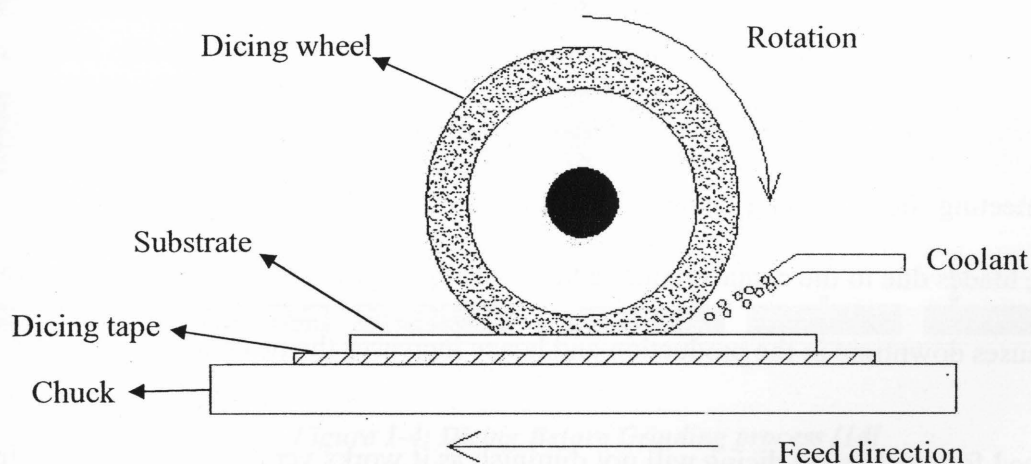


Figure 1-3: Mechanical Blade dicing

Wafers are first mounted on a wafer cutting ring and aligned. A diamond stud blade is mounted on a spindle perpendicular to the wafer. It spins at a high speed and travels along the street, cutting the die apart. Usually the blade cuts 100% through the wafer and 1 to 3 mils into the wafer tape. The blade can travel either forward or reverse across the wafer. Once all the parallel streets are cut, the chuck is then rotated 90 degrees and all of the orthogonal streets are cut. Once the wafer is fully sawn, the individual dies are removed from the wafer tape and transferred to an appropriate carrier for further processing.

Blade dicing is the most commonly used silicon wafer dicing process. However, since blade dicing is a mechanical process, it produces undesirable mechanical vibrations and stress in the dies [10-12]. These induce mechanical damage in dies, consisting of cracks, chippings, delamination and peel-off of top layers [13].

In order to meet the demand for smaller devices, the industry is moving towards thin wafers with thickness less than 100 μ m, for advanced manufacturing. Saw dicing has been preferred in the industry due to its processing speed capabilities. But as the wafer thickness reduces to less than 100 μ m, serious reliability issues arise due to the high cutting speed and contact nature of the saw dicing technique. In order to compensate for these issues, processing speeds need to be reduced significantly, which in turn is not viable for the industry. Processing speed being one of the most important specifications for industry, saw dicing is considered unviable for meeting the upcoming demand of throughput and yield for thin wafers. Also, the wearing of the blades due to the contact nature adds to the operating cost. Changing of the blades and spindle causes downtime in the production and hence increases the production cost.

The need for mechanical dicing will not diminish as it works very well for thicker silicon wafers. However, the industry is looking for an alternative technique to offset some of the yield loss caused by mechanical dicing of thin flexible wafers. Some of the techniques that have been proposed to offset some of the above mentioned challenges are discussed hereafter.

1.3.3 DICING BEFORE GRINDING

Dicing Before Grinding (DBG) reverses the usual process of fully dicing the wafer after grinding (DAG-Dicing After Grinding). Traditionally, the silicon wafers are 650-800 μ m thick,

which are then grinded and thinned down to the desired thickness. These wafers then undergo a number of deposition, lithography, etching and developing processes to create the desired circuit. After completion of the transfer of circuits on to the wafer, the wafer is completely diced, to separate each chip. However, in DBG, this process is reversed and the wafer is cut half way into its thickness before being grinded and thinned down. The half-cut wafer is then mounted on a tape from topside. The wafer is grinded from the back side until die singulation occurs, when the wafer is thinned below the bottom of the cut. Figure 1-4 shows a typical dicing and then back grinding process.

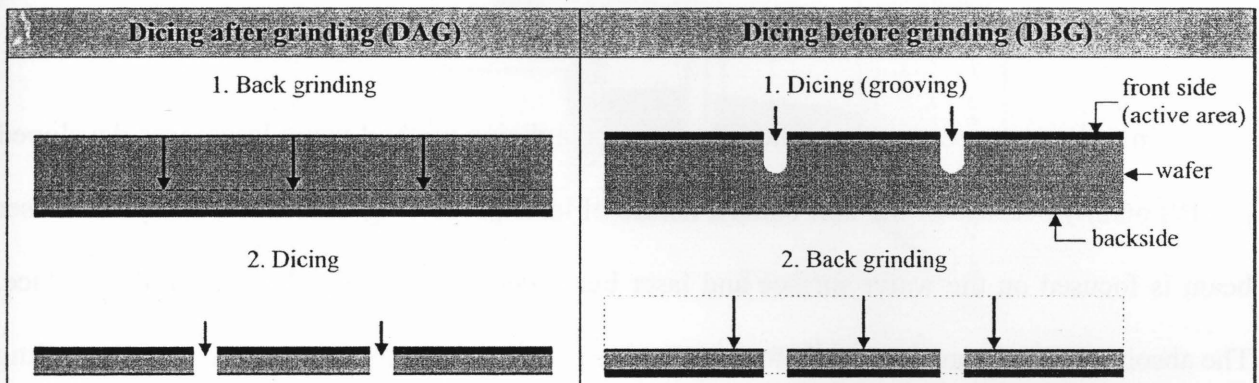


Figure 1-4: Dicing Before Grinding process [14]

The wafer then goes to the in-line DBG mounter, which gently peels off the protective grinding tape. In DBG, as the thinned wafers are never transported, wafer-level breakage is greatly reduced, and because die separation occurs during the grinding process, the backside chipping associated with thin-wafer dicing is kept to a minimum, hence increasing the die strength. For these reasons, DBG is an excellent process for processing 300 mm wafers into high-quality dies.

The drawback of diamond back grinding is that it can cause serious wafer damage, which, under the mechanical constraints of sawing, can lead to die chipping and hidden micro damage. Back chemical etching can be used to reduce some of the internal stress caused by diamond back grinding [15]. However, it cannot repair all damages, and any remaining internal mechanical stresses, can lead to outright failures or, for power devices, device reliability problems in the field due to possible frequent large surging currents. Also, mounting the wafer on the active topside (the side with the circuit already built on) is not desirable since it may cause damage and contamination to the delicate circuitry.

1.3.4 CONVENTIONAL LASER DICING

In order to overcome blade-dicing problems, a dicing method using lasers was developed [16,19] mainly because of the non-contact nature of laser processing. In these techniques, a laser beam is focused on the wafer surface and laser beam energy is absorbed on the wafer surface. The absorbed laser beam energy ablates or changes the properties of the wafer surface depending on the quantity of absorbed energy.

Nanosecond lasers have been widely used for material removal and micro-fabrication [18,20,21,22]. In principle, any type of nanosecond laser with intensities above the ablation threshold could potentially be utilized as the light source for silicon dicing. There are many nanosecond lasers available, with repetition rates varying from a few Hertz to few thousand Hertz and pulse widths from a few nanoseconds to a few tens of nanoseconds. Most commonly used commercially available, nanosecond lasers are Nd-YAG, Diode pumped Solid State (DPSS), Excimer laser, etc. The material removal rate and the quality of resultant features are the

most important considerations for selection of laser source. Figure 1-5 show a typical laser dicing setup.

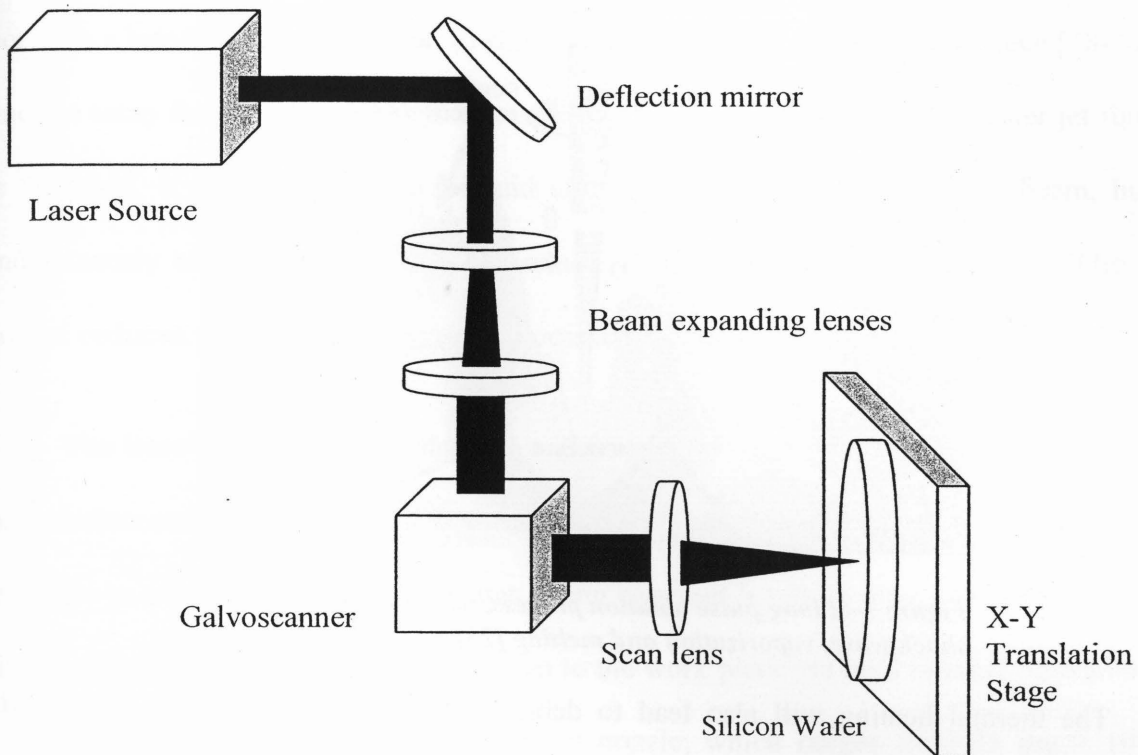


Figure 1-5: Setup for laser micromachining

The physical process of laser-silicon interaction in the nanosecond time regime is a complex process, involving many aspects of laser-matter interaction. As a laser beam with intensity above the ablation threshold illuminates the surface, the heat waves penetrate into the bulk of the silicon, generating vapor and melt. At the same time, surface plasma is formed by the ejected atoms species. The surface plasma absorbs and reflects laser energy and the expansion of the plasma generates shockwaves. Cracks and fractures might appear as a result of the impact of the shock waves. Figure 1-6 shows a long laser pulses irradiation of a surface and its effects on the material breakdown.

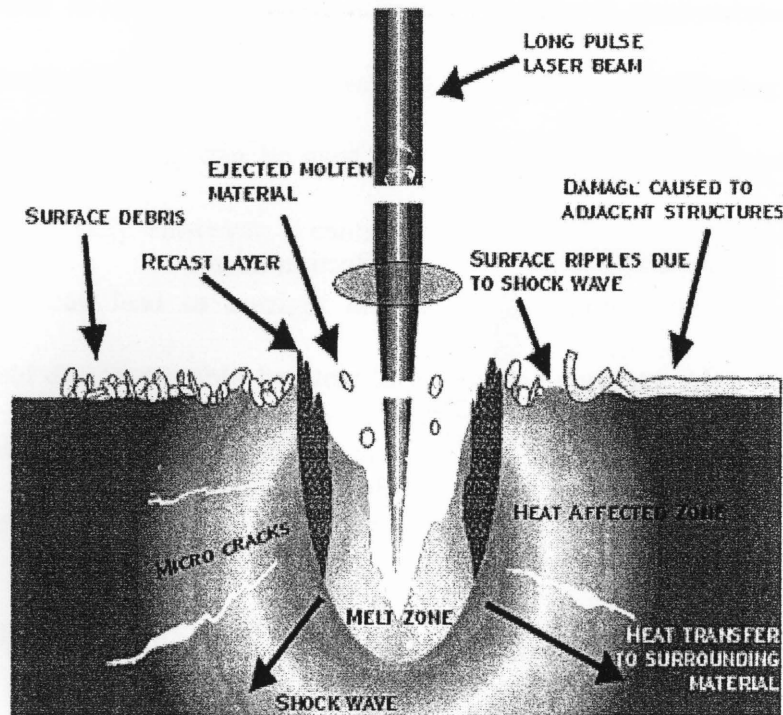


Figure 1-6: long pulse ablation process, which includes plasma, shock wave, vaporization and melting [23]

The thermal heating will also lead to debris and a heat affected zone (HAZ) where properties of the material are thermally altered. The direct affect of these defects is the degradation of die strength [24]. For a thin chip, low die strength tends to induce failure of the chip during the packaging process. Etching processes including wet-etch and dry-etch were attempted to recover the die strength by removing the chip sidewall damages. Results from previous studies indicated that, before etching, the laser diced sidewalls were with rough surfaces, voids and microcracks. After etching, the surfaces got smooth and most of the voids and microcracks were removed [25,26]. Chip strength measurement also verified the partial die strength recovery after the etching process. However, etching increases the cost of production significantly. Hence, the most challenging problems with conventional laser dicing are the die strength degradation due to thermal damage, chipping and formation of microcracks on die sidewalls. This has been considered as a limitation of laser dicing technology [27]

1.3.5 LASER WATER-JET CUTTING TECHNIQUE

The water jet-guided laser technology combines the advantages of a high power pulsed laser with a hair-thin jet of water jet, to simultaneously cut and cool the work-piece [28-30]. The principle setup for this technology is shown in Figure 1-7. The low-pressure water jet functions are threefold. It acts, not only as a liquid optical fiber for guiding the laser beam, but also simultaneously cools the work piece and removes the molten material and debris. The water coolant reduces the thermal damage associated with laser dicing.

The laser beam is focused through a glass window on to the surface of the nozzle. The glass window and the nozzle, together form a tiny pressurized water chamber. The water jet exits the nozzle as a low pressurized jet, having a long coherent length (a long and stable water jet of uniform diameter), and guides the laser down to the work piece via total internal reflection at the air/water interface. The diameter of the water nozzle, which ranges from 25 μm – 100 μm , directly controls the cutting diameter of the laser. The control of the geometries of both the chamber and nozzle are crucial for efficient coupling of the laser beam into the water jet. The long cylindrical water jet avoids the need of focus control. It carries the laser beam down to the bottom of the cutting kerf and hence, allows to machine materials with a high aspect ratio. The machining result is independent of the machining direction, as problems related to the conventional dry laser process, such as beam ellipticity and astigmatism, no longer exist.

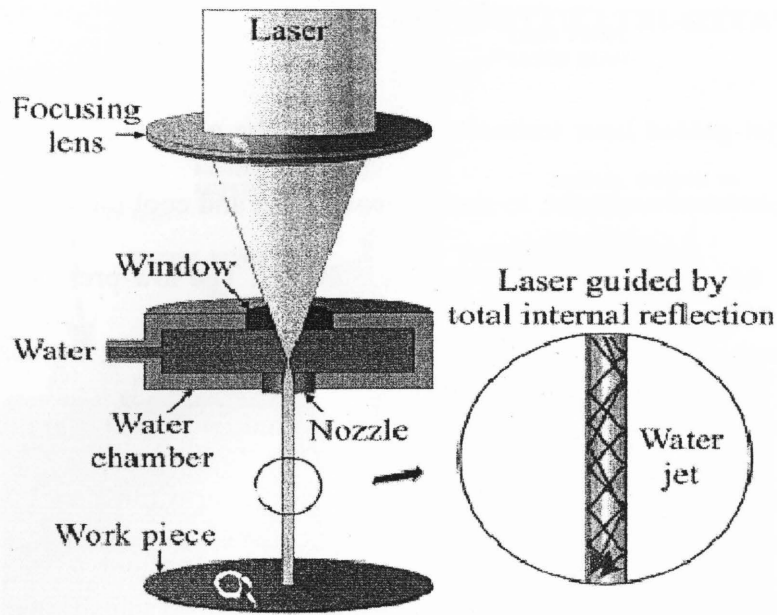


Figure 1-7: Principle of the LMJ, coupling of a laser beam into a water jet [29]

The water-jet-guided laser requires no complicated adjustments for spindle speed or cutting wheel selection. For thin silicon wafers, this technique can cut faster than the conventional diamond wheel with high-quality kerfs. High throughput, significantly lower de-ionized water usage, and the lack of blade and spindle maintenance costs provide much improved cost of ownership compared with the conventional diamond saw.

This technique offers a processing capacity for large wafer diameters and can place cuts with high accuracy. The kerf width that can be obtained is the same as the diameter of the water jet. Hence, controlling the water jet nozzle diameter can lead to smaller kerf width. Even though this machine can cut with a kerf smaller than 50 μm , currently it is limited to a kerf no smaller than 80 μm . Curved cuts can be made as easily as straight cuts. This process works very well with thin materials. Thicker wafers are usually more efficiently cut using conventional dicing processes. The main advantage of this technique, compared to the traditional laser dicing, is that

heat conduction is minimized, therefore resulting in a better quality and thus higher dice strength. In addition, focusing is not necessary as cutting can be accomplished along the entire water jet. However, the usage of water is not preferred in many semiconductor applications as it may damage the circuitry and other sensitive devices. Also, this technique needs a water permeable dicing tape and a special chuck to drain water, which makes this tool incompatible with current assembly line setups.

1.3.6 FEMTOSECOND LASER DICING

The development of femtosecond (fs) lasers and their initial application to the machining of a variety of materials has created huge interest in their micromachining potential [31-36]. Current reasoning suggests that the pulsewidth of a femtosecond laser is too short to allow for heat conduction into the bulk of the ablated material. Therefore, defects associated with thermal heating during ablation can be eliminated and superior machining quality can be obtained. Figure 1-8 shows an image of material processing using a femtosecond laser pulses.

Femtosecond laser is an attractive alternative for dicing, as it provides a way to obtain very clean removal of materials. The main advantage of using femtosecond laser pulses for the ablation of materials is that compared with using nanosecond laser pulses, the heat diffusion into the target is negligible, which results in highly localized ablation and precise patterning of the sample without much thermal damage to the surroundings [35-36].

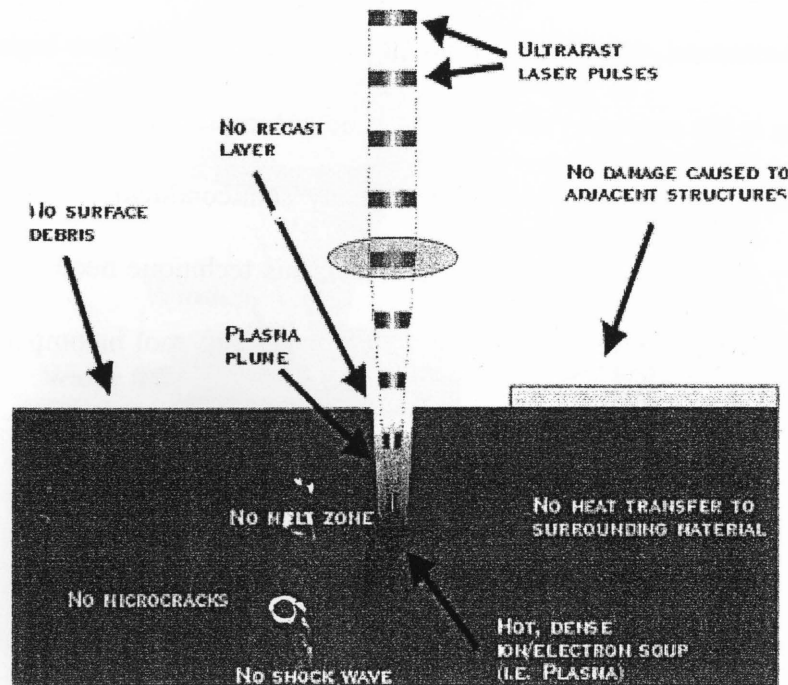


Figure 1-8: Femtosecond laser pulse ablation process [23]

One significant difference between femtosecond laser-matter interaction and nanosecond laser-matter interaction in terms of transferring laser energy into thermal energy of the target is that electrons and ions are not in equilibrium during the laser pulse in the Femtosecond laser ablation case. This is because the electron-ion relaxation time, which is in the range of a few picoseconds to a few tens of picoseconds, is much longer than the sub-picosecond pulse length. Therefore, for the interaction of femtosecond laser pulses with solid materials, the laser energy is first deposited into the thermal energy of electrons and then transferred to the lattice on a picosecond time scale after the laser irradiation. With new techniques in fiber amplification, a high power femtosecond laser is coming to the market. Therefore, using a femtosecond laser for dicing could be considered a feasible and a promising industrial tool.

1.3.7 SUMMARY OF DICING TECHNIQUES

Traditionally, silicon wafers are diced or singulated by the saw blade dicing method. Since blade dicing is a mechanical process, it tends to cause greater stresses on the wafer, resulting in increased chipping, cracking and mechanical stress. Also, due to the contact nature of this technique, severe wafer damage is observed when used for wafers thinner than 100 μm .

There are a number of other dicing techniques suggested to meet the stringent requirements and overcome the challenges imposed by thin wafer singulation. Each of these techniques interweaves some advantages along with drawbacks. Water jet guided laser cutting is a highly efficient technique being recently adapted. The advantage of using a water jet laser is that water helps to cool the workpiece and removes the molten material and debris, resulting in a better quality. However, the usage of water is not preferred in many semiconductor applications as it may damage the circuitry and other sensitive devices. Furthermore, this technique needs a water permeable dicing tape and a special chuck to drain water, which makes this tool incompatible with current assembly line setups. Back grinding is also another techniques proposed for thin wafer singulation. But it creates wheel pattern, fracture load and wafer warping. There are a number of pre and post dicing preparations to be made for use of this technique, leading to numerous modifications in the assembly lines and hence inducing high operating cost.

The typical conventional laser source produces pulses with the duration in the range of nanoseconds to milliseconds. Besides the advantages of cutting with laser, it has several limitations. The thermal load in the material due to the heat conduction is relatively high which results in large heat affected zone that may damage the delicate circuitry in the vicinity and also

leads to degradation of the mechanical strength of the dice. Moreover a large amount of melting also affects the quality of finishing. Dicing of silicon wafers with a non-contact nature and a fast processing speed, the femtosecond laser provides a novel alternative method for the thin wafer dicing.

As a summary for this chapter, it can be said that in order to meet the future demand for microelectronic devices using thin wafers below 100 μ m, the femtosecond laser can be considered a viable solution.

1.4 RESEARCH OBJECTIVES

Even though the feasibility of using femtosecond lasers has been predicted for over a decade now, industrial application of this technique is still awaited due to the challenges faced in terms of laser parameters and inadequate experimental studies in this area. The main aim of this thesis is to study the high repetition rate high average power femtosecond laser system and its effect on thin wafer dicing.

Researchers have been predicting the advantages of using ultra fast laser systems for more than a decade now, but the capabilities of the laser systems used in previous studies did not have the potential of overcoming the throughput and die strength requirement. One of the major factors influencing the reliability or die strength is the sidewall quality which greatly depends upon the repetition rate and laser power. Hence, the outline of the research objectives of this thesis can be summarized as

1. Verify the capabilities of the proposed high-repetition-rate-high-average-power femtosecond laser system for dicing.

2. Optimize the laser parameters like pulsewidth, repetition rate, polarization and cutting speed and evaluate the influence of these parameters on kerf width and depth of cut.
3. Study the influence of the pulsewidth, repetition rate and cutting speed on the sidewall quality.
4. Evaluate the influence of laser parameters on die strength and suggest a range for each parameter that can provide best cutting quality in terms of side wall roughness and die strength.

1.5 OVERVIEW OF THESIS

In chapter 2, the pulsed laser ablation mechanism is discussed in general. Existing mechanism and theories describing laser-matter interaction during the long pulse and short pulse ablation of silicon are summarized, with special attention to femtosecond laser ablation.

Details of the experimental setup, are presented in chapter 3. The important laser parameters, the role of aberration and other important parameters are identified and discussed.

A systematic experimental study of the influence of pulsewidth using a high-power-high-repetition-rate femtosecond laser is investigated and the results are presented and discussed in chapter 4. Crucial parameters such as the ablation threshold and depth of cut are deduced as a function of pulsewidth. The ablation depth is found to decrease and the ablation threshold increases slightly with the increase in the pulsewidth. The spherical shaped debris and its dependence upon the repetition rate and the scan speed have been found. The results obtained contribute to the experimental analysis of the effect of pulsewidth on the machining quality using femtosecond lasers with high repetition rate in Mega Hertz.

A systematic study of the influence of the laser parameters on the kerf width, depth and quality of machining is discussed in chapter 5. A number of different experiments were performed. The experimental results obtained by using the high-powered-high-repetition-rate femtosecond laser are promising for dicing of thin wafers. It is also the first time that a high-repetition-rate femtosecond laser has been demonstrated for real world industrial application for micromachining. A cutting speed of 40 mm s^{-1} , with acceptable quality of sidewalls, depth of cut and kerf width, is demonstrated during the experiments which can be considerable when applying for industrial usage.

In chapter 6, the dependence of die strength and sidewall surface roughness, on laser parameters, such as pulsewidth and repetition rate, is reported. The $80 \text{ }\mu\text{m}$ wafers used in this study are polished on both sides, and hence the role of die edge defects in determining the die strength is discussed. Results obtained for the sidewall and average surface roughness will be discussed. Die strength tests using the three point bending test are discussed and reasons for the strength reduction due to die sidewall surface defects are evaluated. The effect of the gas assist like Nitrogen and Helium, on the surface roughness and sidewall quality of the thin singulated dice are discussed.

Chapter 7 summarizes the results obtained from this research work. Also, the achievements and applications of the proposed dicing technique using the high-repetition-rate-high-power femtosecond laser system are discussed. This chapter also includes suggestions for further research that can be carried out.

CHAPTER 2

LASER ABLATION MECHANISM

2.1 INTRODUCTION

The efficient use of lasers for precise material processing is difficult to understand without thorough knowledge of the fundamental physics governing the interaction of laser radiation with matter. The physical process of laser-matter interaction is indeed very complicated and involves rich variety of different phenomenon, underlying the different aspects of laser matter interaction. Many fundamental researches have been done to determine the physical mechanisms involved and their relative contributions in this complex and highly non equilibrium laser-matter interaction process [35-37]. These mechanisms are not only of fundamental interest, but also are very important for engineering application. For example, the primary concerns of manufacturing inkjet printer are the throughput, precision and quality of laser micromachining processes. There are vast varieties of laser parameters to choose from, including laser intensity, pulse length, wavelength, repetition rate etc. Therefore, understanding of the physical processes in laser-matter interaction becomes very crucial in choosing the optimal operating conditions. The ablation mechanism is dependent on the properties of the sample material. Silicon material prevails in semiconductor industry and hence is selected as the subject of this study. This chapter focuses on the fundamental physical mechanisms and characteristics of laser-silicon interaction. Number of researchers have shown that the mechanism of laser ablation is determined by pulsewidth [35-40]. Depending on the pulsewidth regimes, the mechanism can be thermal or non-thermal in nature. To better understand the advantages of ablation with femtosecond laser,

laser-matter interaction mechanisms are discussed both for femtosecond and nanosecond pulsewidth.

2.2 MECHANISMS IN LASER ABLATION PROCESS

The process of laser ablation can be briefly summarized as follows. Upon irradiation of the laser beam on the surface, the heat waves penetrate into the bulk of the substrate, generating vapor and melt. As more heat is supplied, due to the rapid heating and heating-induced instability, evaporated particles are explosively ejected from the surface. Also the surface plasma is formed by the incident laser beam. The surface plasma is a large population of loosely bound electrons and ions which absorbs and reflects laser energy. The surface plasma absorbs and reflects laser energy. The expansion of plasma on the surface and the rapid ejection of removed material create shockwaves. Fractures might appear as a result of the propagation of the large shock-wave pressure-induced and thermal-induced stress.

Figure 2-1 shows a schematic illustration of the ablation process, which includes heat transport, plasma, shock wave, and vapor and melt formation. For nanosecond or longer pulses, the physical process of laser-matter interaction is characterized by thermal diffusion and plasma absorption which results in the partitioning of laser energy between plasma and bulk material; whereas for Femtosecond or ultrashort pulses, it is characterized by the formation of hot and dense plasma, plasma heating and then heat diffusion.

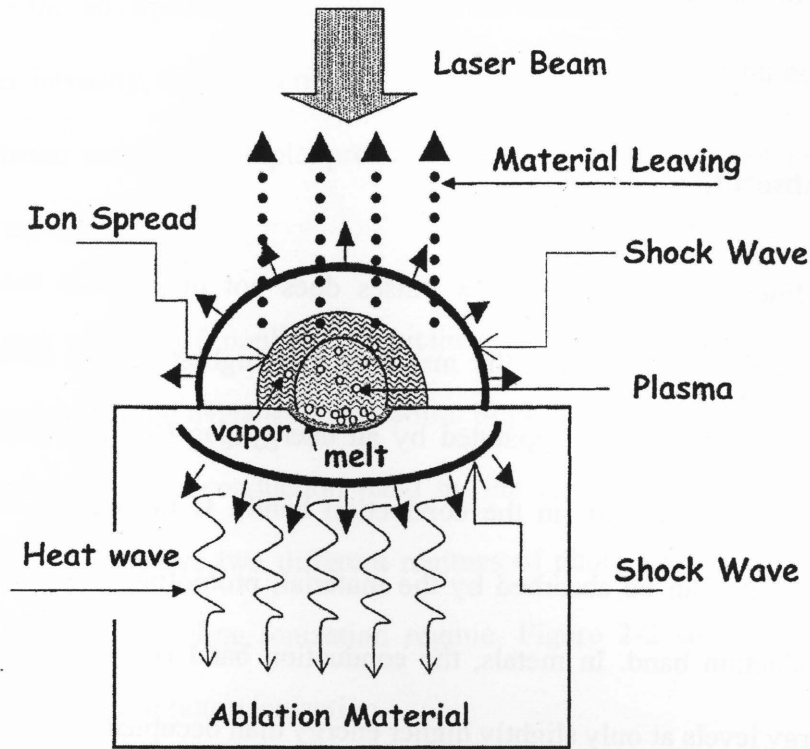


Figure 2-1: Laser Ablation of material

In the following sections, various mechanisms associated with laser ablation are discussed respectively.

2.2.1 ABSORPTION AND IONIZATION

The absorption of laser light occurs through excitation of the outer atomic electrons. When the excitation energy exceeds the binding energy of the target material, bond breaking may occur [36]. The interaction of short pulses (< 1 ps), with materials, differs from the interaction of longer pulses or continuous wave light in two ways. First, the energy deposition occurs on a timescale that is shorter compared to the electron-phonon relaxation time. The laser energy is absorbed by the electrons, leaving the ions cold, and only after the laser pulse is gone does thermalization take place. Second, the intensity of a short pulse, even with very moderate energy, is high enough to drive highly nonlinear absorption processes in materials that do not

normally absorb at the laser wavelength. This implies that material breakdown is wavelength dependent for short pulses.

2.2.1.1 Linear Absorption

Overall, linear absorption of laser pulses does not differ from the linear absorption of any other light field. In non-metallic materials, the highest energy level occupied by an electron (in the valence band) is separated by an energy gap (the bandgap) from the lowest energy level that is unoccupied (in the conduction band). If the photon energy exceeds the bandgap energy, light can be absorbed by the material, promoting electrons from the valence band to the conduction band. In metals, the conduction band is partially occupied, providing unoccupied energy levels at only slightly higher energy than occupied ones. In this case, photons can be absorbed through free-carrier absorption, a three-body interaction where an electron gains energy by absorbing a photon, and gains momentum through an interaction with a phonon (a lattice vibration) to move to a higher-lying level in the conduction band. In addition, there remains the possibility for interband transitions between the conduction band and higher-lying bands, as in insulating materials. If sufficient laser energy is deposited into the surface of a material through linear absorption, material ablation can occur.

2.2.1.2 Nonlinear Absorption

In samples that are transparent to the laser wavelength, a single photon of light does not have enough energy to excite an electron from the valence to the conduction band, and absorption of laser energy can occur only through nonlinear processes. If enough laser energy is deposited into the material by this nonlinear absorption, ablation or permanent structural changes

can occur. Because the absorption is nonlinear, i.e., the absorption probability is a nonlinear function of the laser intensity, the absorption can be confined to the bulk of a sample by tightly focusing the laser beam inside the sample, producing a much higher laser intensity in the focal volume than at the surface.

There are two classes of nonlinear excitation mechanisms that play a role in this absorption, photo ionization and avalanche ionization. In photo ionization, electrons are directly excited from the valence to the conduction band by the laser field. Depending on the laser frequency and intensity, there are two different regimes of photo ionization, the multi photon ionization regime and the tunneling ionization regime. Figure 2-2 shows the schematics of avalanche ionization and multiphoton ionization.

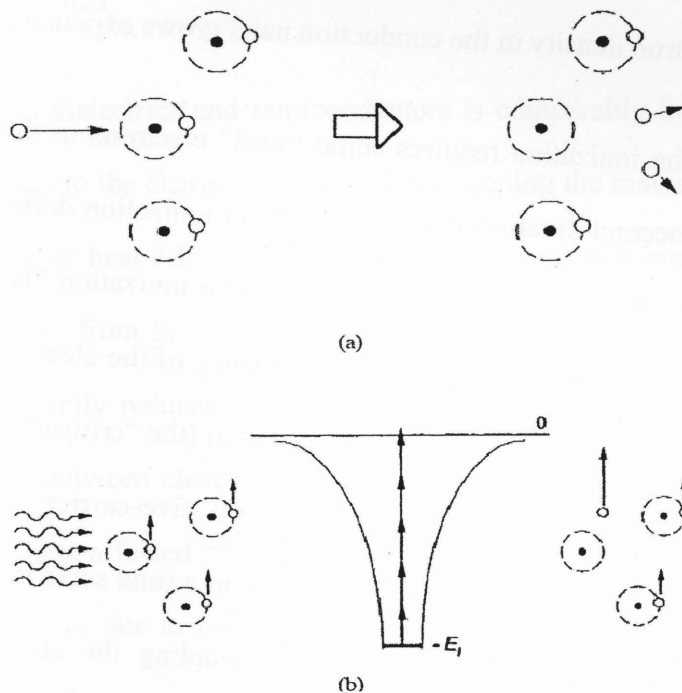


Figure 2-2: (a) Schematics of electron avalanche by collisional impact ionization (b) The multiphoton ionization process [41]

In tunneling ionization, the electric field of the laser suppresses the potential that binds a valence electron to its parent atom, allowing the electron to tunnel out and become a free electron. This type of nonlinear ionization dominates for strong laser fields and low laser frequency. At higher laser frequencies (but still below that required for linear absorption) nonlinear photoionization occurs due to the simultaneous absorption of multiple photons by an electron. The sum of the energy of all the photons absorbed must exceed the bandgap energy.

Avalanche ionization involves free carrier absorption by an electron already in the conduction band of the material followed by impact ionization. An electron in the conduction band sequentially absorbs several laser photons until its energy exceeds the conduction band minimum by more than the bandgap energy, then collisionally ionizes another electron, leaving two electrons at the conduction band minimum. As long as the laser field is present, this process repeats, and the electron density in the conduction band grows exponentially.

The avalanche ionization requires some "seed" electrons in the conduction band of the material. For femtosecond duration laser pulses, photo ionization during the leading edge of the laser pulse provides these seed electrons for avalanche ionization. The electron density grows through avalanche ionization until the plasma frequency of the electrons in the conduction band approaches the frequency of the incident laser radiation (the "critical" plasma density). This high density plasma strongly absorbs laser energy by free-carrier absorption. For ultrashort pulsewidths, the absorption described above occurs on a time scale that is short compared to the time scale for energy transfer to the lattice, decoupling the absorption and lattice heating processes. At the end of the laser pulse, what essentially left are, "hot" electrons and a "cold" lattice.

2.2.2 ENERGY RELAXATION

The laser radiation interacts primarily with the electronic states of the valence and the conduction bands. The time to deposit the energy within these states is determined by the laser pulsewidth. For very short laser pulses the resulting energy distribution of the electrons at the end of the laser pulse may be non-thermal. Within a fraction of a picosecond this non-thermal energy distribution will relax to a Fermi-Dirac distribution, which can be properly characterized by a temperature. Later on, the deposited energy is redistributed over the various energy states of the system, i.e. energy is transferred from the electrons to the lattice. In order to understand the difference in the interaction of ultrashort and long laser pulses with matter, it is instructive to consider the characteristic time scales involved.

2.2.3 HEAT TRANSPORT

Heat transport in dielectrics and semiconductors is comparably low, since the electrons are not able to escape due to the charge separation force keeping the material neutral. In general, metals show much stronger heat diffusion, since the hot electrons moving into the target can be replaced by cold electrons from the adjacent region. However, even in the case of metals heat diffusion can be significantly reduced when ultrashort pulses are used, due to the strong non-equilibrium interactions between electrons and lattice. The main advantage of using ultrashort laser pulses is reduced heat affected zone (HAZ), less molten material due to absence of liquid phase and less debris. Also, due to reduced HAZ, thermal defects like cracking, chipping and delaminated can be reduced.

2.2.4 THE LASER GENERATED PLASMA

The characteristics of laser generated plasma depend on the material, the laser pulse length, wavelength and laser intensity as well as the ambient conditions. Figure 2-3 shows a schematic illustration of the composition of plasma at a distance from the surface of the target.

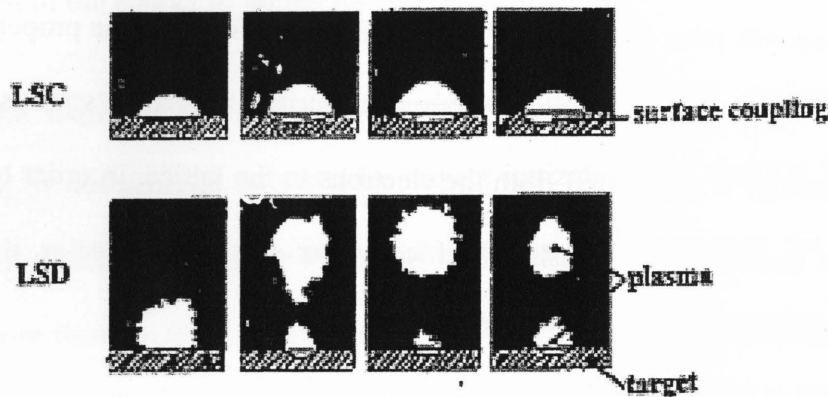


Figure 2-3: Formation of plasma during laser ablation [41]

The region closest to the target is the central or core region where the plasma temperature is maximal and the plasma density is highest. It is also the region where most plasma ionization through collision and most plasma absorption of the incident laser energy take place.

2.2.5 THE MELT FLOWS IN LASER ABLATION

To characterize the melt flow under laser heating, a hydrodynamic model was proposed, which finds good agreement with experimental measurements for nanosecond or longer laser pulses. Wherein based on the thermal property of the ablating material and the laser pulse length, the laser ablating is classified as volumetric laser ablation and superficial laser ablation. Shorter pulse length will reduce the melt pushups and hence reduce the melt recast and therefore improve ablation quality.

2.2.6 SHOCK WAVE

When the ambient environment for ablation is a gas, such as air, a shock wave is produced by the expansion of the plasma plume. The shock wave above the ablating material into the ambient gas is caused by the compression of the gas by the high velocity portion of the spreading of the ionized species, and by the high velocity expansion of the evaporated particles. A shock wave in the solid is caused by the generation and the expansion of the hot plasma, as well as by the subsequent heat conduction into the bulk. In the bulk of the ablating material, the shock wave overtakes when the heat conduction is slowed down by the occurrence of a phase transition.

When a shock wave propagates through the bulk of the solid target, a failure process called spallation or scabbing, can occur around the rear surface. The spallation is due to the crossing of two release waves: one of these rarefaction waves is generated by the unloading, starting from the front surface of the plate; the other one is the reflection of the first shock wave by the rear surface. The compressive stress wave interacts with the reflected tensile stress wave within the target, and a sufficiently large tensile stress will lead to internal dynamic fracture. In reality, the propagation of the shock wave in the material is more complicated since the shock wave loses its energy as it propagates to create permanent strain. In general, at the beginning of the laser pulse, the shock pressure increases and the shock wave start to penetrate the target. The laser intensity determines the initial pressure of the shock wave, which determines its velocity. The thickness of the target and the shock (changing) velocity determine the travel time, and the travel time together with the initial velocity determine the shock attenuation and its pressure at the back surface.

2.3 NANOSECOND LASER ABLATION

Nanosecond laser pulses have been widely used for material removal and micro-fabrication [18,20,21,22]. In principle, any type of nanosecond laser with intensities above the ablation threshold could potentially be utilized as the light source for silicon machining. There are many nanosecond lasers available, with repetition rates varying from a few 10's of kHz to a few Hz, having a maximum average per pulse intensity from a few GW/cm^2 to up to a thousand GW/cm^2 , and pulse lengths from a few nanoseconds to a few tens of nanoseconds. The efficiency of laser pulse utilization in terms of removing material is an important aspect that needs to be known before choosing laser sources.

The physical process of laser-silicon interaction in the nanosecond time regime is a complex process, involving many aspects of laser-matter interaction. As a laser beam with intensity above the ablation threshold illuminates the surface, the heat waves penetrate into the bulk of the silicon generating vapor and melt. Also, the surface plasma is formed by the incident laser beam. The surface plasma absorbs and reflects laser energy, and shock wave loading on the surface is created primarily by the expansion of the plasma. Cracks and fractures might appear as result of the large shock wave pressure and thermal stress. As the laser intensity increases the laser-silicon interaction could be divided into three distinct regimes based on laser intensity; namely, the low ablation intensity regime, the medium high intensity regime and the high intensity regime.

The major physical processes that dominate in these three regimes include the nonlinear physical processes between laser and the condensed matter in the low intensity regime, the physical processes within the ablation generated vapor plume in the medium intensity regime,

and the physical processes between laser ionized vapor plume and the ablating condensed matter in the high intensity regime. In the low-laser-intensity regime, the absorption of the incident beam by the laser excited surface plasma is assumed to be insignificant. This assumption is valid only for low to moderate light intensities. At higher laser irradiance, the laser beam ionizes the target at the early part of the pulse through the multi-photon ionization process. The growth of the free electron and ion population forms a plasma layer above the surface, which is non-transparent to the incident laser beam, and effectively keeps the laser energy from penetrating into the ablating materials beneath. Due to this plasma shielding effect, the laser silicon ablation speed will slow down and saturate as laser intensity increases.

The interaction of laser energy with silicon evaporates the target, generating a plasma and vapor plume; in addition, the strong laser field also creates high density electron and hole pairs in the bulk of the target. As a result, the absorption of laser energy is further modified. Also, thermal and photon-initiated free-electron emissions from the electron hole plasma, together with the multi-photon ionization are the sources for providing the "seeds" in surface plasma growth. Due to the continuous modification of the incident light by the vapor plasma and the electron-hole plasma during the pulse, the steady-state approximation of surface evaporation is no longer valid. Assuming again that the laser spot size is much larger than the heat affected zone, the heat conduction and evaporation front propagation are described by the one-dimensional heat transport equation.

With further increase the laser energy, the vapor plasma will further decouple the incident laser energy from penetrating into the ablating material. Meanwhile, at high laser irradiances, the energy absorbed by the vapor plasma increases with laser intensity and becomes non-negligible.

It is therefore believed that in the high laser-irradiance regime, the laser-heated hot plasma attains enough energy during the laser pulse to redistribute the incident energy through re-radiation after the laser pulse. The plasma is now treated as a secondary heating source, which presumes the continued energy exchange with the ablating material after the laser pulse and considerably accelerates the ablation process. The delayed ejection phenomenon or mechanisms for this kind explosive ejection at a very high heating rate could be established by considering the explosion of a metastable liquid. At the high laser irradiance regime, the short heating time and the great shock wave pressure allow the ablating system to enter deeply into the metastable state. The evaporation from the melted surface is rather weak and the primary mechanism for material removal is through the phase explosion of the metastable liquid.

The difference in the mass (volume) removal rate and the average ablation depth rate is due to the increased material ejections in the lateral directions caused by the increased plasma dimensions in the transverse direction and the strong shock wave. The strong shock wave mainly introduced by the plasma expansion can reach hundreds of kbar for laser intensity above 100 GW/cm^2 . A strong shock wave is accompanied by the strong shock heating effect, where acoustic energy transforms into heating. The shock heating helps to further increase, especially in the lateral direction, the material ejection speed.

2.4 FEMTOSECOND LASER ABLATION

Femtosecond laser pulses provide an attractive choice for laser dicing, as it provides a way to obtain very clean removal of materials. The main advantage of using femtosecond laser pulses for the ablation of materials is that compared with using nanosecond laser pulses, the heat diffusion into the target is negligible, which results in much localized ablation and precise

patterning of the sample without great thermal damage to the surroundings [35,36]. One significant difference between femtosecond and nanosecond laser-matter interaction in terms of transferring laser energy into thermal energy of the target is that electrons and ions are not in equilibrium during the laser pulse in the Femtosecond laser ablation case. This is because the electron-ion relaxation time, which is in the range of a few picoseconds to a few tens of picoseconds, and is much longer than the sub-picosecond pulse length. Therefore, for the interaction of Femtosecond laser pulses with solid materials, the laser energy is first deposited into the thermal energy of electrons and then transferred to the lattice on a picosecond time scale after the laser pulse.

For the Ultrashort lasers, the pulsewidth is too short for the heat to be conducted away from the surface during illumination. In this regime, the laser beam deposits its energy into the surface of the material, excites electrons to the conduction band and generates an excess of electrons. The laser pulsewidth is shorter than the electron relaxation time, which is on the order of picoseconds. By the time the laser beam is turned off, the system is out of equilibrium as the electrons are at a much higher temperature than the ions [42]. In this case, absorption of the laser and heating of the electrons in the surface layer, diffusion of the hot electrons into the bulk of the material, and energy exchange between the electron and phonon subsystem happen nearly simultaneously. It has been postulated that the highly concentrated energy heats the material quickly past the melting phase to the vapor phase. Since the heat does not have time to diffuse, the heat affected zone is greatly reduced. The depth of the optical absorption determines the thickness of the heated layer and is independent of the pulsewidth [43].

This indicates that ablation occurs via a direct solid-vapor transition. The timescale of ablation is sufficiently short to ignore all thermal effects, to the first order [36] and all hydrodynamic motion [42]. One indication of this phenomenon is the absence of an observable heat affected zone. Harzic et al did not observe a heat affected zone in Al, using a femtosecond laser, but concluded that the heat affected zone was smaller than their observational limit of 2 μm [44].

Another theory is that heating can occur electronically via fast Auger recombination. The presence of amorphous silicon in certain experiments indicates rapid thermal effects because amorphous silicon forms from rapid cooling of liquid silicon [45,46]. In the nanosecond timescale, where thermal melting occurs, melt expulsion by vapor pressure “pushes” molten material above the surface, leaving behind an amorphous ring [47]. This process was observed for the picosecond timescale as well when amorphous rings were seen to form around an ablated hole [46]. Ablation would occur by a homogenous nucleation of gas bubbles at the surface causing an explosion and expelling of material [48]. This would indicate that even though the laser beam is not directly heating the substrate, the ablation process can be explained using traditional thermal models.

Third, the mechanism may be delayed Auger recombination [49]. Here, heating of the substrate is a two step process, the first involving direct heating of the substrate by the laser pulse and the second by indirect heating from recombination effects [50]. During direct heating, photons from the laser are absorbed by the carriers in the semiconductor and are promoted to an excited state until all the free states are occupied. When this happens no more energy can be deposited. Since the electron relaxation timescale is in the order of 1-10 ps [51], the femtosecond

laser beam is off by the time most of the heating occurs in the substrate. Results show that the temperature of the lattice rises considerably on the picosecond timescale, far after the laser has been turned off. As the excited carrier fall back to equilibrium, the substrate is heated by phonons emitted either directly through recombination is on then or indirectly through the thermalization of carriers due to Auger recombination. The timescale of Auger recombination is in the order of several hundred picoseconds. In the fs regime, the Auger heating is dominant and can be described by the equation

A fourth model is of plasma annealing [52,53] which explains a change in structure via a non thermal annealing process. The rise in surface reflectivity observed in time-of-flight spectroscopy, which is usually the attributed to presence of a liquid phase, is instead interpreted as the result of an electron-hole plasma of sufficient density that exceeds the energy of the photons used to determine the reflectivity. The electron plasma then softens the covalent bonds in the lattice allowing for the rearranging of atoms into a crystalline state. Amorphization occurs when the electron loses its mobility before the material had a chance to establish long range order.

Much work has been done to identify the mechanism for ablation. Some work indicates a thermal effect. In some time-of-flight spectroscopy of GaAs, it has been observed that within a few hundred fs there is a rise in reflectivity in the center of the laser beam, indicating ultrafast electronic melting. After a few hundred picoseconds, the reflectivity of the entire spot increases. This timescale is significantly longer than the time needed for energy relaxation, indicating a thermal process by delayed Auger recombination. Once thermalization is complete, the material is molten and is then carried away by the hydrodynamic forces [54].

Some work indicates a combination of thermal and non thermal effects. Cavalleri et. al. describes five fluences regions where at the lowest fluences, delayed Auger recombination dominates. At higher fluences, melting occurs through ultrafast, non thermal effect. Above the ablation threshold, material is removed [55]. In metals, it has been shown that the energy not used in expelling material will induce a liquid phase leading to an amorphous or polycrystalline phase during solidification [51,56]. There has also been report on the oxidation of the ablated hole in addition to amorphization [57].

In this research, the ablation mechanism is a thermal effect. In this work, ablation is performed slightly above the single-shot ablation threshold, yet some heat effect zone and surface morphology can be seen, which can be attributed to a thermal process. A possible explanation of this phenomenon is that melt expulsion is occurring even in the femtosecond regime. This would indicate that electronic melting is occurring and that ablation happens by homogeneous nucleation of gas bubbles in the liquid phase [58].

2.5 THEORY FOR NS AND FS LASER ABLATION

During the interaction of low intensity short laser pulses with targets, the laser energy is absorbed by free electrons due to the inverse Bremsstrahlung [36]. Then the evolution of the absorbed laser energy involves thermalization within the electron subsystem, energy transfer to the lattice, and energy losses due to the electron heat transport into the target. If it is assumed that the thermalization within the electron subsystem is very fast and that the electron and the lattice subsystems can be characterized by their temperatures (T_e and T_i), the energy transport into the metal can be described by the following one-dimensional, two-temperature diffusion model [36]:

$$C_e \frac{\partial T_e}{\partial t} = -\frac{\partial Q(z)}{\partial z} - \gamma(T_e - T_i) + S \quad \text{Eq 2-1}$$

$$C_i \frac{\partial T_i}{\partial t} = \gamma(T_e - T_i) \quad \text{Eq 2-2}$$

$$Q(z) = -k_e \frac{\partial T_e}{\partial z}, \quad S = I(t)A\alpha \exp(-\alpha z) \quad \text{Eq 2-3}$$

Here z is the direction perpendicular to the target surface, $Q(z)$ is the heat flux, S is the laser heating source term, $I(t)$ is the laser intensity, A is laser absorptivity and α are the surface transmissivity and the material absorption coefficient, C_e and C_i are the heat capacities (per unit volume) of the electron and lattice subsystems, γ is the parameter characterizing the electron-lattice coupling, k_e is the electron thermal conductivity. In the above equations, a thermal conductivity in the lattice subsystem (phonon component) is neglected. The electronic heat capacity is much less than the lattice heat capacity and therefore electrons can be heated to very high transient temperatures. When the electron temperature (in units of energy) remains smaller than the Fermi energy, the electron heat capacity and the nonequilibrium electron thermal conductivity are given by $C_e = C_e' T_e$ (where C_e' is a constant) and $k_e = k_0(T_i) \cdot T_e/T_i$ where $k_0(T_i)$ is the conventional equilibrium thermal conductivity of a metal) [58].

Eq. 2-1, 2-2, 2-3 have three characteristic time scales τ_e , τ_i and τ_L where $\tau_e = C_e/\gamma$ is the electron cooling time, $\tau_i = C_i/\gamma$ is the lattice heating time ($\tau_e \ll \tau_i$) and τ_L is the duration of the laser pulse. These parameters define three different regimes of the laser-metal interaction which are called femtosecond, picosecond and nanosecond regimes.

2.5.1 NANOSECOND PULSES

This section discusses the ablation with nanosecond laser pulses when the condition $\tau_L \gg \tau_i$ is fulfilled. In this case the electron and lattice temperatures are equal $T_e = T_i = T$, and (2-1, 2-2, 2-3) reduce to

$$C_i \frac{\partial T}{\partial t} = \frac{\partial}{\partial z} \left(k_0 \frac{\partial T}{\partial z} \right) + I_a \alpha \exp(-\alpha z) \quad \text{Eq 2-4}$$

Laser heating of metal targets by long laser pulses has been a subject of many experimental and theoretical studies [35,36,59]. In this regime the absorbed laser energy first heats the target surface to the melting point and then to the vaporization temperature. Note that metals need much more energy to vaporize than to melt. During the interaction the main source of energy losses is the heat conduction into the solid target. The heat penetration depth is given by $l \sim (Dt)^{1/2}$ where D is the heat diffusion coefficient, $D = k_o/C_i$. Note that for long-pulse laser ablation of metal targets the condition $D\tau_L \alpha^2 \gg 1$ is usually fulfilled. The energy deposited inside the target per unit mass is given by $E \sim I_a t / \rho l$ where ρ is the density. When at a certain moment $t = t_{th}$, this energy becomes larger than the specific heat of evaporation Ω , significant evaporation occurs. From the condition $E_m \sim \Omega$, $t_{th} \sim D(\Omega\rho/l)^2$ is obtained. Thus, the condition for strong evaporation, $E_m > \Omega$ (or $\tau_L > t_{th}$), can be written as [36]

$$I > I_{th} \sim \frac{\rho \Omega D^{1/2}}{\tau_L^{1/2}}, \quad F > F_{th} \sim \rho \Omega D^{1/2} \tau_L^{1/2} \quad \text{Eq 2-5}$$

for laser intensity and fluence, respectively. The threshold laser fluence which is necessary for evaporation with long laser pulses grows as $\tau_L^{1/2}$. In case of ablation with long laser pulses there is enough time for the thermal wave to propagate into the target and to create a relatively large

layer of melted material. In this case the evaporation occurs from the liquid metal, which makes precise material processing of metal targets in vacuum with nanosecond pulses very complicated.

2.5.2 FEMTOSECOND PULSES

For femtosecond pulses, the laser pulsewidth is shorter than the electron cooling time, $\tau_L \ll \tau_e$. For $t \ll \tau_e$ which is equivalent to $C_e T_e / t \gg \gamma T_e$, the electron-lattice coupling can be neglected. In this case, Eq 2-1 can be easily solved. Since the general solution of this equation is quite complicated, the electron heat conduction term in the formulas is neglected. This can be done when the following condition is fulfilled $D_e \tau_L < \alpha^{-2}$, where $D_e = k_e / C_e$ is the electron thermal diffusivity. Hence Eq 2-1, reduces to [36]

$$C_e \frac{\partial T_e^2}{\partial t} = 2I_a \alpha \exp(-\alpha z), \quad \text{Eq 2-6}$$

and gives

$$T_e(t) = \left(T_0^2 + \frac{2I_a \alpha}{C_e} t \exp(-\alpha z) \right)^{1/2} \quad \text{Eq 2-7}$$

Here $I(t) = I_0$ is assumed constant, $I_a = I_0 A$, and $T_0 = T_e(0)$ is the initial temperature. At the end of the laser pulse the electron temperature is given by

$$T_e(\tau_L) \simeq \left(\frac{2F_a \alpha}{C_e} \right)^{1/2} \exp(-z/\delta) \quad \text{Eq 2-8}$$

where $T_e(\tau_L) \gg T_0$ is assumed, $F_a = I_a \tau_L$ is the absorbed laser fluence, and $\delta = 2/\alpha$ is the skin depth.

The evolution of the electron and lattice temperatures after the laser pulse is described by Eq. 2-1, 2-2 and 2-3, with $S = 0$. Initial conditions for the electron and lattice temperatures are given by Eq. 2-8 and $T_i = T_0$. After the laser pulse the electrons are rapidly cooled due to the

energy transfer to the lattice and heat conduction into the bulk. Since this electron cooling time is very short, Eq. 2-2 can be written as $T_i \approx T_e(\tau_L)t/\tau_i$ (here the initial lattice temperature is neglected). The attainable lattice temperature is determined by the average cooling time of the electrons $\tau_e^a = C_e T_e(\tau_L)/2\gamma$ and is given by

$$T_i \approx T_e^2(\tau_L) \frac{C_e}{2C_i} \approx \frac{F_a \alpha}{C_i} \exp(-\alpha z) \quad \text{Eq 2-9}$$

Note that the problem of the hot electron relaxation dynamics in metals after the excitation by a femtosecond laser pulse has been intensively studied during the last decade [60-61]. It has been shown that the time scale for the fast electron cooling and a considerable energy transfer to the lattice is of the order of 1 ps.

The significant evaporation occurs when $C_i T_i$ becomes larger than $\rho\Omega$, where ρ is the density and Ω is the specific (per unit mass) heat of evaporation. Using Eq. 2-9, the condition for strong evaporation can be written as

$$F_a \geq F_{th} \exp(\alpha z) \quad \text{Eq 2-10}$$

Where $F_{th} \approx \rho\Omega/\alpha$ is the threshold laser fluence for evaporation with femtosecond pulses. Then the ablation depth per pulse is given by,

$$L \approx \alpha^{-1} \ln(F_a/F_{th}) \quad \text{Eq 2-11}$$

The logarithmic dependence of the ablation depth on the laser pulse fluence is well known for the laser ablation of organic polymers. Recently the logarithmic dependence of the ablation depth per pulse has been demonstrated for metal targets with femtosecond KrF-laser pulses [62].

Due to the very short time scales involved in the ablation with femtosecond laser pulses the ablation process can be considered as a direct solid-vapor (or solidplasma) transition. In this case the lattice is heated on a picosecond time scale which results in the creation of vapor and plasma phases followed by a rapid expansion in vacuum. During all these processes thermal conduction into the target can be neglected in a first approximation. These advantages of femtosecond laser pulses allow very precise and pure laser-processing of silicon which is experimentally demonstrated in chapter 4,5 and 6.

2.6 SUMMARY

Thorough knowledge of the fundamental physics governing laser matter interaction is important for efficient use of lasers for precise material processing. The complicated physical process of laser-matter interaction involves variety of different phenomena. The ablation mechanism is dependent on the properties of the sample material along with the laser pulsewidth. For the nanosecond regime the primary mechanism for material removal is through the phase explosion of the metastable liquid. For this regime the ablation process is identified as a thermal process creating heat affected zone, melt redeposition, cracks and shock waves. On the contrary, in the femtosecond regime the primary ablation occurs via a direct solid-vapor transition. The heat diffusion into the target is negligible, which results in much localized ablation and precise machining of the sample without thermal damage to the surroundings. The significant difference between femtosecond and nanosecond laser-matter interaction in terms of transferring laser energy into thermal energy of the target is that electrons and ions are not in equilibrium during the laser pulse in the femtosecond laser ablation case. This is because the electron-ion relaxation

time, which is in the range of a few picoseconds to a few tens of picoseconds, and is much longer than the sub-picosecond pulse length.

CHAPTER 3

EXPERIMENTAL DETAILS AND PARAMETERS

3.1 INTRODUCTION

Selection of laser system and understanding of the laser parameters are most essential for the dicing operation. In this chapter, an overview of the laser system selected for this study is provided. In the first part of the chapter, the experimental setup used for this study is discussed and in the later part, some of the important parameters considered for the laser ablation are explained. These experiments were conducted using a high power high repetition rate femtosecond laser in the Micro and Nano Fabrication research lab at Ryerson University, Toronto, Canada.

3.2 EXPERIMENTAL SETUP

Figure 3-1 shows a schematic drawing of the dicing machine configuration. A Clark-MXR IMPULSE™, an all-diode-pumped, direct-diode-pumped Yb-doped fiber amplified system, capable of producing variable pulse energies up to 10 μ J, is used for this research. Repetition rates can be varied between 200 kHz and 25 MHz. This is more than an order-of-magnitude higher than that of traditionally available one-box ultrashort pulse laser system. The laser system used is capable of producing an output power of 20 W for a repetition rate > 2 MHz and has a fundamental central wavelength of 1030 nm.

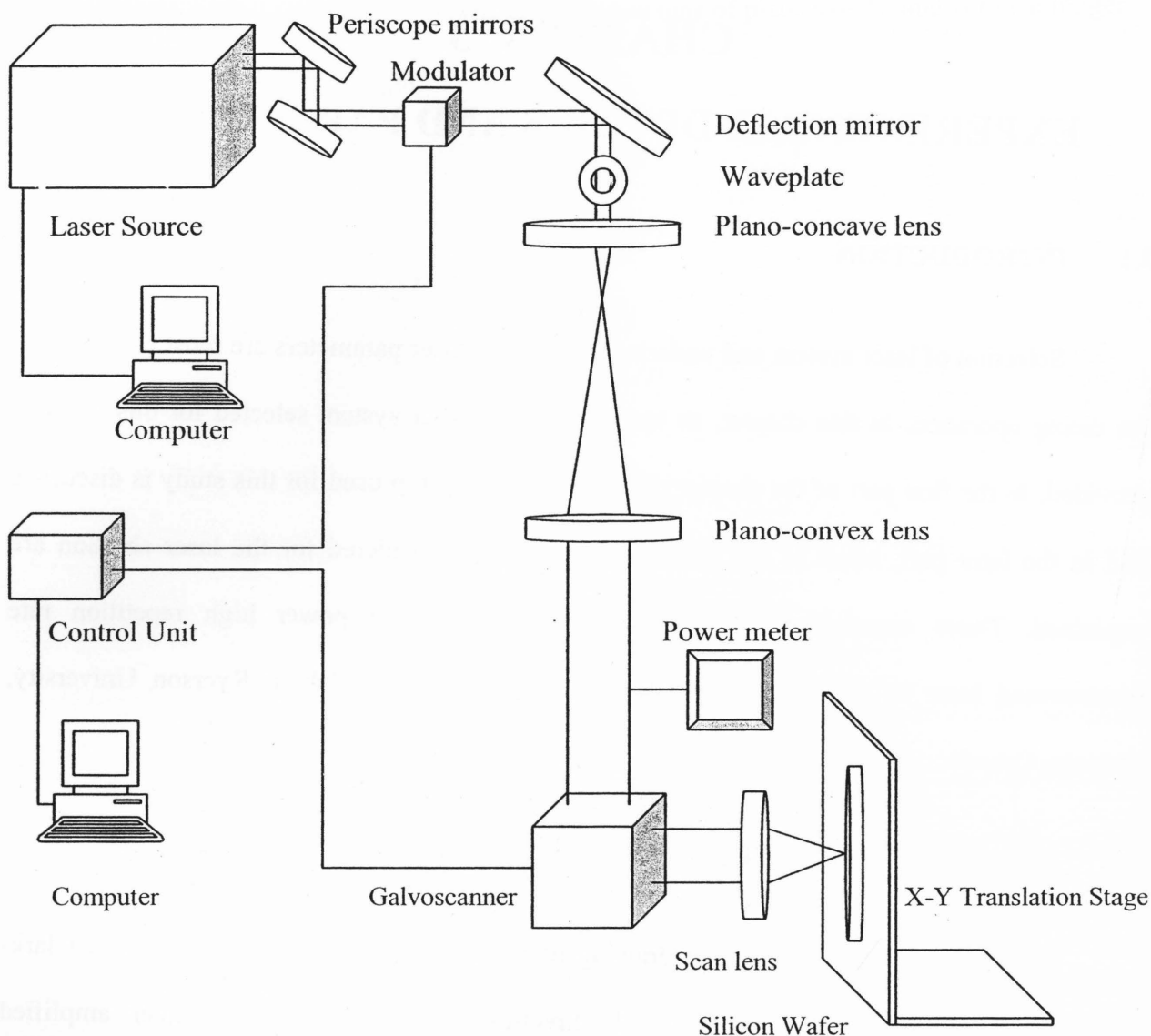


Figure 3-1: Experimental Setup

The collimated output beam from the laser measured approximately 3 mm in diameter. The laser beam before coming out of the system passes through an internal shutter, operating at a very high frequency. The beam then passes through periscope mirrors to bring the laser beam down to a workable height. Polarization of the laser beam has a significant effect on the cutting speed and kerf width, especially when multiple passes are used for cutting [63]. Optical waveplates, more commonly known as waveplates or retardation plates, are transparent plates used for manipulating the polarization of the laser beam. In the current study, the linear

polarization of the output beam from the laser was changed to circular. Circular polarization was maintained throughout the experiment to obtain optimum cutting quality, using a quarter waveplate. Importance of the laser polarization for the current study is discussed in more detail section 3.3.3. The beam was then expanded to 6 mm using a combination of plano-convex and plano-concave lenses with focal length of 100 mm and 200 mm respectively. The expanded beam then passes through a galvo-scanner. The galvo-scanner steers the laser beam across the sample surface in both X and Y axis. An electronic driver that is controlled by a personal computer will control the movements of the galvo-scanner. Galvo-scanners are preferred to a translation stage because of its high scanning speed, which in the current study is 3000 mm s^{-1} . Such higher speed is difficult to achieve, using a mechanical translation stage. In addition, irregular shaped dies can be easily cutout, by programming the laser beam contour using CAD software, which is one of the other advantages of using a galvo-scanner for micromachining. A scan lens with effective focal length of 63.5 mm, was used to focus the laser beam, normal to the work surface. Samples used in this study were P type Boron doped silicon wafer of 50mm diameter, back grinded to 250 μm thickness with orientation of $\langle 100 \rangle$. The silicon wafer was mounted on a vacuum chuck secured by a two-axis translation stage.

Pulsewidth was altered between 214 fs and 3.5 ps by changing the compressor grating position and calibrated using an autocorrelator. The range of pulsewidth selected for the study is limited by the range availability of the laser system. The average power is measured using a calibrated power meter. For each of the pulsewidth selected, repetition rates were changed from 2 MHz to 13 MHz while keeping the ratio of scan speed and number of cycles constant. Number of cycles (N) here means the number of times a beam is scanned at a predetermined speed (S_{scan}) over a particular area. The cutting speed can be obtained by using the equation below

$$S_{cut} = S_{scan} / N$$

Eq 3-1

where S_{scan} is the scan speed and N is the number of passes or cycles. Set of experiments were performed such that the cutting speed remained constant throughout the study. At each of the repetition rates, dice were cut with the ratio of scan speed and the number of cycles as 1000 mm s^{-1} to 25 cycles, 2000 mm s^{-1} to 50 cycles & 3000 mm s^{-1} to 75 cycles, hence resulting in a constant cutting speed (ratio of scan speed to number of cycles or cycles) of 40 mm s^{-1} throughout the study. The total energy deposited (number of effective pulses at center of groove (N_{eff}) x laser fluence (ϕ)) into the substrate at a given repetition rate and a scan speed remained same for each pulsewidth and hence facilitated a meaningful comparison between experiments conducted for different pulsewidth. The machined samples were then examined under a scanning electron microscope (SEM) to evaluate the kerf width, depth of cut and quality of cut in terms of sidewalls, back side chipping and die strength.

All experiments were carried out in ambient atmosphere. Most of results that can be obtained in air can be further improved by using different mediums like vacuum and assist gas. However the associated cost and set up requirement add up to further complexity to the assembly line setups in the industry. Keeping this in mind, all the experiments were conducted in air, such that the changes required on the production line could be kept to minimum.

3.3 PARAMETERS

For the generation of microscopic cuts and grooves, several basic parameters are mainly responsible for the achievable resolutions, processing speed and quality. These include laser fluence, spot size, cutting speed and spot overlap of laser pulses. Moreover, when generating kerfs with high aspect ratios or cutting through the substrate, the beam polarization has a visible

influence on the quality. These parameters and other aspects pertaining to the experiments performed will be discussed in detail in the subsequent sections.

3.3.1 SPOT SIZE

The spot size, also known as the beam waist, is the minimum diameter of the Gaussian beam travelling in a free space. Figure 3-2 shows a schematic diagram of the laser spot size and depth of focus for converging laser beam using a convex lens.

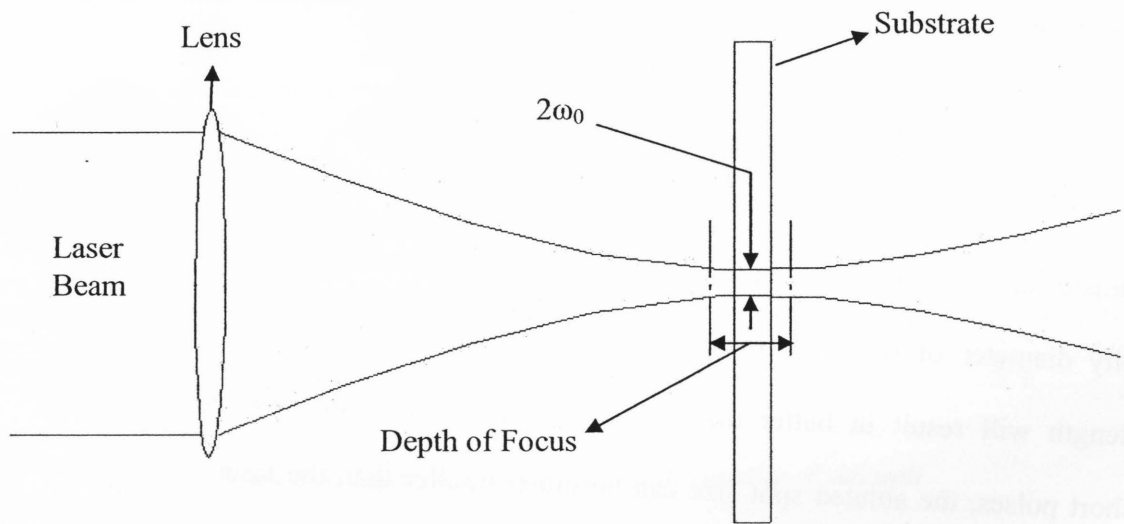


Figure 3-2: Laser spot size and depth of focus for converging laser beam using a convex lens

In order to find the size of the focused beam spot, a single spot can be machined on a thin metal film, with pulse energy well above the material threshold. The size of the machined spot, measured using a Scanning Electron Microscope (SEM), gives the size of the focused beam spot. However, theoretically, the spot size value of the tightly focused laser beam can be calculated using Eq 3-2 [64],

$$2\omega_0 \approx 1.27 \lambda_0 f_l / D$$

Eq 3-2

where λ_0 is the wavelength of the laser beam (1030 nm), f_l is the effective focal length of the scan lens (63.5 mm) and D is the diameter of the laser beam at the input of the galvo-scanner (6mm). The spot diameter was calculated as 13.64 μ m. During the experiment the spot size may be bigger due to scatter and misalignment. Generally, smaller spot size results in higher laser fluency, which in turn decreases the dicing speed. On the other hand kerf, width decreases as the laser spot size reduces [65]. With a thick substrate, the narrow kerf may cause difficulty for the molten silicon to eject from the bottom of the opening. The trapped molten material deposits in the ablated cavity and has to be removed using subsequent scanning cycles and therefore might result in a decrease in dicing speed.

X.Liu and group (1997) conducted a detailed study of the ultrafast lasers ablation mechanism and concluded that since the smallest diffraction-limited focus spot (given as the intensity diameter of the laser focus spot) is proportional to the laser wavelength, smaller wavelength will result in better machining resolution [42]. They also concluded that with ultrashort pulses, the ablated spot size can be much smaller than the laser focus spot size, and therefore the micromachined spot size is no longer limited by the smallest focus spot size given by the wavelength. The machined feature size, the size of the transition layer between machined part and unaffected substrate, can be even smaller.

3.3.2 SPOT OVERLAP

Spot overlap is an important factor for pulsed laser cutting using a more than one number of scan cycles. Figure 3-3 (a) depicts a situation where a certain spot overlap is inadequate to achieve a complete through cut in the material since bridges of uncut material remain. Complete cutting is only possible by increasing the extent of spot overlap. Figure 3-4(b) depicts a situation

with a wafer completely cut but the obtained sidewall quality would be wavy and further processing would be need to removed the curvy edge. Figure 3-3 (c) shows a relatively smooth and clean through cut which is desirable. This kind of sidewall surface can be obtained by two ways: first by slowing down the scan speed hence creating a high overlap ratio and secondly by using high repetition rate.

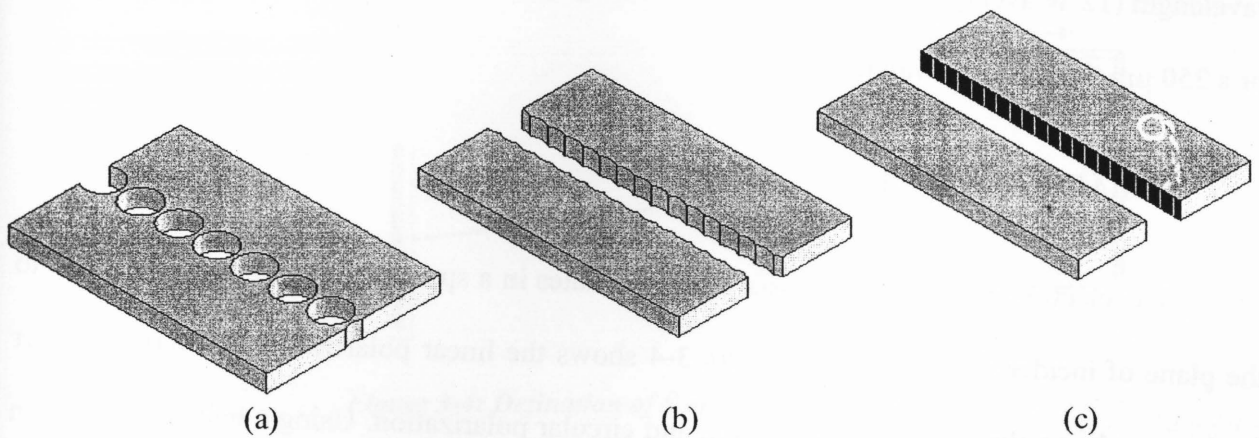


Figure 3-3: Effect of spot overlap on the quality of sidewall

Spot overlap depends on two parameters scanning speed of the laser beam and the repetition rate of the laser system. The optimal scanning speed depends on the laser spot size at the focal point and the repetition rate of the laser beam such that there is overlap of the successive laser pulse for scanning. Higher repetition rate results in more than one number of pulses to be incident on groove center. The effective number of laser pulse incidents on the centre of the groove, N_{eff} is given by [66]

$$N_{eff} = \sqrt{\frac{\pi}{2} \frac{\omega_0 f}{v}} \quad \text{Eq 3-3}$$

where f is the repetition rate of the system, ω_0 is the focused beam diameter and v is the scanning speed. The Eq. 3-3 shows that the number of pulses N_{eff} increases with the increase in beam diameter and repetition rate. But for an optimal cutting speed the repetition rate of the laser system and the laser beam diameter should be optimized depending on the ablation threshold of the material and the thickness of the substrate. In this study, the scanning speed was optimized at 3000 mm s^{-1} , at which it gave the highest overall cutting speed for die singulation at 1030 nm wavelength (12 W average power). The overall cutting speed obtained at 1030 nm was 40 mm s^{-1} for a $250 \text{ }\mu\text{m}$ thick silicon wafer.

3.3.3 POLARIZATION

The electronic vector of the laser beam oscillates in a specific direction with reference to the plane of incidence of the beam. Figure 3-4 shows the linear polarization states of the laser beam, namely s polarization, p polarization and circular polarization. Using a half-wave plate in front of the focusing lens, the polarization state of the beam can be converted to s from p and visa versa. These types of s or p polarization are also known as linear polarization. In order to get a circular polarization the half wave plate can be replaced by quarter waver plate placed 45° to the plane of incidence of the beam.

The influence of the orientation of the polarization on machining efficiency and feature shape has been well studied for the laser micromachining applications [65,67,68]. Due to the different reflectivity at different incident angles, a linearly polarized laser spot has a higher intensity at the bottom of the cut in the direction perpendicular to the polarization.

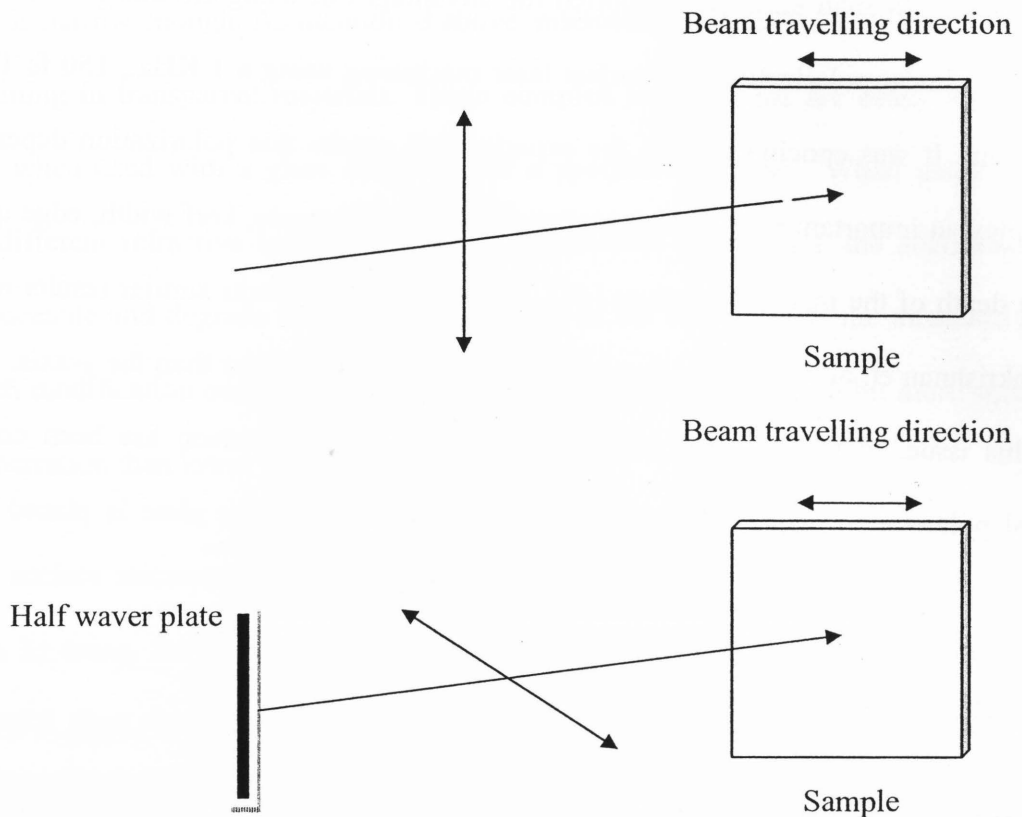


Figure 3-4: Defination of S and P polarization

The uneven intensity distribution of the laser spot will result in kerf-width variation when the laser spot cuts in various directions [63]. Figure 3-5 shows the cutting lanes in x and y axis.

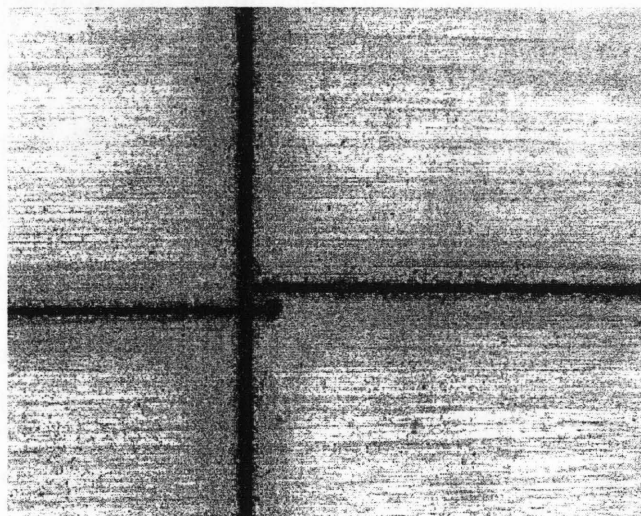


Figure 3-5: Unequal kerf widths in X and Y axis with a linearly polarized beam [63]

Venakatakrisnan et. al [63] reported the advantages of using circular polarization when compared to linear polarization in ultrafast laser machining using a 1 KHz., 150 fs Ti-sapphire laser system. It was concluded from the experimental results that polarization dependent hole pattern play an important role in determining the laser cutting rate, kerf width, edge quality and ablation depth of the machined feature [63]. Figure 3-5 also reflects similar results reported by Venkatakrisnan et. al, and shows that lane in x-axis is visibly wider than the y-axis. In order to avoid this issue, in this research experiments, the linear polarization has been converted to elliptical polarization, using a quarter wave plate. A quarter wave plate is placed before the focusing lens and is tuned to obtain equal kerf widths on both axis.

3.3.4 FOCUSING AND ABERRATION

When dealing with a focused femtosecond laser beam, one must consider two issues that can arise: self-focusing and aberrations. Self-focusing is a process by which the spatial variation in intensity across a laser beam leads to a spatial variation in the refractive index, which acts as a lens and causes the beam to focus itself. This process leads to a more intense laser beam and can cause catastrophic collateral damage when micromachining precise structures. Fortunately, there are ways to minimize self-focusing when micromachining with femtosecond laser pulses. By keeping the peak power below the threshold for self-focusing, while keeping the intensity above the threshold for damage, one can ensure precise micromachining. This is done by using high numerical aperture (NA) focusing optics.

Aberrations arise as distortions to the laser beam at or near the focus and are a result of the focusing process. Spherical and chromatic aberrations are two types that should be considered for micromachining, though chromatic aberrations may be neglected if the bandwidth

of the laser is narrow enough. As mentioned above, microscope objectives are typically used for micromachining in transparent materials. These complex lens systems are often corrected for aberrations when used with a glass cover slip of a specific thickness. When using different materials (different refractive index) or different thicknesses of material, the aberrations may become noticeable and degrade the focus. The change in the focus affects the threshold energy above which modification occurs. Higher numerical aperture objectives exhibit more significant spherical aberration than lower NA objectives.

For surface micromachining, focusing should be aberration free to achieve the finest feature size, by using, for example, a microscope objective lens that is designed to form a sharp focus without a glass coverslip. Only when using very high pulse energies does self-focusing in the air in front of the sample become a problem. Such high-energy machining is usually associated with the use of projection masks to ablate a large, patterned area at once, rather than with the point-scanning systems discussed here. The self-focusing can be avoided by placing the sample in a vacuum chamber.

3.3.5 PULSEWIDTH AND DISPERSION

Micromachining of silicon is an intensity dependent process. Ablation will only start when pulses, above the intensity threshold, are incident on the substrate surface. The laser intensity, as mentioned earlier in the section 3.3.5, is inversely proportional to pulsewidth. Pulsewidth is limited by the spectral width of a laser pulse, with a wider spectrum, implying, a shorter attainable pulsewidth. Dispersion is a process whereby different frequencies of light travel at different speeds inside of a material. Dispersion separates frequency components of a femtosecond pulse temporally, therefore increasing the pulsewidth. When using multi-element

focusing optics such as a microscope objective large amounts of dispersion can be induced. Because the pulsewidth is lengthened by this dispersion, there is a risk that the threshold intensity cannot be reached at the focus, and microstructures will not be created. In order to avoid this, measures must be taken to compensate dispersion. A micromachining setup may include a compression scheme whereby the pulses can be pre-chirped to compensate for the dispersion induced by the focusing lens and other optics to ensure that dispersion does not affect the laser writing process.

3.4 SUMMARY

In using short laser pulses as an alternative for silicon micromachining, laser parameters including wavelength, pulse length, pulse intensity and beam shape must be optimized to satisfy the requirements of specific tasks and to maximize the efficiency of laser power usage. Among other parameters of laser light-matter interaction, removal rate is an important performance factor that determines whether laser machining is appropriate for silicon processing for certain specific applications. Different multiple physical processes dominate under different laser operating conditions and at different ablation stages. Through estimating the impact of each physical process, the laser parameters that affect the removal speed, degree of debris, mechanical properties, aspect ratio and other quality factors can be determined.

Table 2 and Table 3 show the laser and dicing parameters analyzed and evaluated in this study.

Laser Parameters		Effect
Power Output	(20 W)	Throughput
Wavelength	(1030nm)	Feature size
Beam polarity	(circular)	Feature shape & size
Pulse energy	(1μJ-7μJ)	Quality, throuput
Pulsewidth	(214 fs-3.5 ps)	Size of Heat Affected Zone
Repetition rate	(2MHz-13MHz)	Quality, throughput
Spot Diameter	(10 μm -13.5)	Feature size

Table 2: Laser parameters

Dicing Parameters		Effect
Kerfwidth (Minimize)		More dies per wafer, Mfg. cost
Depth of cut (Maximize)		Throughput
Scanning speed (Maximize)		Throughput
Debris & contamination(Minimize)		Die strength, Reliability
Surface roughness (Minimize)		Die strength, Post processing cost
Die strength (Maximize)		Reliability

Table 3: Dicing parameters

CHAPTER 4

EFFECT OF PULSEWIDTH

4.1 INTRODUCTION

Ablation threshold fluence is the fluence needed to initiate the removal of material as a consequence of removing a few angstroms from the surface during vaporization or can be simply defined as the point at which absorbed laser energy is sufficient to break the bonds between molecules of a material. Laser ablation occurs when the laser fluence exceeds a certain threshold value, typical of a given condensed matter, which could also depend on the laser parameters like pulsewidth. Ablation threshold is hence seen as an important parameter for understanding the physical mechanism underlying laser ablation at various pulsewidths.

A significant amount of research in pulsed laser ablation and laser processing of material has been done employing pulses from nanosecond to femtosecond time regime. The mechanisms responsible for material ejection are strongly dependent on the physical properties of the solid, the laser fluence and in particular the pulsewidth or pulsewidth [69-72]. Laser pulse absorption and the associated thermal energy transport in materials have been studied through computer modeling of heat conduction process with appropriate source and sink terms applicable to the system [40,73,74]. Pronko et. al. reported experimental data and theoretical results of a systematic computer simulation study done from femtosecond to the nanosecond regime, as an assessment of the problems and benefits associated with various laser pulsewidths and their use in processing optically absorbing media [35]. B.N.Chichkov and group (1996) were among the first groups to experimentally demonstrate the advantages of femtosecond lasers for precise

material processing, using a Ti-Sapphire laser for pulsewidth ranging from 0.2 - 5000 ps [75]. B.K.A.Ngoi et al. (2001) studied laser induced damage thresholds in micromachining of silicon using 300 fs pulsewidth and 1KHz repetition rate system [76]. A.Yokotani (2002) and group investigated the influence of laser conditions such as pulsewidth and fluence on the cutting depth and diameter in order to develop a new photo-dicing technique for very thin ICs. In their experimental results, conducted using a Ti-Sapphire laser with repetition rate of 10 Hz and pulsewidth of 100-500 fs, no dependence of kerf width on pulsewidth was found for the range of pulsewidth selected [69]. J. Bonse and group (2001) investigated laser induced modification threshold and ablation of silicon surfaces with laser pulsewidths in the range between 5 fs and 400 fs. With respect to the feasibility of using femtosecond pulses for microstructuring, they reported that a reduction of the pulsewidth below 500 fs does not offer significant advantages, because of the nearly constant ablation threshold fluence [38]. Chen and Gupta (2005) conducted a systematic study of the influence of the laser pulsewidth in femto to picosecond time regimes on laser micromachining of silicon and stainless steel to determine an optimum pulsewidth for material processing. They used a 1 KHz, Ti-sapphire laser system and suggested pulsewidth of 5 ps for melt free ablation of silicon and 2.5 ps for stainless steel [77]. A study of comparison of femtosecond versus picosecond laser ablation was conducted by Ostendorf and group (2005) using a 12 ps, 50 KHz. and 130 fs, 1 KHz. Laser system [78]. In the study, they concluded that high repetition rate picosecond laser produce a higher thermal loading and hence for drilling microholes femtosecond laser was a better choice. However, they suggested, use of high repetition rate picosecond laser for the producing high quality cuts in metals and other heat conducting materials. Harzic and group (2005), compared ablation with low and high energy densities for steel, Cu and Al with ultrashort pulses, using a 80 MHz femtosecond laser system

and found femtosecond laser offers advantages over longer pulse lasers. They also concluded that the loss of ablation efficiency is associated with the low fluence regime of femtosecond ablation could be compensated by using a higher repetition rate femtosecond lasers, which were not commercially available then [79]. In the study conducted by Fujita and group (2007), irradiation of the femtosecond laser pulses induced amorphization in crystalline silicon, which lead to the increase in the laser absorption and hence decrease in ablation threshold [80]. An investigation of silicon melting, under femtosecond laser irradiation, was presented by Korfiatis and group (2007). This study revealed the dependence of fluence thresholds on wavelength and pulsewidth, and found that the threshold increases with the pulsewidth following a power law [81].

Despite intensive investigations and considerable progress achieved over the last decade, the mechanisms of ultrashort laser ablation are still an issue of much debate. The dependence of the ablation threshold on pulsewidth and the effect of the mega hertz high repetition rate and high power on the substrate have been never investigated due to the non availability of a laser system with such capabilities.

In this study, the influence of the pulsewidth on ablation threshold, kerf width, ablation depth, fluence and debris were analyzed. Pulsewidth for this study ranged from 214 fs to 3.5 ps. The observations of the experimental results have been presented with an emphasis on the dependence of ablation threshold, kerf width, ablation depth and debris on pulsewidth.

4.2 EFFECT OF PULSEWIDTH ON ABLATION THRESHOLD FLUENCE

In femtosecond laser ablation, feature size is determined by the maximum laser fluence, ϕ_0 , which must exceed a certain threshold value to cause an irreversible change on the surface. This modification threshold fluence, ϕ_{th} , depends essentially on the material and number of laser pulses, applied at each scanning point. For laser pulses with Gaussian intensity profile, the feature size obtained is related to the maximum laser fluence ϕ_0 on the sample surface by [82]

$$D^2 = 2\omega_0^2 \ln \sqrt{\frac{\phi_0}{\phi_{th}}} \quad Eq\ 4-1$$

where ω_0 is the beam radius, ϕ_0 is maximum laser fluence and ϕ_{th} is threshold fluence. The maximum laser fluence is related to the measured pulse energy E_{pulse} by [83]

$$\phi_0 = \frac{2E_{pulse}}{\pi\omega_0^2} \quad Eq\ 4-2$$

In order to find the threshold fluence of the silicon wafer used in the study, circular pits were machined at different pulse energies, using a circularly polarized laser beam. According to Eq.4-1, the threshold fluence ϕ_{th} , is the laser fluence ϕ_0 at which the diameter of the ablated pit equals to zero. Hence, threshold fluence can be determined from the plot of squared diameter, D^2 , of the circular pit versus the laser fluence, ϕ_0 , by extrapolation of the fits to $D^2=0$.

This procedure yields thresholds close to, or slightly higher than, that for vaporization. By extrapolating to zero emission, it is being assured that the energy obtained will be closer to the actual threshold value for vapourization. Number of results have been reported for the measurement of ablation threshold fluence by extrapolating the linear fit of the plot of the squared diameter against the maximum fluence, to $D^2=0$ [84,85]. However for this study the

ablation threshold fluence values were calculated from minimum power required to start the ablation process. For each combination of pulsewidth and repetition rate, power was recorded for the point at which ablation started. Ablation threshold fluence was calculated from the minimum pulse energy required to start ablation at the particular combination of pulsewidth and repetition rate. These threshold fluence values are plotted against pulsewidth, as shown in Figure 4-1.

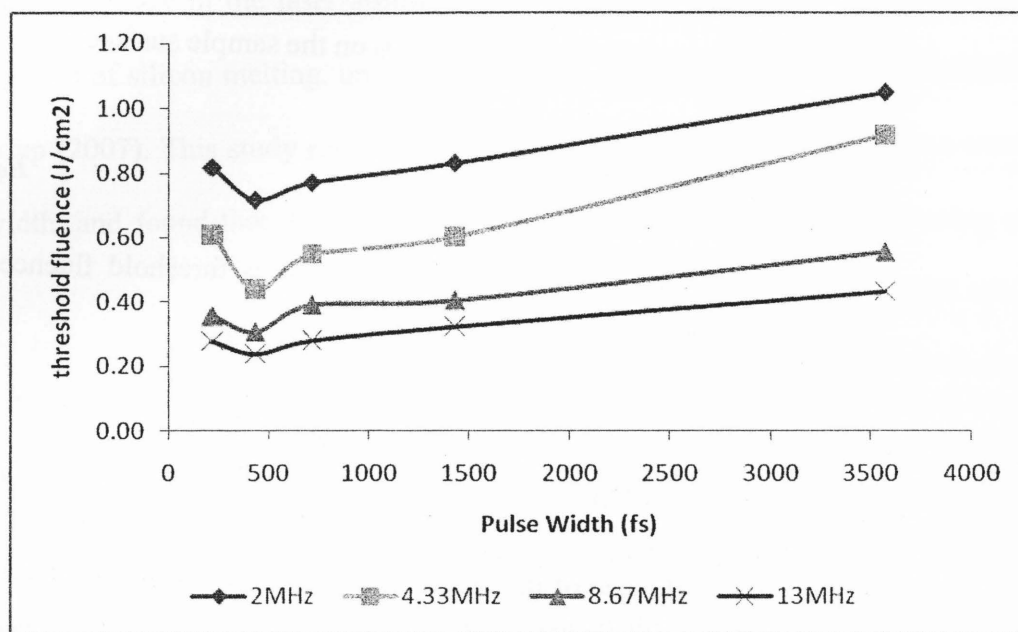


Figure 4-1: Influence of pulsewidth on threshold fluence at repetition rate of 2 - 13 MHz

Dependence of ablation threshold fluence on the pulsewidth can be clearly observed from the plot of threshold fluence and pulsewidth. The threshold fluence is found to increase with the increase in the pulsewidth from 429 fs to 3.5 ps. This trend of increase in threshold fluence can be associated with the thermal diffusion of the input pulse energy. The longer the pulsewidth the more time is available for the heat to diffuse into the bulk before the vaporization stage is achieved. However, the rate of increase observed in the current study seems to be considerable small and hence threshold can be considered nearly constant except for 429 fs pulsewidth where, a slight dip in the measurement is observed for all the repetition rates. This can be explained by

the thermo-physical effects occurring in this range of pulsewidth which include the finite velocity of the vapor front relative to the underlying material as well as the structure of thermal gradients at the surface where vapor is supported and deeper in the material where the bulk diffusion occurs [35]. The thermal gradient in the bulk and on surface will increase with the decrease in the pulsewidth. The finite velocity of the vapor front determines the relaxation of the near surface gradient while the bulk diffusion determines the temperature profile in the bulk of the material. These two gradients together determine the amount of energy lost to the vaporization of material and to the bulk. Increase in the amount of energy drawn into the bulk will result in increase of the threshold values. Decrease in pulsewidth results in commensurate changes in the fraction of the pulse energy that is distributed among the solid, liquid and vapor phases, as the incoming pulse goes through the entire process of absorption. For the pulsewidth less than of 429 fs the energy that might otherwise be lost to the plasma, is being absorbed and stored by the material in a superheated state at the surface. This would result in the increase in the maximum surface temperature at the threshold for ablation. Hence it can be said that the change in trend of threshold fluence, with decrease in pulse, from decreasing to increasing, is due to complex thermodynamic processes associated with the vapor front and the bulk temperatures. Depending upon the amount of energy being absorbed in the bulk or that being extracted by the vapor front, the pulsewidth and the internal bulk temperature profile determines the threshold fluence.

4.3 INFLUENCE OF PULSEWIDTH ON KERF WIDTH

Kerf width is an important criterion for the evaluation of various dicing techniques. A decrease in the kerf width can significantly increase the dice density, which in turn reduces

manufacturing cost. Here, the influence of pulsewidth on kerf width is investigated. To determine the effect of the pulsewidth and the repetition rate, on the thin silicon wafer, experiments were performed by varying the scan speed and the number of cycles such that the total pulse energy delivered to the sample, remained constant for a given repetition rate. These experiments were repeated for pulsewidth ranging from 214 fs to 3.5 ps.

Figure 4-2 shows the SEM images of the grooves cut at a repetition rate of 2 MHz and a scan speed of 3000 mm s^{-1} . Kerf width was measured from the SEM images at three different points long the cut and an average of the values were taken. These values came out to be within 2 % variation and were plotted against the pulsewidth as shown in Figure 4-3.

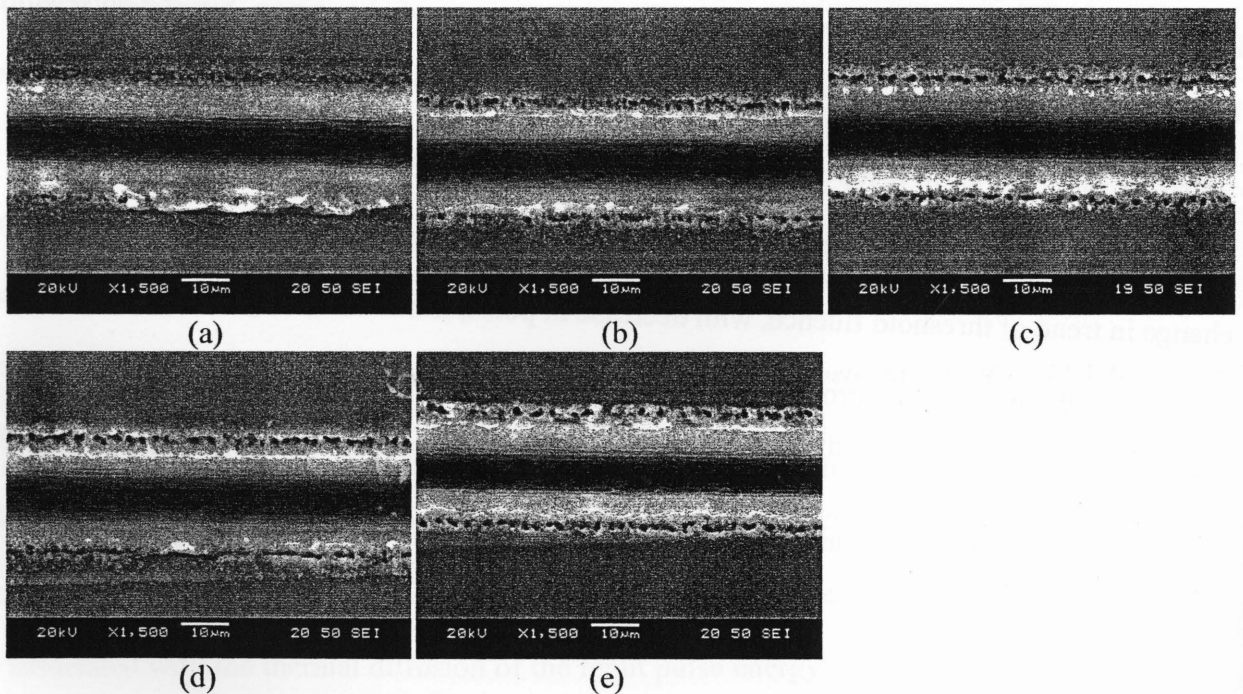


Figure 4-2: Kerf width cut at repetition rate of 2 MHz at scan speed of 3000 mm/s at pulsewidth of (a) 214 fs, (b) 429 fs, (c) 714 fs, (d) 1429 fs and (e) 3571 fs

The results show that the kerf width in general show an overall trend of increase in kerf width with increase in pulsewidth for all the repetition rates studied, except for the decrease in

the kerf width measure at 429 fs. This could be a directly related to the value of the lower ablation threshold fluence measured at this point as explained in section 3.1.

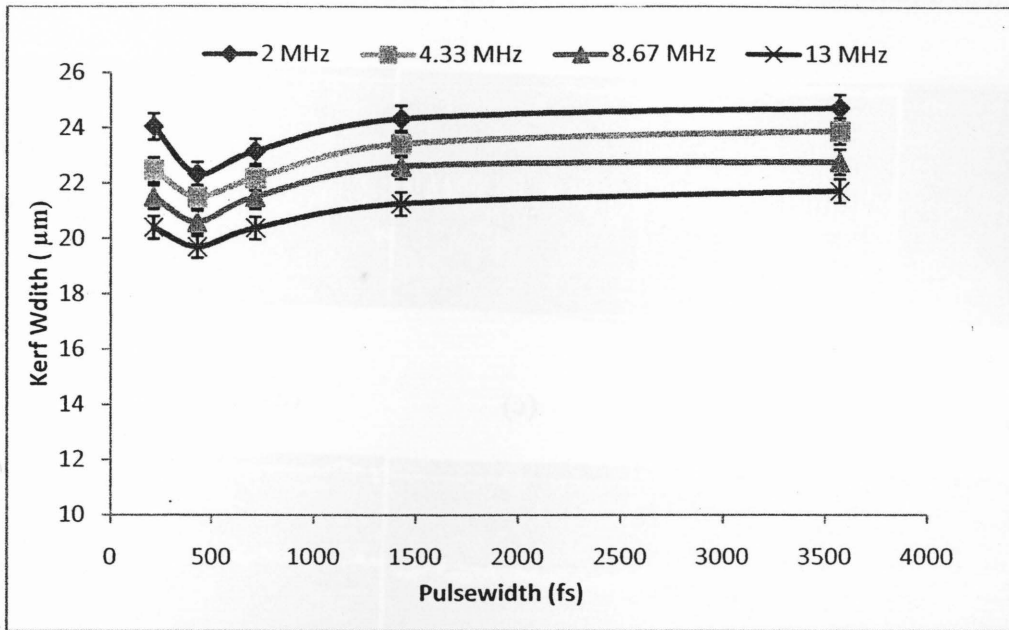


Figure 4-3: Influence of pulsewidth on kerf width at repetition rates of 2–13 MHz

It is known that with decrease in the pulsewidth, peak laser intensity increases for the same pulse energy and hence a reduction in the feature size is achieved. However in this study the kerf is observed to stay nearly the same throughout the range of pulsewidth for all the repetition rates studied. This could be due to the extra amount of energy being deposited by extra number of cycles than needed for the shorter pulsewidth, which leads to increase in the kerf width. These observations agree well with the previous studies [77,79,86].

4.4 EFFECT OF PULSEWIDTH ON ABLATION DEPTH

Grooves were cut into the Si substrate at different pulsewidth ranging from 214 fs to 3.5 ps. Fluence was used to make a comparison between different pulsewidths. At pulsewidth of 214 fs grooves were cut at scan speed of 1000 mm s^{-1} (25 cycles), 2000 mm s^{-1} (50 cycles) and 3000

mm s⁻¹ (75 cycles) at repetition rates from 2 MHz to 13 MHz. These set of experiments were repeated for pulsewidth ranging from 429 fs to 3.5 ps. Depth of cut were measured using a SEM and recorded as a function of pulsewidth as shown in Figure 4-4.

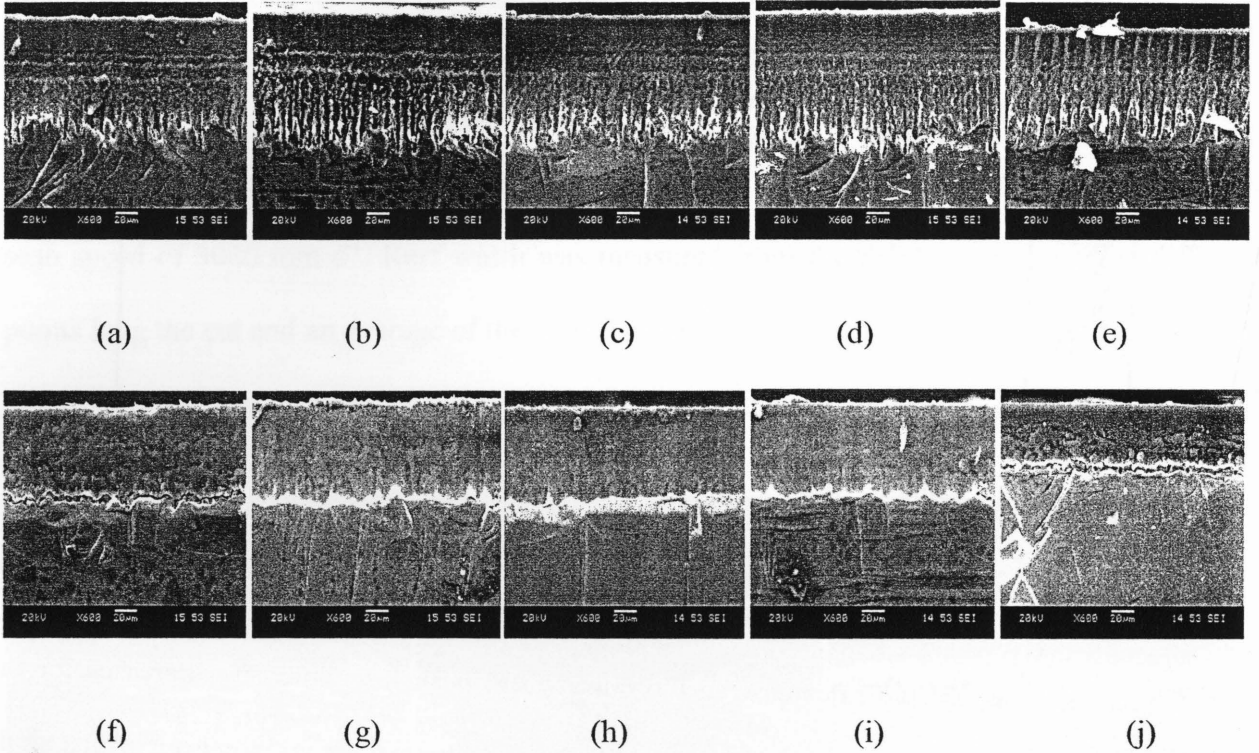


Figure 4-4: Ablation depth cut at repetition rate of 2 MHz and scan speed of 3000 mm/s at pulsewidth of (a)214 fs, (b)429 fs, (c)714 fs, (d)1429 fs and (e) 3571fs and for repetition rate of 13 MHz at scan speed of 3000 mm/s at pulsewidth of (f)214 fs, (g)429 fs, (h)714 fs, (i)1429 fs and (j) 3571fs

An approximate change in depth of cut of about 17-25µm is observed when the pulsewidth was changed from 214 fs to 3.5 ps when repetition rate was varied from 2 to 13 MHz. The depth obtained is the highest at pulse width of 214 fs, repetition rate of 2 MHz and a scan speed of 1000 mm s⁻¹. It can be observed that for the same repetition rate and total deposited energy, the depth of cut reduces with the increase of pulsewidth. This can be explained with respect to the laser intensity and pulse energy. For a pulsed laser system, with the increase in pulsewidth, the laser peak intensity decreases, hence, resulting in a reduction of the depth of cut. Moreover, at a given pulsewidth, the depth obtained is higher for the lower repetition rate. This

can be attributed to the higher pulse energy at lower repetition rate for a constant laser power. With increase in the repetition rate for a constant power, the pulse energy decreases and hence results in a reduction in the ablation depth. This can be observed from Figure 4-5.

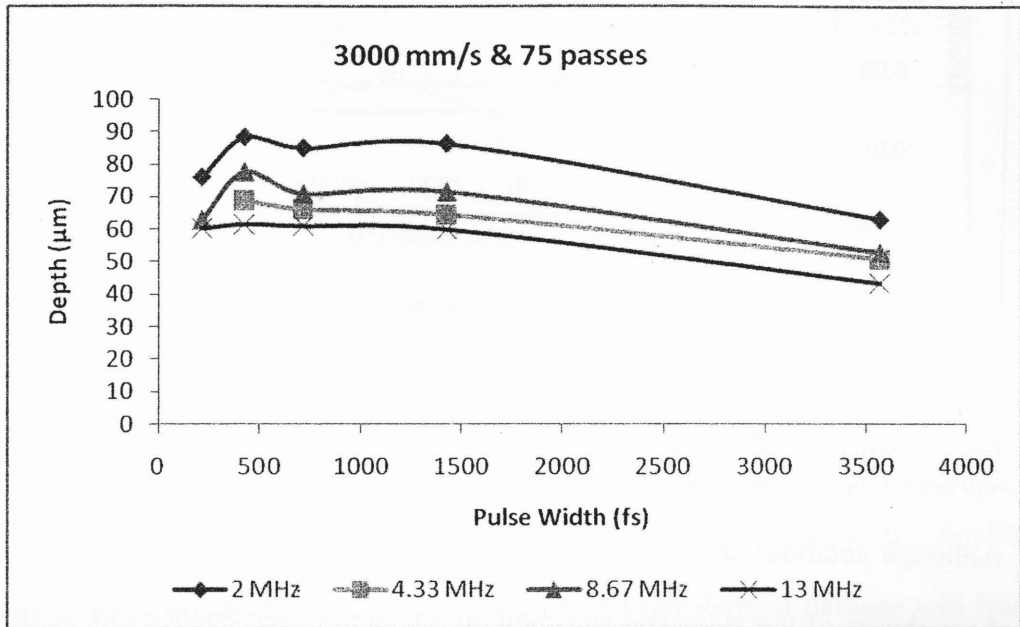


Figure 4-5: Influence of pulsewidth on Ablation depth at different repetition rate (2MHz – 13 MHz) having the same total energy deposited (30.34 J cm⁻², number of pulses x laser fluence)

Ablation rate was calculated from the total depth of cut and the effective number of pulses delivered on a spot at a given repetition rate and scan speed. Figure 4-6 shows the plot of ablation rate against the pulsewidth. A decrease in ablation rate was observed with an increase in pulsewidth from 214 fs to 3.5 ps. The decrease in ablation rate seen at 2 MHz is higher compared to that observed at 13 MHz. At 13 MHz the ablation rate remained almost constant for the range of pulsewidth selected. As pulse energy reduces with the increase of repetition rate, the ablation rate decreases accordingly. At lower repetition rate, the pulses have higher energy and hence result in a greater ablation rate [87].

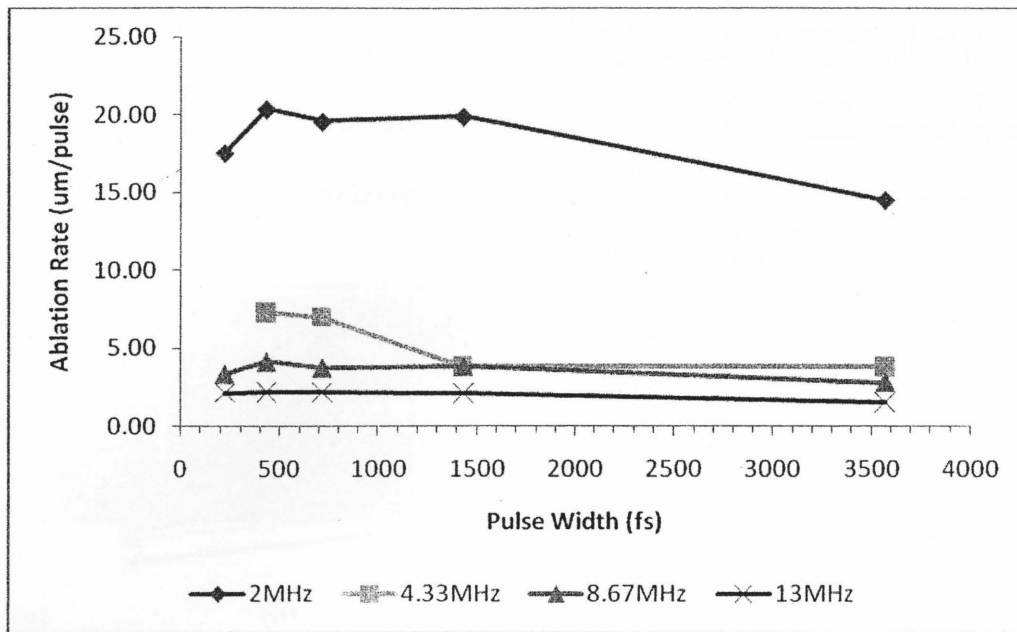


Figure 4-6: Influence of pulsewidth on Ablation Rate at different repetition rate having the same total energy deposited (30.34 J cm^{-2} , number of pulses \times laser fluence)

Although ablation rate is low at higher repetition rate, the quality of finish is better in terms of roughness of the sidewalls and thermal damage. Laser fluence just slightly above the ablation threshold is preferred for efficient and clean dicing. Figure 4-7 plots laser fluence against the repetition rate. It can be observed that at the lower repetition rate of 2 MHz, the laser fluence is about 7 times more than the threshold fluence, resulting in more energy being deposited into the substrate thus causing higher degree of thermal damage. However at 13 MHz the calculated laser fluence is close to the measured ablation threshold fluence, therefore, dice presents smooth sidewalls free of thermal defects.

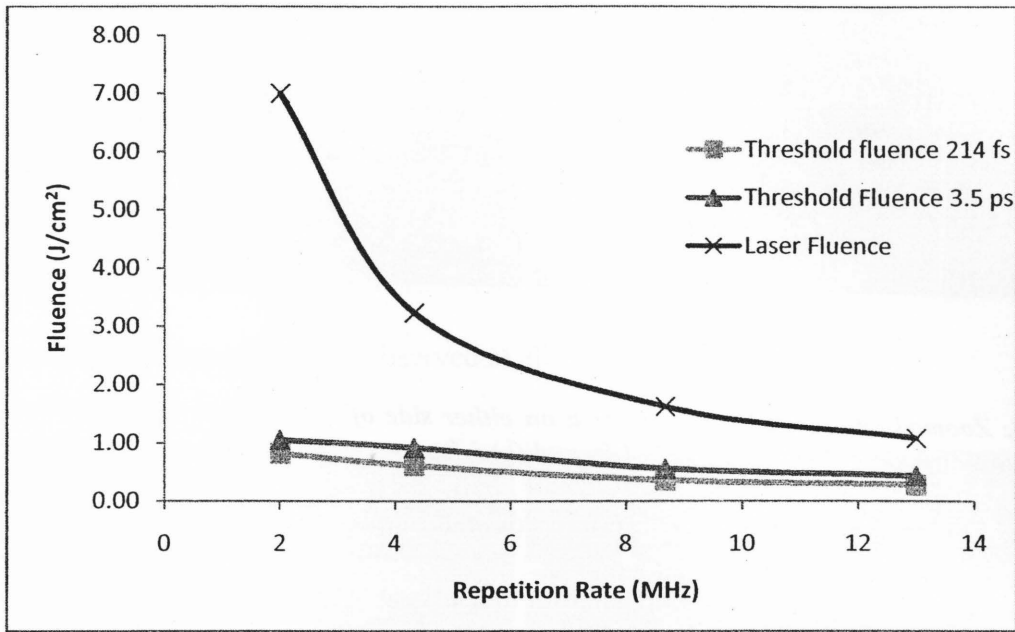


Figure 4-7: Plot of laser fluence and threshold fluence for pulsewidth of 214 fs and 3.5 ps at repetition rate from 2 MHz to 13 MHz

Thermal heat affected zone is a critical factor that determines the dicing quality and strength of the dice. Increase in the heat affected zone (HAZ) or thermal damage will lead to a significant decrease in the dice strength. The HAZ depends on thermal diffusion length l , which can be defined by [88]

$$l \sim (D\tau)^{1/2} \quad \text{Eq 4-3}$$

where D is the thermal diffusivity constant and τ is the laser pulsewidth. It can be seen from the above equation that the thermal diffusion length is directly proportional to the pulsewidth and hence will increase with the increase in the pulsewidth. This means a larger HAZ generated at the pulsewidth of 3.5 ps will be larger than that at the pulsewidth of 214 fs. Figure 4-8 (a) and (b) show a zoomed image of the surface area on either side of the grooves cut with pulsewidth of 214 fs and 3.5 ps at repetition rate of 2 MHz.

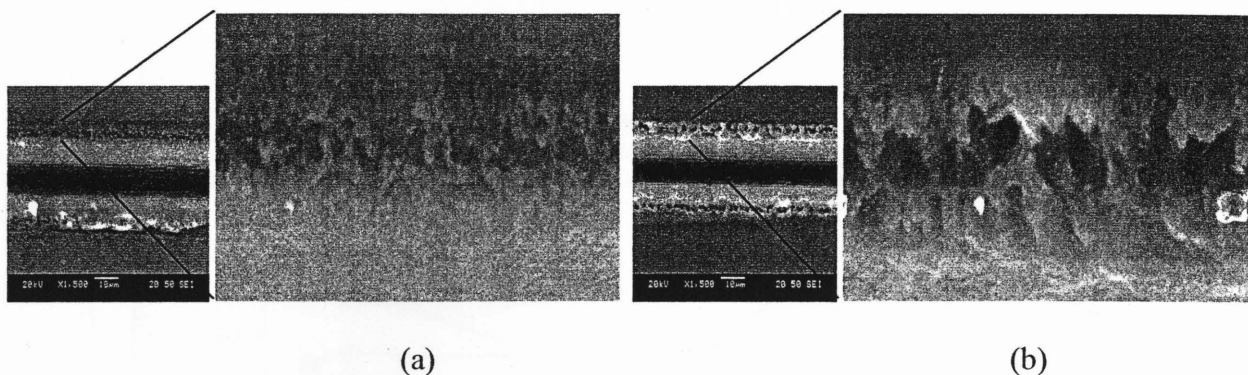


Figure 4-8: Zoomed image of the surface area on either side of grooves cut with repetition rate of 2 MHz at scan speed of 3000 mm s^{-1} at (a) 214 fs and (b) 3.5 ps

Cavities or sites of explosive vaporization can be seen in the Figure 4-8 (b), which can be associated with the amount of heat deposited in the surface area on either side of the cut and also on the high number of pulses resulting on a spot. More number of pulses will land at given spot with increase in the number of cycles at constant repetition rate, resulting in excessive energy being deposited onto the surface and hence resulting in a larger HAZ. The cavities seen in the Figure 8 (b) can be resulted from explosive vaporization on the adjacent areas of the ablated region. Such explosive vaporization has been reported to be seen in picosecond laser ablation and is characterized as function of superheating [89].

4.5 DEBRIS & CONTAMINATION

Many researchers have studied and investigated the influence of important laser parameters like the laser power, repetition rate, scan speed, pulsewidth, beam profile and spot size. Along with these parameters, the contaminations and debris formation greatly affect the quality and strength of the dice. While dicing of silicon dies, it is interesting to notice the formation of spherical structures along the cutting edges. This phenomenon has never been observed in laser dicing using the nanosecond lasers or amplified femtosecond lasers with

repetition rate in kHz or Hz. The sphere size is found to increase with the increase in the repetition rate and with the decrease in the scan rate.

As seen in the Figure 4-9, at the same scan speed, formation of the spherical structures is more predominant at repetition rate of 13 MHz as compared to that at repetition rate of 2 MHz. Infact, the structure formation is not observed at all at 2 MHz.

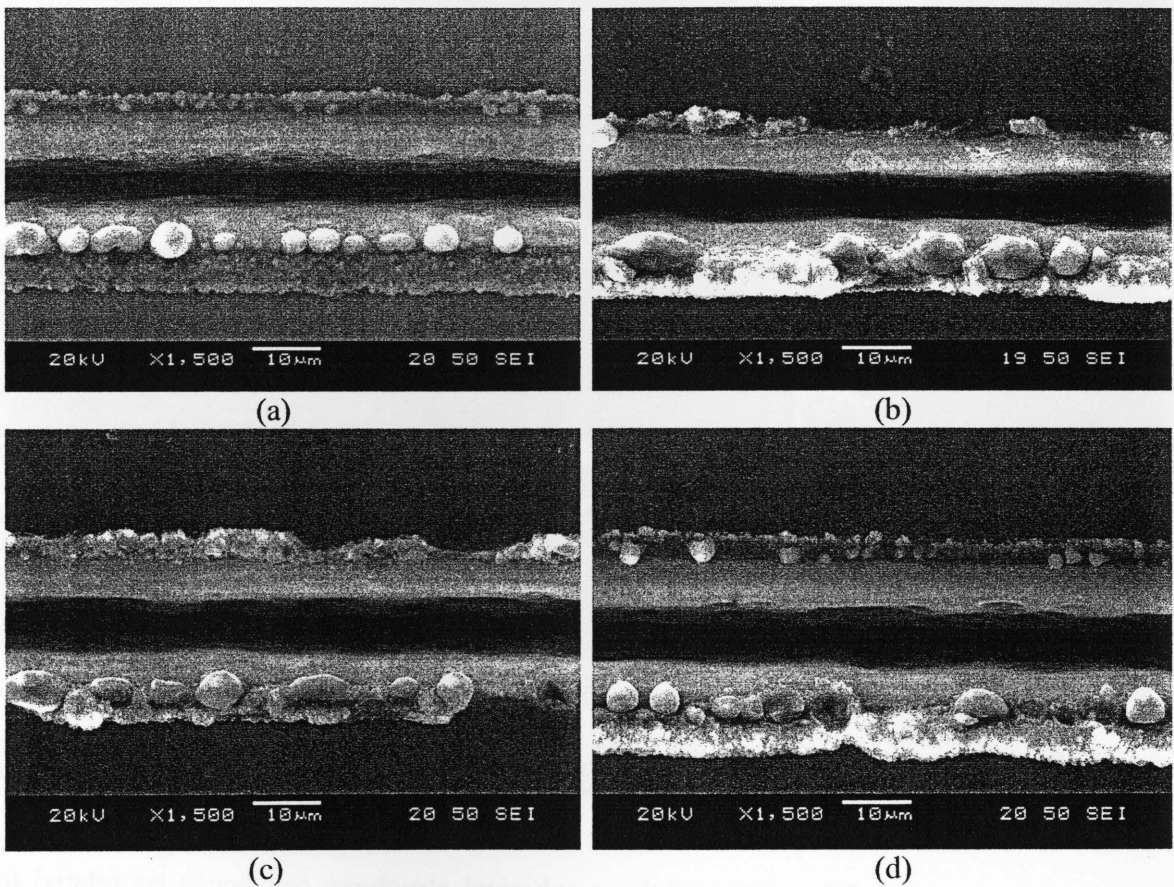


Figure 4-9: Grooves cut at repetition rate of 13 MHz and scan speed of 3000 mm s^{-1} at pulsewidth of (a) 214 fs, (b) 429 fs, (c) 714 fs, (d) 1429 fs

Hence, this phenomenon of structure formation can be related with the lower pulse energy, obtained at the high repetition rate, for a constant power.

The structure formation also seems to be affected by the number of effective pulses or the scan speed. As seen from the Figure 4-10, with increase of the scan speed, size of the structure seems to reduce.

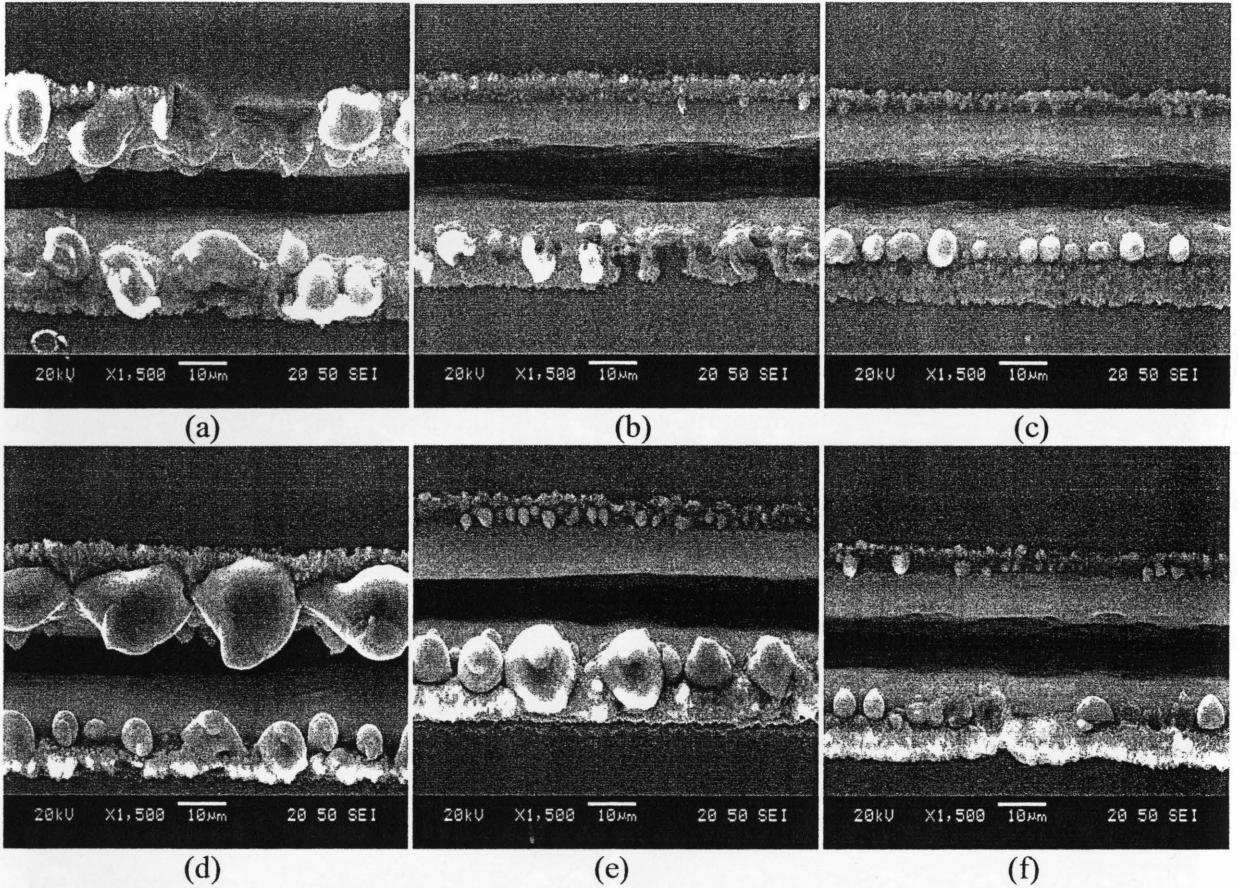


Figure 4-10: Grooves cut at repetition rate of 13 MHz and pulsewidth of 214 fs at scan speed of (a) 1000 mm s^{-1} , (b) 2000 mm s^{-1} , (c) 3000 mm s^{-1} and at pulsewidth of 1429 fs at scan speed of (d) 1000 mm s^{-1} , (e) 2000 mm s^{-1} , (f) 3000 mm s^{-1}

The mechanism of formation of these spherical structures can hence be related to the repetition rate and the scan speed or the number of effective pulses incident at the center of the groove. A systematic study of similar structural features in silicon laser ablation has been studied by Bleiner et al [90]. It was observed by Bleiner et al. that the formation of such structure in air medium is characterized by a rounded core. These rounded particulate adhere firmly to the sample and capture fine particle from the ejected ablated spheres and grow larger in size. The

size of these rounded structures can vary depending on the duration of ablation. Further analysis of these spherical structures was not within the scope of this study. A future study of the composition and dependence of structure size on the laser parameters can be performed to better understand the phenomenon related to formation of these structures.

4.6 SUMMARY

The experimental analysis of the influence of change in the pulsewidth from 214 fs to 3.5 ps for high-power-high-repetition-rate femtosecond laser system was performed successfully. The ablation threshold was deduced to be a function of the pulsewidth and was found to decrease with the decrease in pulsewidth until the pulsewidth of 429 fs, after which a further decrease in pulsewidth leads to an increase in the threshold fluence. However the change is comparatively small for the range of pulsewidth selected. The kerf width did not seem to change significantly, with increase in pulsewidth. The depth of cut reached the maximum at 214 fs and was found to reduce significantly with the increase in the pulsewidth. During the study, formation of spherical structures were observed at higher repetition rate of 13 MHz and were found to be dependent upon the repetition rate and the scan speed or the number of pulses. It is concluded that pulsewidth has some effect on kerf width, ablation rate and ablation depth, but in general the effect is not significant. However its effect on debris is more prominent. Theoretically longer pulsewidth would have more thermal damage. At the same control parameters long pulses would result in lower die strength. As the thin wafers are more sensitive to HAZ, shorter pulses are preferred to maintain the mechanical strength of the dice. From the experimental data observation, in the range of pulsewidth that has been studied there was no significant effect of pulsewidth on visible thermal damage or edge defects.

All the analysis in this study were done using SEM images. So the defects and damages observed here are referred to as “visible defects”. Effect of pulse width on die strength cannot be evaluated by visual observation, and is therefore not analyzed here. However, it has greater effect on die strength which must be analyzed in depth for thin wafer dicing.

CHAPTER 5

EFFECT OF REPETITION RATE

5.1 INTRODUCTION

femtosecond laser systems are becoming more established in industrial applications and have demonstrated high potential in thin wafer dicing [91-93]. Although much research have been carried out to push femtosecond laser into industrial application, the main obstacle of thermal damage and throughput still remain. The heat damage due to high pulse energy, low die strength and low throughput, must be overcome. Increasing the processing speed by applying high pulse energies usually leads to a significant quality loss. Using high pulse repetition rates with low pulse energies may provide a solution to minimize the thermal effects, but the repetition rate of commercially available laser sources is mostly restricted to one to several kHz with pulse energy in the microjoule range. There are two considerations to be taken care when attempting to minimize thermal effect, throughput and quality. Throughput commands for high average power, while the reduction of thermal effect demands for lower pulse energy. The high average power Mega Hertz femtosecond laser system satisfies both the criterions. It gives pulse energy of few microjoules when using high repetition rate. High repetition rate should improve the sidewall quality. Hence both considerations indicate that MHz repetition rate femtosecond laser might be the best suit for dicing applications.

To demonstrate the advantages of using high repetition rate femtosecond laser system, cuts and grooves using different motion parameters, pulse repetition rate and number of scan

cycles are presented for silicon samples. However, a systematic investigation of further relevant parameters enables the processing quality and speed to be optimized.

For the generation of microscopic cuts and grooves, several basic parameters are mainly responsible for the achievable resolutions, for the processing speed, and for the quality of the results. The pulse energy is, together with the focusing optics, responsible for the fluence in the ablation plane. The other main parameters are the cutting speed, the number of cutting cycles and the pulse energy. With regard to the focusing strategy, it has been shown earlier that by using linear focus shapes in the direction of the cut, cutting speeds can be increased while maintaining high edge qualities of the cuts and grooves. However in the current study circular polarization is used. The presented results prove the potential of high repetition-rate femtosecond lasers for high quality cuts in different industrially relevant materials. Also, when generating kerfs with high aspect ratios or cutting through thick material, the beam polarization has a visible influence on the quality [93,94]. This effect is avoided by rotating the polarization from linear to circular with the help of a half wave plate in the beam path. In this experiment, static focusing with lenses is used, which, in combination with a precise workpiece movement, enables to process large structured areas with constant properties. To achieve obvious differences in quality while still ablating roughly the same amount of material per time, the velocity of the workpiece movement and the number of these movements (cutting repetitions) can be adapted.

The silicon wafer was mounted on a two-axis translation stage. Dice were cut at repetition rate of 2 MHz, 4.33 MHz, 8.67 MHz and 13 MHz. The repetition rate for this laser system could be changed from the computer console of the laser system. The cutting speed of 40 mm s^{-1} is achieved during this study and was kept constant throughout the study. By varying the ratio of

scan speed and number of cycles to obtain a constant cutting speed, it is ensured that total the energy being deposited into the substrate remained constant for the given scan speed at any repetition rate and hence the comparison between different repetition rates could be made. At each of the repetition rate, dice were cut at scan speed and number of pass of 500 mm s^{-1} and 13 passes, 1000 mm s^{-1} and 25 passes, 1500 mm s^{-1} and 38 passes, 2000 mm s^{-1} and 50 passes, 2500 mm s^{-1} and 63 passes & 3000 mm s^{-1} and 75 passes. Therefore, the cutting speed remained constant, 40 mm s^{-1} throughout the study. The machined samples were then examined under a Scanning Electron Microscope (SEM) to evaluate the quality and depth of cut.

The experimental results in regards to the study of the effect of high repetition rate on the silicon wafer dicing are discussed in this chapter. The main emphasis on the dicing quality has been explained in terms of number of effective pulses, scan speed and pulse energy.

5.2 EFFECT OF SCAN SPEED AND EFFECTIVE NUMBER OF PULSES

The cut made in silicon wafer using a laser is generally fabricated by a multiple passes of laser beam scanned to obtain the desired feature. The focus of the laser beam is kept unchanged during the process. The cutting process, using pulsed laser, involves overlapping a series of individual holes, generated by each pulse. The effect of the pulse to pulse overlap has been discussed earlier in the chapter 3. In order to facilitate understanding of the cutting process with repetition rate femtosecond laser, as well as to appreciate significance of issues such as spot size and spot overlap, analysis of the several parameter were performed.

As seen from the Eq. 3-3, the effective number of pulses (N_{eff}) at the center of the groove is directly proportional to the spot size and the ratio of repetition rate to the scan speed. A set of

experiments were performed to study the influence of number of pulses on the dicing parameters. Graphical representation of the variation of the depth of cut at various scan speed is plotted in Figure 5-1.

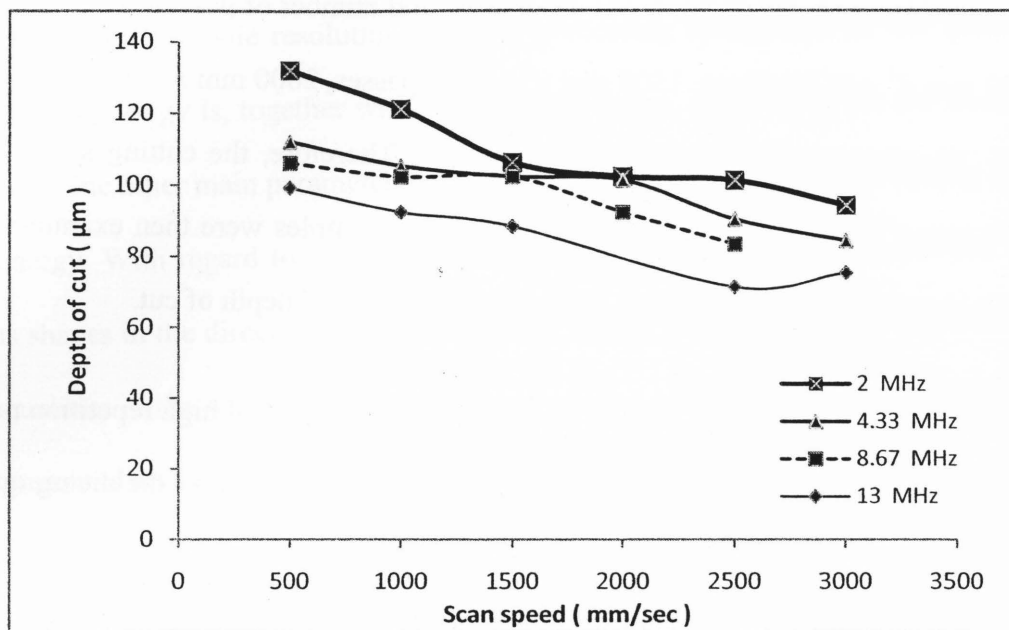


Figure 5-1: Influence of Scan speed on the depth of cut at repetition rate of 2 MHz, 4.33 MHz, 8.67 MHz & 13 MHz

Decrease in the depth of cut results from a decrease in number of pulses at a spot. At a given spot size and a repetition rate, the number of pulse decrease with an increase in the scan speed as seen from the Eq. 3-3. Reduction in the depth of cut can be observed from the Figure 5-1. The number of effective pulses at 13 MHz was calculated to be 222, at a scan speed of 500 mm s⁻¹ compared to 37, at a scan speed of 3000 mm s⁻¹, resulting in the depth of cut of 99μm and 75μm respectively.

Hence it can be clearly seen from the Figure 5-2 (a) & (b) that with the decrease in number of pulses at the same repetition rate, the depth of cut decreases.

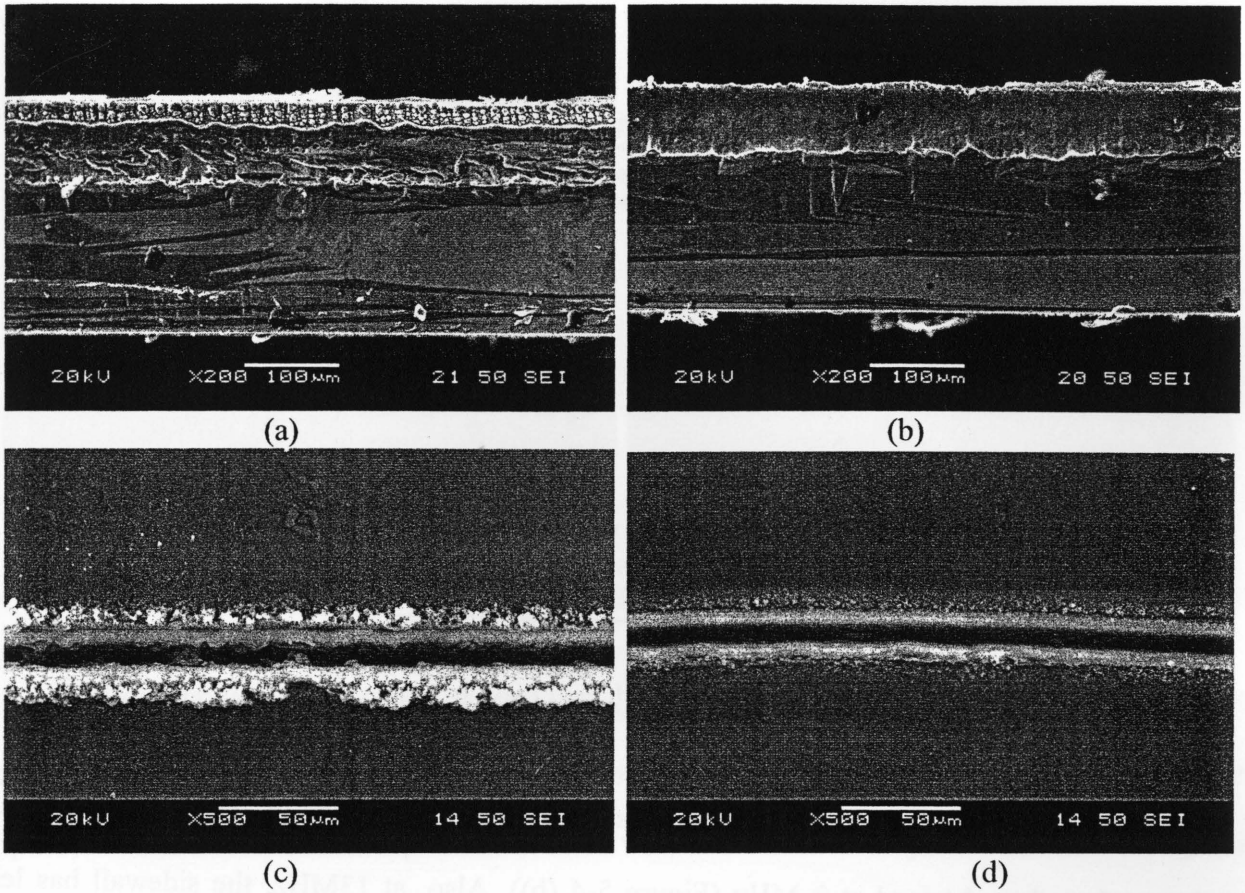


Figure 5-2: Cross section of grooves cut on a thin Si wafer at 13MHz, scan speed of (a) 500 mm s^{-1} , (b) 3000 mm s^{-1} and top surface view for 13 MHz at scan speed of (c) 500 mm s^{-1} (d) 3000 mm s^{-1}

The kerf width also increases with the number of incident pulse as seen from the Figure 5-3 (c, d) and the plotted results in the Figure 5-3. Because of the more number of pulses on the incident area, the kerf width obtained at lower scan speed is wider than that obtained at the higher scan speed.

The quality of sidewall is a function of number of effective pulses and overlap ratio. With increase in the repetition rate more number of pulses are incident at the groove center, hence resulting in greater pulse overlap leading to a better sidewall quality.

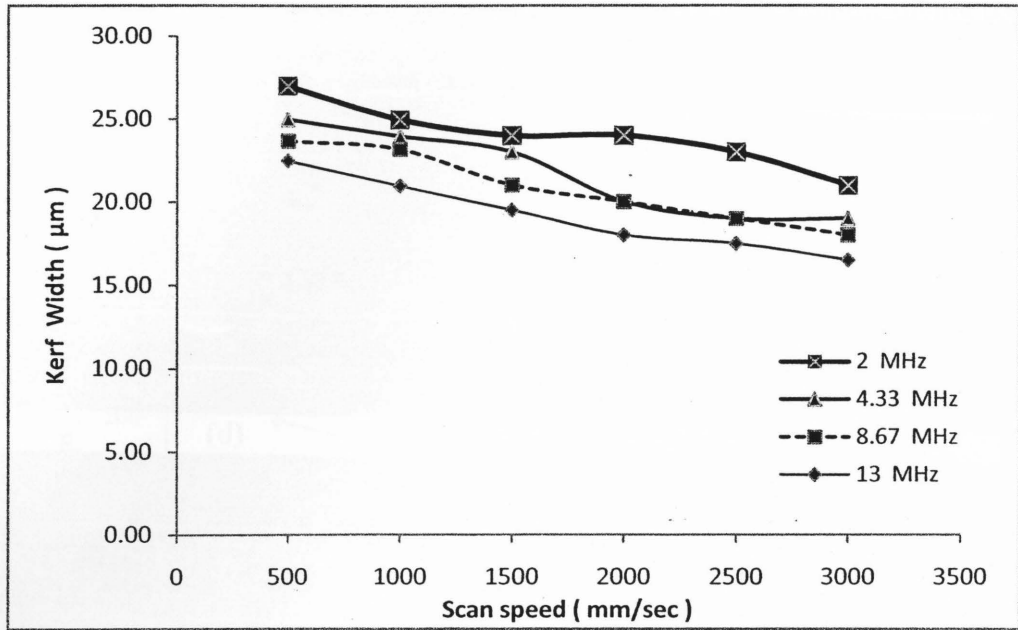


Figure 5-3: Influence of Scan speed on the kerf width at repetition rate of 2 MHz, 4.33 MHz, 8.67 MHz & 13 MHz

The sidewall quality obtained at a scan speed of 1000 mm s^{-1} for 13 MHz (Figure 5-4 (a)) is better than that obtained at 2 MHz (Figure 5-4 (b)). Also, at 13MHz, the sidewall has less recasted molten material and an even bottom area at the higher scanning speed. This relation is in agreement with the results of Ameer-Beg et al. for grooves cut in fused silica and silicon [96]. To a good approximation, the groove depth appears to be proportional to the effective number of pulses, with a greater depth increment at the lower repetition rates. The groove depth measured at 500 mm s^{-1} scan speed was $99 \mu\text{m}$ at 13 MHz and increased to $132 \mu\text{m}$ at 2MHz.

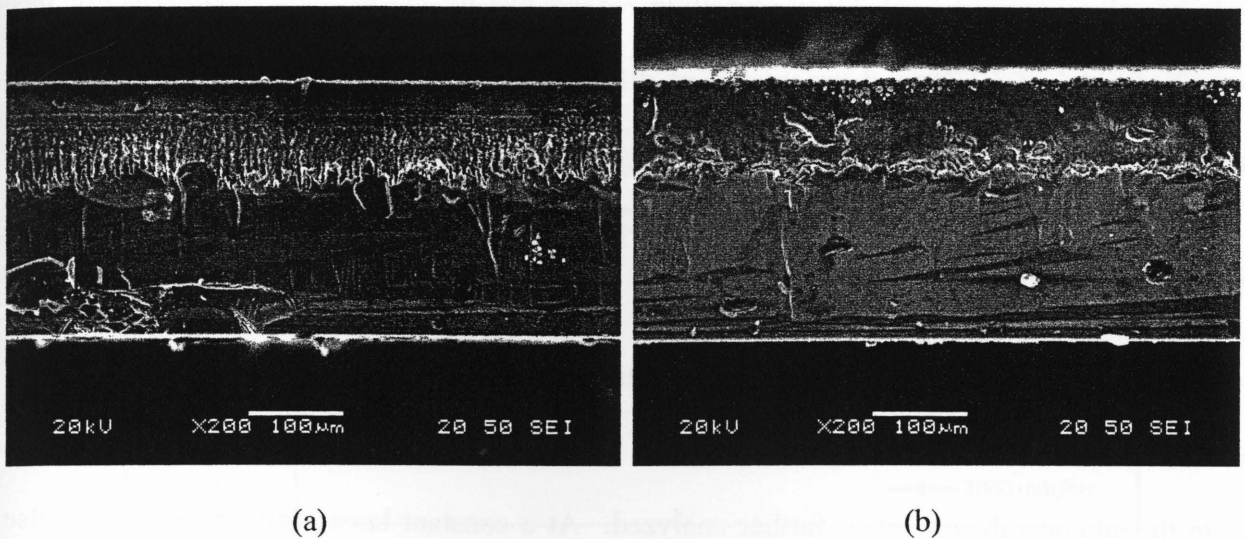


Figure 5-4: Cross-section view of a groove cut on the Si wafer at 1000 mm s^{-1} for repetition rate of (a) 2 MHz, (b) 13 MHz

From the Eq. 3-3, it could be seen that the number of effective pulses at the center of the groove is directly proportional to the repetition rate at a given scan speed. At the same scan speed, the number of effective pulses increases with increase in the repetition rate, resulting in a higher ablation depth. At a scan speed of 500 mm s^{-1} for 2 MHz, the effective number of pulses incident at the center of the groove is 222 compared to 34 at 13 MHz, resulting in a cut depth of 132 µm for the former as opposed to 99 µm for the latter.

For a dicing application, the ablation rate is seen to decrease with the increase in scan rate. The mechanism of this effect could also be considered as follows. As the depth of cut increases, the groove starts to act as a hollow waveguide. The initial pulse first travels to the bottom of the groove, where majority of the ablation takes place. During the pulse propagation through the groove the pulse energy decreases due to scattering and absorption resulting in a diminished energy available for the ablation at the bottom of the groove. At some final depth, the propagation losses are sufficiently high to bring the pulse energy below the ablation threshold, leading to an unavoidable taper. Furthermore, with the increasing depth, the ablated material at

the bottom has a greater probability of getting redeposited on the walls. Similar behavior has been observed in femtosecond processing of different glasses [97]. Moreover, the quality of sidewalls and the amount of debris seen, decreases at a higher scan speed of 3000 mm s^{-1} .

5.3 EFFECT OF PULSE ENERGY

Precise control of the pulse energy is vital to obtain an optimum machining quality. In order to study the effect of laser pulse energy on the depth and the kerf width, the set of grooves cut in the silicon substrate were further analyzed. At a constant laser output power, the pulse energy decreases with the increase in the repetition rate. Figure 5-5 shows the increase in depth of cut with increase in the pulse energy from $0.85 \text{ }\mu\text{J}$ to $5.5 \text{ }\mu\text{J}$ for a scan speed ranging from 500 mm s^{-1} to 3000 mm s^{-1} .

The kerf width and the depth of cut measured for the higher pulse energy of $5.5 \text{ }\mu\text{J}$ and a scan speed of 500 mm s^{-1} , is measured to be $27 \text{ }\mu\text{m}$ and $132 \text{ }\mu\text{m}$, respectively. With decrease in the pulse energy to $0.85 \text{ }\mu\text{J}$, values for the kerf width and the depth reduced to $22.5 \text{ }\mu\text{m}$ and $99 \text{ }\mu\text{m}$, respectively. At the higher pulse energy of $5.5 \text{ }\mu\text{J}$, the depth of cut was found to be higher but of poorer sidewall quality and also wider kerf width. Figure 5-4 (a) & (b) shows the scanning electron microscope (SEM) images of grooves cut at a scan speed of 1000 mm s^{-1} for 2 MHz and 13 MHz respectively. The images show that as the pulse energy decreases from $5.5 \text{ }\mu\text{J}$ (2 MHz) to $0.85 \text{ }\mu\text{J}$ (13 MHz), the kerf width and the depth of cut reduces and the quality of sidewalls improves.

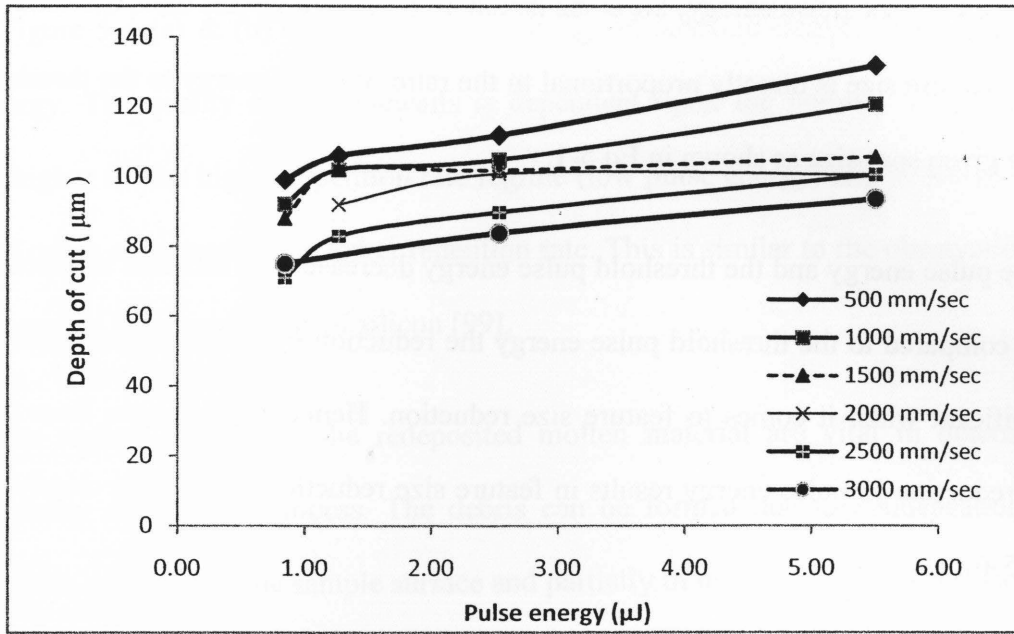


Figure 5-5: Influence of pulse energy on the depth of cut at scan speed ranging from 500 mm s^{-1} to 3000 mm s^{-1}

The cutting depth is governed by the intensity dependent penetration depth for a femtosecond pulsewidth [38]. The penetration depth obtained by a pulse of higher energy is much greater than that obtained at lower pulse energy. At higher pulse energy the depth of cut is observed to be increasing more significantly than the increase observed at lower pulse energy. This is in good agreement with the previous studies [98].

In a femtosecond laser ablation of thin films, the dependence of the threshold fluence and hence the feature size on pulse number and scanning resolution is reported [66]. The feature size in terms of pulse energy can be expressed as [65]

$$D^2 = 2\omega_0^2 \ln\left(\frac{E_0}{E_{th}}\right)$$

Eq 5-1

where E_0 is the pulse energy, E_{th} is the threshold pulse energy and ω_0 is the focused beam radius. The feature size is directly proportional to the ratio of pulse energy to the threshold pulse energy at a given spot size as shown in Eq 5-1.

The pulse energy and the threshold pulse energy decrease with increase in repetition rate. But when compared to the threshold pulse energy the reduction in the pulse energy seems to be more significant when it comes to feature size reduction. Hence, as it is seen from the above equation, reduction in pulse energy results in feature size reduction and can be clearly observed in Figure 5-6.

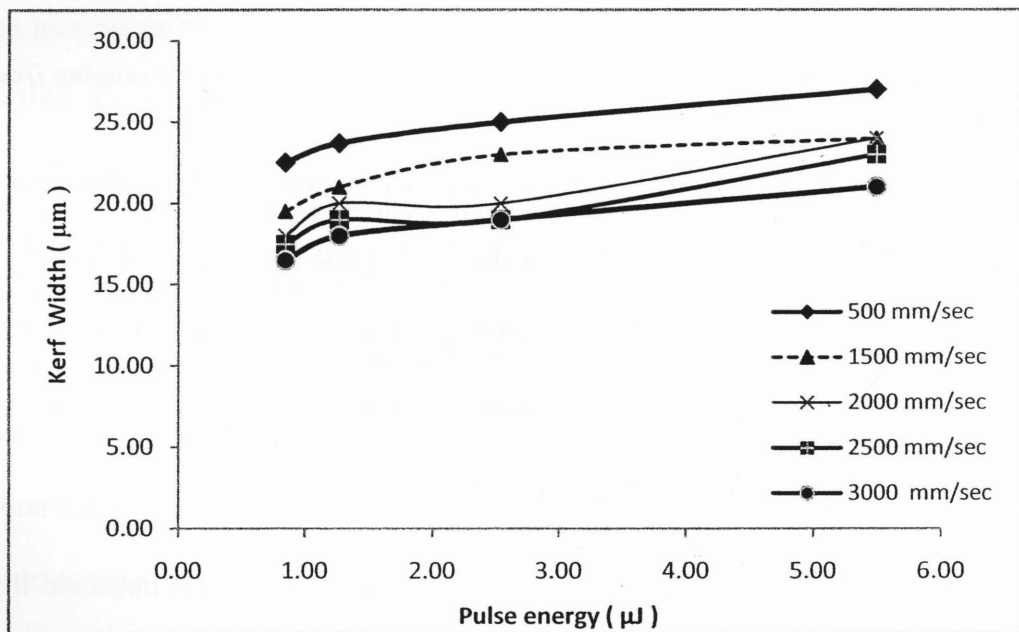


Figure 5-6: Influence of pulse energy on the kerf width at scan speed ranging from 500 mm s^{-1} to 3000 mm s^{-1}

This is in good agreement with previous observations and the theoretical model developed by K.Venkatakrishnan et al [66]. In terms of the sidewall quality, from the results obtained it can be clearly depicted that the quality improves with the reduction in the pulse

energy. Figure 5-4 (a) & (b) clearly show the change in sidewall quality with decrease in the pulse energy. The quality of the sidewalls is dependent upon the number of pulses incident, which is higher for the higher repetition rate regime (low pulse energy) and hence gives a better quality of cut as compared to the lower repetition rate. This is similar to the observation made in the femtosecond laser machining of silicon [99].

The surface debris and the redeposited molten material are vital in determining the surface quality of a dicing process. The debris can be formed due to condensation of super cooled vapors, partially on the sample surface and partially in the gas phase via collision with the ambient gaseous molecules. The majority of the vapor initially ejected eventually finds itself back on the perimeter of the ablated surface and inside the groove. The debris also reduces ablation efficiency, since contamination left from the previous scan can block the laser beam path for the next scan. The amount of debris reduces as the scan speed is increased at a higher pulse repetition rate. At a lower scanning speed of 500 mm s^{-1} at 13 MHz, more debris is observed as seen in Fig. 3 (c). This is due to the high number (222) of the low pulse energy pulses at the center of groove.

5.4 SUMMARY

This experimental study emphasizes on important of tuning the laser parameters in order to obtain a clean and defect free cut. The important laser parameters such as the cutting speed, repetition rate and energy fluence, were analyzed and evaluated. Analysis of these parameters has shown that the proposed laser system has the capability to overcome the limitations encountered by the currently used thin wafer dicing techniques, in terms of quality and throughput. Clean side wall and acceptable machining speed were achieved.

In this experiment, the feasibility of using a high-powered-high-repetition-rate femtosecond laser, for thin silicon wafer singulation was studied. Scan speed of 3000 mm s^{-1} resulting in a cutting speed of 40 mm s^{-1} was demonstrated during the experiment, which can be considerable when applying for industrial usage. A kerf width of $16.5 \text{ }\mu\text{m}$ and a depth of cut $75 \text{ }\mu\text{m}$ were obtained with an acceptable machining quality and cutting speed that could meet the industrial requirement of throughput. The influence of number of pulses, pulse energy and scanning speed on the machining quality and the feature size were studied successfully.

CHAPTER 6

ANALYSIS OF DIE STRENGTH AND SURFACE ROUGHNESS OF SIDEWALLS

6.1 INTRODUCTION

Maximizing the silicon wafer fracture strength is important as it improves the ability of the wafers to survive the mechanical and thermal stresses. The die is subjected to stresses during wafer handling and further processing as in packaging and during service operation. Although a thin wafer below 100 μm has higher degree of flexibility than a thick wafer, the flexibility achieved by devices significantly depends on the die strength. There are two major factors governing die strength, surface fracture strength and edge fracture strength. The surface fracture strength is generally improved by stress relief processes such as chemical mechanical polishing, spin etching and dry polishing. These processes improve the surface roughness and relieve the stress in the dies, hence improving the die strength. Since the surface fracture strength can be improved by post-manufacture processes, the resultant die strength is determined more by the quality of die edges.

The high edge fracture strength can be achieved if the cutting edge is smooth, the sidewall is of small surface roughness and the material is free of residue stress. Also, the dicing process that provides the flexibility of cutting round contour is preferred since the edge fracture strength can generally be enhanced by adopting round corners. (Traditionally, silicon dies have sharp corners.) Short-pulsed laser dicing is a promising tool for retaining the strength of thin dies

because of its non-contact nature and high-localized thermal heating process. Die fracture strength using laser processing depends on the following factors:

- the heat-affected zone length;
- micro cracks formed by laser ablation;
- chipping of edges during laser singulation/dicing;
- recast material along the side wall and on the top surface of the dies.

In order to move the ultrashort laser dicing towards industrial application, these concerns associated with die strength need to be resolved. In this study, through the experimental analysis of the thin dice, it is shown that the ultra short pulse laser dicing is a promising tool for retaining the strength of thin dies because of its non contact nature, negligible thermal damage, higher side wall quality and no backside chipping. In this study, the focus is on the effects of the laser parameters such as repetition rate and pulsedwidth on die strength along with the influence of different gas atmosphere on singulated die.

6.2 METHODOLOGY

Rectangular silicon dies of 10mm x 2.5 mm were cut, using a pulsedwidth of 214 fs and repetition rate of 2 MHz, 4 MHz and 8 MHz at scan speed of 1000 mm sec⁻¹, 2000 mm sec⁻¹ and 3000 mm sec⁻¹. The pulsedwidth was changed by changing the compressor grating position and measuring the output using an autocorrelator. The repetition rate was changed from the laser control panel. The number of cycles used for the through cut were derived by performing a number of precuts to get the desired control and repeatability.

The surface, microstructure and geometry of the dice were then observed using a scanning electron microscope (SEM). The surface roughness of the dice sidewalls were

examined and measured, using an optical microscope. In order to obtain the stress in the dice cut using the high repetition rate high average power pulsed laser, a three point bending test was performed on the dies. In this test, the dies were subjected to bending load created by lowering a pin on the dice supported by two identical cylindrical pins, as shown in Figure 6-1. The load at which the dice fails is recorded for each dice cut with different pulsewidth, repetition rate and scan speed combination. Die Stress was calculated by using the equation [100]:

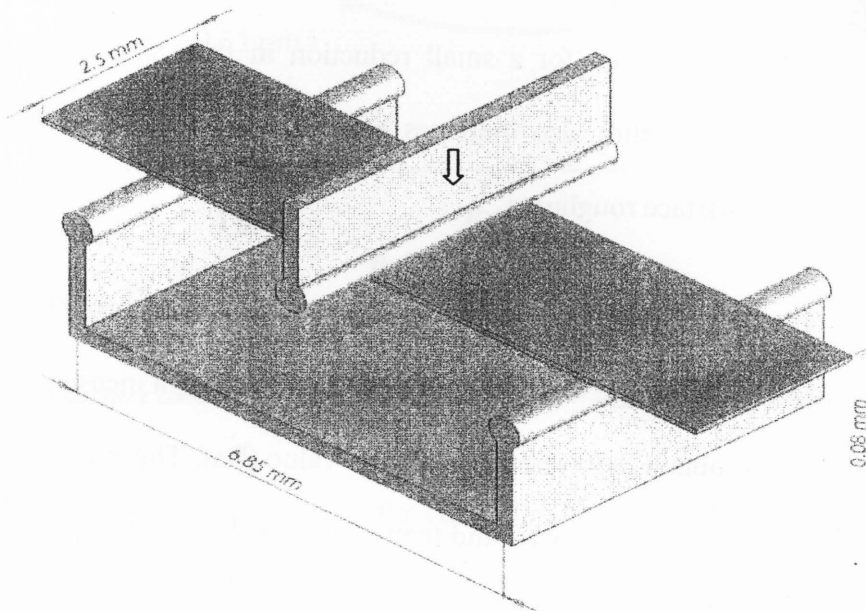


Figure 6-1: 3-Point bending test configuration

$$\text{Stress} = \sigma = \frac{3F_b L}{2wt^2} \quad \text{Eq 6-1}$$

Where, F_b is breaking load (N), L is support length (6.85 mm), w is width of specimen (2.5 mm), t is thickness of specimen (0.08 mm).

6.2.1 SURFACE ROUGHNESS

Surface roughness has been an important factor affecting the die strength. The peak and especially the crests on the machined surface act as stress concentrator and crack initiation sites

when subjected to external load. Die failure is usually initiated from surface flaws, and the failure condition is described by linear elastic fracture mechanics and can be expressed as [101],

$$K_I = Y\sigma\sqrt{\pi c} = K_{IC} \quad \text{Eq 6-2}$$

where K_I is the stress intensity factor, Y is the geometric factor, σ is the nominal applied stress or failure stress, c is the flaw size and K_{IC} is the fracture toughness of the die material. For a given fracture toughness value and geometric factor, the failure stress is inversely proportional to root of the flaw size, which means that for a small reduction in flaw size the failure stress will increase significantly. This in turn also indicates higher strength for the dice with smoother surface or lower average surface roughness.

In the current study, the surface roughness was measured using a ZYCO make (Model : Newview 6300) optical microscope. A rectangular surface area with a measurement field of 0.33 by 0.03 mm was used to obtain the average roughness value (Ra). The Ra values were recorded at three different locations on the sidewall and then average value was used for the plotting. The Ra values recorded were then plotted against the pulsewidth for two different repetition rates for comparing the surface characteristic of the cut sidewalls.

6.3 RESULTS AND DISCUSSION

6.3.1 SURFACE ROUGHNESS OF SIDEWALLS

Figure 6-2 shows the plot of the Ra values at different pulsewidths for repetition rate of 4.33 MHz and 8.67 MHz. For these experiments the average laser power of 15.5 W was used. From the plot it can be seen that the Ra of the sidewalls cut at repetition rate of 4.33 MHz increases with increase in the pulsewidth from 214 fs to 3.5 ps.

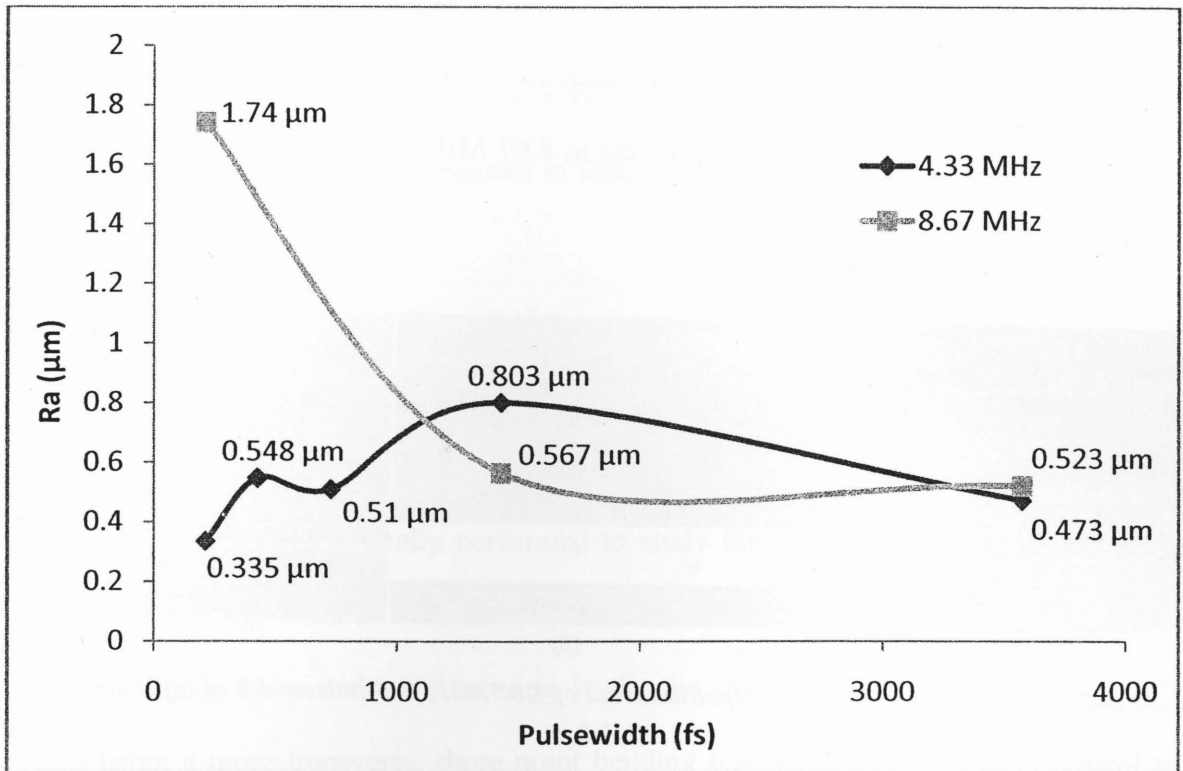


Figure 6-2: Plot of surface average surface roughness value at different pulsewidth for 4.33 MHz and 8.67 MHz

Figure 6-3 shows the cross section view of the cut surface of the silicon dice using the 4.33 MHz starting with 214 fs up to 3.5 ps.

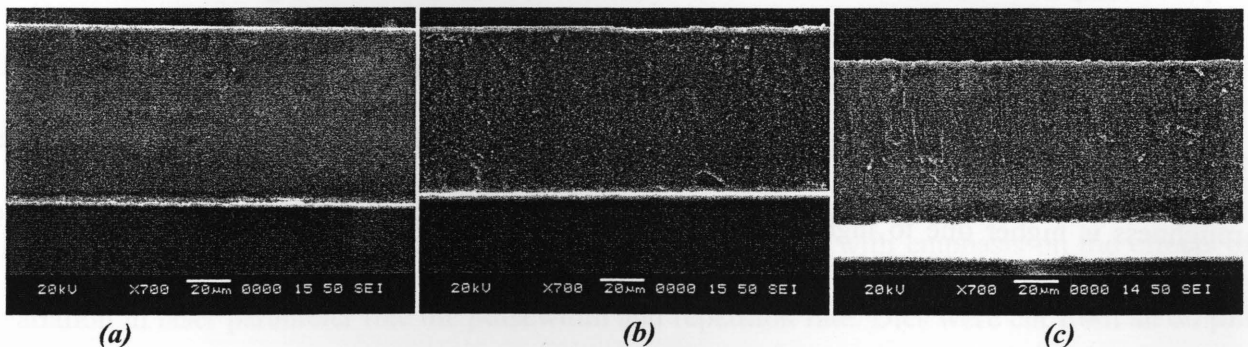


Figure 6-3: Sidewalls of si dice cut at repetition rate of 4.33 MHz and pulsewidth of (a) 214fs, (b) 1.4ps, (c) 3.5 ps

However, unlike the results obtained at repetition rate of 4.33 MHz, the Ra value of the sidewalls cut at repetition rate of 8.67 MHz is found to decrease with increase in the pulsewidth. Figure 6-4 shows the cross section view of the dice cut at 8.67 MHz and pulsewidth of 214 fs, 1.4 ps and 3.5 ps.

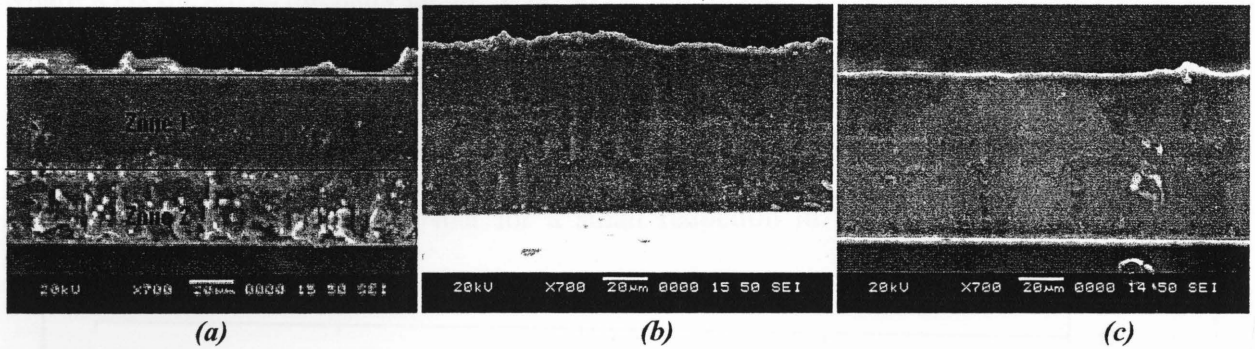


Figure 6-4: Sidewalls of si dice cut at repetition rate of 8.67 MHz and pulsewidth of (a)214fs, (b)1.4ps, (c)3.5 ps

One crucial observation found from Figure 6-2, Figure 6-3 and Figure 6-4, is that the Ra of the sidewalls cut at shorter pulsewidth of 214 fs and repetition rate of 4.33 MHz and 8.67 MHz show a significant difference in roughness. However as the pulsewidth becomes longer (> 0.7 ps), the change in the repetition rate seems to make a small difference and Ra values come in closer proximity for both repetition rate.

The surface roughness could vary along the kerf due to the different material removal mechanism [102] and also the pulse to pulse overlap. At repetition rate of 4.33 MHz, the surface roughness is higher due to higher pulse to pulse overlap. At repetition rate of 8.67 MHz, the surface roughness can be divided into two zones.

From top surface to the middle of the die thickness, seems to be very smooth and comparable with the roughness obtained at 4.33 MHz. As we goes closer to the bottom the

surface quality degrades. This could be due to the dynamics of the flow of ablated material and the fact that at higher repetition rate the laser fluence is not sufficient to evaporate the material and does not have sufficient vapor pressure to force the molten material out from the bottom of the die.

6.4 DIE STRENGTH

Die strength of a material is defined as the maximum applied stress at the moment of die breakage. Tensile tests are normally performed to study the stress-strain behavior of material. However silicon being a brittle material it is difficult to prepare a test specimen of required geometry and grip them without fracturing it. In the current paper silicon die strength is evaluated using a more transverse, three point bending test technique. Test arrangement is as show in Figure 6-1. This method is commonly used for testing of brittle materials where by a breaking load obtained for silicon dice is used for calculating the die strength using Eq 6-1. This helps provide a better understanding of the amount of stress accumulated in the die before failure. The die strength generally not only depends on the material property but also on the flaw size in it. For a singulated dice, flaws exist as cracks, notches and surface roughness. Upon loading the stress intensity begins to build up at the crack tip and when applied stress becomes larger than the fracture toughness of the material, fracture or failure will occur in the material.

In this section, fracture strength of thin silicon die was studied with emphasis on the effects of variation in laser parameter like the pulsewidth and repetition rate. Dies were cut from an 80 μm thick silicon wafer using pulsewidth of 214 fs and 1429 fs at repetition rate of 4.33 MHz and 8.67 MHz. The scan speed was kept at 3000 mm s^{-1} . Die strength or fracture strength of these dice was calculated using the breaking load obtained from the 3-point bending test done on each

dice and using Eq 6-1. The values of the die strength calculated are as plotted in the Table 2. From these values it can be seen that die strength obtained for the 214 fs (shorter pulsewidth) is higher than the 1429 fs (longer pulsewidth) at repetition rate of 4.33 MHz as well as 8.67 MHz. Also it is observed that the die strength measured for the dice cut at pulsewidth of 214 fs and repetition rate of 4.33 MHz is higher than that of 8.67 MHz. Same was observed for pulsewidth of 1429 fs.

MHz	Die strength at 214fs (N/mm²)	Die strength at 1429fs (N/mm²)
4.33	882.37	729.01
8.67	601.09	495.51

Table 4: Die strength at different repetition rate and pulsewidth

It should be noted that die strength is a combined effect of die thickness, back surface roughness and die edge defects. In this study as the die thickness remains the same for all the samples and as the wafer used for dicing is polished on both sides the possibility of these factors influencing the die strength are negligible and hence the die edge roughness plays a decisive role in determining die strength. From Figure 6-3(a) and Figure 6-4(a) it is seen that for the dice cut at 214 fs pulsewidth and 4.33 MHz repetition rate, the sidewall quality is higher than that obtained for same pulsewidth and 8.67 MHz. By comparing Figure 6-3(a) and (b), it can be seen that for repetition rate of 4.33 MHz the sidewall quality obtained is higher than that obtained at 1.4 ps. At 1.4 ps, striations as well as some notches or chipping are observed in the sidewalls hence degrading the die strength. At 8.67 MHz, the sidewalls show a significant amount of defects or flaws like the melt reflow, notches and rougher surface as compared to that obtained at

4.33 MHz. These surface flaws in turn directly affect the die strength value and hence lowering it for 8.67 MHz. This can also be seen from Eq. 6-2, that as the flaw size increases the die strength drops for a given geometric factor and material toughness.

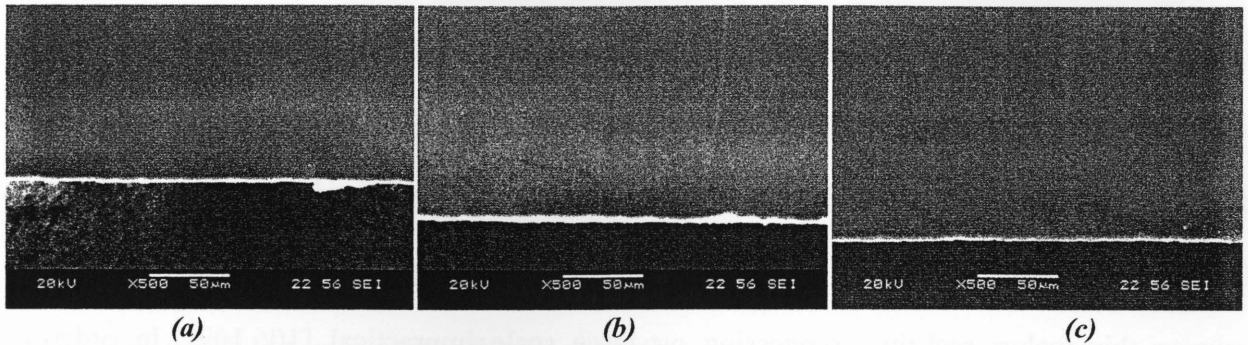


Figure 6-5: Backside surface finish of si dice cut at 4.33 MHz and (a) 214fs, (b) 728fs (d) 3.5ps

Chipping of backside surface is one of the major concerns with laser dicing. Figure 6-5 shows the SEM images of the dice cut at repetition rate of 4.33 MHz and different pulsewidth. Chipping occurs when a high pulse energy laser beam is scanned on a thin wafer. As the laser beam ablates the material, a high recoil pressure is built up in the substrate due to the plasma and as a result the last remaining thin layer before through cut cannot withstand the plasma pressure and it bursts away, resulting in chipping. Unlike results obtained by Barsch et. al. [103], chipping effect is not observed at all while using this laser system. This is due to the high repetition rate capabilities of this laser system, which enables it to dice thin wafers using low pulse energy.

6.5 EFFECT OF ASSIST GAS

Ultrafast laser micromachining is realized by focusing a femtosecond laser beam to a small spot where very high intensity is achieved at the workpiece. With such an unprecedented high intensity, many new possibilities are provided for laser matter interaction and material processing. However, there is one problem that arises during this, ionization of the propagation

medium. Often, however, the beam must pass through a gas, e.g air, before reaching the workpiece. At the very high laser intensities associated with femtosecond laser, the gas can ionize, resulting in a rapid increase in free electron (plasma) density, which in turn decreases the gas refractive index, resulting in plasma defocusing and self phase modulation. Plasma induced effects, distort the temporal and spatial profile of the laser beam, which degrade feature quality and repeatability of ultrafast laser micromachining [104]. In addition plasma absorption reduces the energy available for materials processing, resulting in a decreased material removal rate [105]. To avoid these effects, processing has traditionally been performed in a vacuum chamber, however this makes real-time processing on large scale impractical [106,107]. In order to improve the machining quality, using different assist gas to study the change in dice surface quality obtained against that obtained in air, was studied. By these experiments, a beam delivery technique that uses inert gas as the beam propagation environment instead of air or vacuum chamber is shown.

To compare the machined quality, thin silicon wafers were cut using Air, Helium and Nitrogen gas assists. Although Nitrogen is not completely inert, it is the most commonly employed gas due to its low chemical activity and low cost compared to other pure inert gases like Helium. Through the results obtained, it is observed that Nitrogen gas under pressure not only helps cool the substrate but also drives the melt out of the cutting zone and therefore improves the surface quality of the cut zone. Figure 6-6 shows the dice cut in air and with Nitrogen and Helium gas assist. The surface values of sidewalls were measured for all the dices cut using air and Nitrogen.

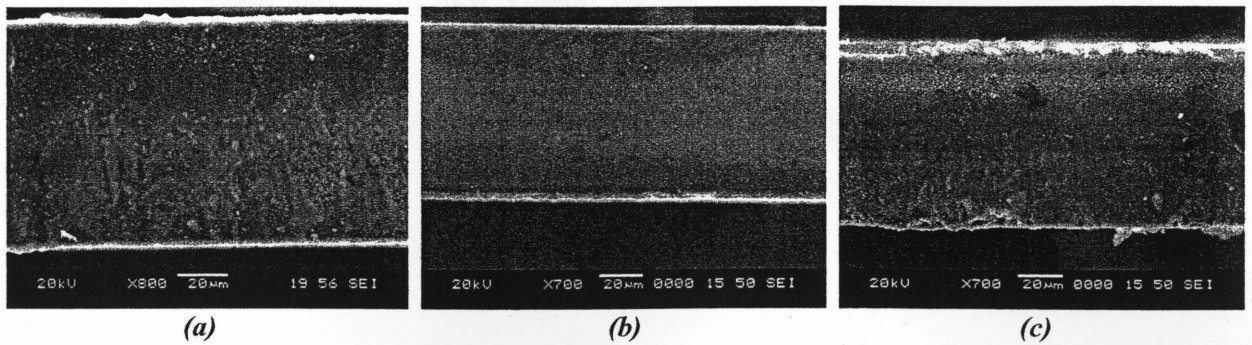


Figure 6-6: Sidewall quality in (a) Air and (b) Nitrogen (c) Helium gas assist

These results indicate that by applying gas assist during machining process can significantly reduce the redeposition of the ablated material and hence improve the surface roughness of the cut surface, which in turn improves the die strength.

6.6 SUMMARY

In this part of the work, die strength and surface roughness of the dice sidewalls were studied. Die strength and surface roughness were found to be dependent upon the laser parameters repetition rate and pulsewidth. Die strength was found to increase with decrease in the pulsewidth and surface roughness. The dicing quality in terms of sidewall surface roughness and back side chipping, obtained by proposed laser system, were found to compatible with those obtained by subsequent etching or polishing processes. The back side chipping is one of the biggest concerns in thin wafer dicing. In the current study, chipping free thin dice using a mega hertz repetition rate high average power femtosecond laser were obtained, which can be considered a significant step towards industrial application of femtosecond lasers for thin wafer dicing. The die strength obtained in this study for the thin dice can be further improved by using better quality dicing tape and dice handling equipment. In the current study, a comparison between Nitrogen, Helium and air assist for dicing of thin wafers was performed . The results

show a significant improvement in the sidewall quality while using Nitrogen gas assist as compared to the air.

CHAPTER 7

SUMMARY, CONCLUSIONS AND FUTURE WORK

7.1 SUMMARY

The objective of this thesis report was to propose, investigate and develop a femtosecond laser dicing technique that can overcome the challenges faced by the conventional and mechanical dicing techniques for thin wafer dicing.

In this thesis, the currently used dicing techniques including mechanical scribe and break, saw blade dicing, dicing before grinding, conventional laser dicing, laser water-jet dicing and dicing using ultrashort lasers were studied along with identification of the advantages and the limitations of each of these techniques. Choosing of the dicing techniques plays an important role in thin wafer dicing. Due to the increase in demand for usage of thin wafers in microelectronics manufacturing, the femtosecond laser dicing technique was identified to be most capable of achieving the desired function of high throughput, high quality, least mechanical or thermal damage, along with being capable of producing dies with high die strength.

Even though the feasibility of using the femtosecond lasers has been predicted for a while now, industrial application of this technique is awaited due to the challenges faced in terms of laser parameters, inadequate experimental studies in this area and subsequent processing need for the dies. For precise material processing, thorough knowledge of the fundamental physics governing the interaction of laser radiation with matter is eminent. The physical process of laser-matter interaction is indeed very complicated and involves a variety of different phenomena, underlying the different aspects of laser matter interaction. These processes were successfully

studied and also the mechanisms and phenomena involved in the laser matter interaction for both nanosecond and femtosecond regimes were explained.

For this research work, a high repetition rate femtosecond laser capable of producing high output power was chosen. General models for the experimental setup were developed after studying the capabilities of the proposed laser system. The laser parameters like pulsewidth, repetition rate, laser beam polarization and cutting speed were optimized and were evaluated to study the influence of these parameters on cutting quality in terms of side walls and die strength. Evaluation of the laser parameters with respect to dicing quality were justified successfully by conducting a number of experiments and evaluating the results.

The experimental analysis of the influence of the pulsewidth from 214 fs to 3.5 ps was successfully performed. The ablation threshold was deduced to be a function of the pulsewidth and was found to decrease with the decrease in pulsewidth until the pulsewidth of 429 fs, after which a further decrease in pulsewidth leads to an increase in the threshold fluence. SEM results showed that the depth of cut reached the maximum at 214 fs and was found to reduce significantly with the increase in the pulsewidth. It was also found that the formation of spherical structures, observed at a higher repetition rate of 13 MHz, is dependent upon the repetition rate and the scan speed or the number of pulses. It is also concluded that pulsewidth has some effect on kerf width but in general the effect is not found to be significant. From analyzing the experimental data, in the range of pulsewidth that has been studied, no significant effect of pulsewidth on visible thermal damage or edge defects was found.

Several experiments were conducted to emphasize the importance of tuning the laser parameters in order to obtain a clean and defect free cut. The laser parameters such as the cutting

speed, repetition rate and energy fluence were evaluated and analyzed. The experimental results showed the ability to overcome the limitation encountered with the conventional laser dicing technique for thin wafer dicing, namely, quality and throughput. Dies with clean side walls and acceptable machining speed, were machined using this dicing.

Die strength is an important criterion for industrialization of any dicing technique. Dicing of 80 μ m thin silicon wafers was successfully performed. Die strength and surface analysis of dies cut using the proposed technique were measured. From the analytical results, it was found that the die strength decreased with increase in pulsewidth along with the surface roughness of the side walls for double side polished wafers. The dies had no backside chipping, and side wall roughness was comparable to that obtained after subsequent etching or polishing processes. The side wall quality of the dies was further improved using different gas mediums like Helium and Nitrogen.

7.2 CONCLUSIONS

- The proposed high repetition rate femtosecond laser with high power output is capable of dicing 80 μ m thin silicon wafers, with acceptable quality and throughput.
- The high repetition rate femtosecond laser dicing setup does not require any significant changes or special arrangements to the existing production lines.
- Die strength of 882.37 N/mm², side wall surface roughness of 0.335 μ m and kerf width of about 15 μ m were achieved on 10mm x 2.5 mm x 80 μ m dies, using high repetition rate of 4 MHz at pulsewidth of 214 fs and cutting speed of 40 mm s⁻¹.
- Dies with high die strength and no visible defects like chipping, cracks and heat affected zone (HAZ) can be diced using the proposed thin wafer dicing technique.

- Usage of assist gases like Nitrogen and Helium can improve the side wall quality such that no further processing to improve surface roughness is required.

7.3 FUTURE WORK

Silicon has dominated the semiconductor wafer market for more than three decades. This research has achieved industrially viable results for dicing of thin silicon wafers. However, this study can be extended to various kinds of other material used in the semiconductor industry like the Gallium Arsenide (GaAs) wafers.

During this research study, a galvoscaner was used to scan the laser beam over the silicon wafer. It can be found that, with the available galvoscaner, a maximum scan speed of 3000 mm s^{-1} was achieved. However, for further investigation of the results, more experiments can be done using a higher speed galvoscaner or piezoscaner. This could help achieve even higher cutting speeds, hence increasing throughput. Moreover, even with the proposed laser system capable of operating at 26 MHz, due to the speed limitation of the galvoscaner, results for 26 MHz were not obtained, which could be done as a future work.

In this research, a fundamental wavelength of 1030nm was used. As a future work, these experiments can be performed at lower wavelengths by using second harmonics and third harmonics. Even with the loss of laser power associated with the frequency doubling or tripling, this kind of setup can find application for thin film patterning and creating micro or nano channels for biomedical applications.

REFERENCES

- [1] Carson, F. "3D Packaging Developments and Trends." *Advancing Microelectronics* 33.1 (2006): 14-8.
- [2] Black, B., Annavaram, M., Brekelbaum, N., Devale, J., Lei, J., Loh, G.H., McCauley, D., Morrow, P., Nelson, D.W., Pantuso, D., Reed, P., Rupley, J., Shankar, S., John, S., Webb, C., "Die Stacking (3D) Microarchitecture" *Proceedings of the Annual International Symposium on Microarchitecture, MICRO*, (2006), 469-479
- [3] Liao, Z. L., Danielson, L.R., Fourspring, P.M., Hu, L., Chen, G., Turner, G.W., "Reduction of Thermal Conductivity in Wafer-Bonded Silicon." *Applied Physics Letters* 93.2 (2008).
- [4] Kröninger, W., Mariani, F., "Thinning and Singulation of Silicon: Root Causes of the Damage in Thin Chips." *Proceedings - Electronic Components and Technology Conference*, (2006), 1317-1322
- [5] "Expected thickness evolution of thin wafers", Fraunhofer-Institute for Mechanics of Materials, 2004
- [6] Curran, L., "Diamond Scribes Start to Give Way to Laser Machines, Slurry Saws, New Etch Methods." *Electronics* 43.24 (1970): 70-5.
- [7] Perrottet, D., Dunne, K., Walsh, G., Diggin, B., "Using Lasers to Dice Thin Silicon Wafers." *Advanced Packaging* 17.3 (2008).
- [8] Vittu, J., Perrottet, D., Buchilly, J.M., Richerzhagen, B., "Damage-Free Dicing of Low-K Wafers." *Future FAB Int.* (2004).
- [9] Schmidt, M., Eßer, G., "The Future of Lasers in Electronics." *ICALEO (2003) - 22nd International Congress on Applications of Laser and Electro-Optics*, Congress Proceedings
- [10] Cunningham, P., Delivorias, P., "Dicing's Impact on the Final Product." *Proceedings of SPIE - The International Society for Optical Engineering*, (2002), 4217, 239-245
- [11] Takyu, S., Kurosawa, T., Shimizu, N., Harada, S., "Novel Wafer Dicing and Chip Thinning Technologies Realizing High Chip Strength." *Materials Research Society Symposium Proceedings*, (2007), 970, 281-292
- [12] Cheung, A.T. "Dicing Advanced Materials for Microelectronics." *2005 10th International Symposium on Advanced Packaging Materials: Processes, Properties and Interfaces*. Irvine, CA, March (2005).
- [13] Danyluk, S., Ebbutt, R., Weisshaus, I., "Machining and Dicing of Silicon." *VDI Ber.* (1996), 1276, 371-381

- [14] Perrottet, D., Housh, R., Richerzhagen, B., Manley, J., "Heat Damage-Free Laser-Microjet Cutting Achieves Highest Die Fracture Strength." *Proceedings of SPIE - The International Society for Optical Engineering*, (2005), 5713, 285-292
- [15] Chen, S., Shih, I.G., Chen, Y.N., Tsai, C.Z., Lin, J.W., Wu, E., "How to Improve Chip Strength to Avoid Die Cracking in a Package." *Thermomechanical Phenomena in Electronic Systems -Proceedings of the Intersociety Conference*, (2004), 2, 268-273
- [16] Sibailly, O., Richerzhagen, B., "Laser Dicing of Silicon and Composite Semiconductor Materials." *Proceedings of SPIE - The International Society for Optical Engineering*, (2004), 5339, 394-397
- [17] Wu, X. D., Dijkkamp, D., Gozdz, A.S., Venkatesan, T., "Nanosecond Dynamics Of Excimer Laser Induced Thermal Decomposition Of Thin Polymer Films." *Materials Research Society Symposia Proceedings*, (1987), 74, 275-280
- [18] Hardway, G.A. "Applications Of Laser Systems To Microelectronics And Silicon Wafer Dicing." *Solid State Technology* 13.4 (1970): 63-7.
- [19] Brannon, J. "Laser Material Processing: An Industrial View of Packaging Applications." *Proceedings of SPIE - The International Society for Optical Engineering*, (2002), 4637, 474-478
- [20] Kolomenskii, Al A., Schuessler, H.A., Mikhalevich, V.G., Maznev, A.A., "Interaction of Laser-Generated Surface Acoustic Pulses with Fine Particles: Surface Cleaning and Adhesion Studies." *Journal of Applied Physics* 84.5 (1998): 2404-10.
- [21] Henry, M., Wendland, J., Harrison, P.M., "Nanoscale Analysis of Laser Ablated Thin Films used in Industrial Manufacturing of Flat Panel Displays." *ICALEO (2006) - 25th International Congress on Applications of Laser and Electro-Optics*, Congress Proceedings
- [22] Leiderer, P., Boneberg, J., Dobler, V., Mosbacher, M., Muenzer, H.J., Chaoui, N., Siegel, J., Solis, J., Afonso, C.N., Fourier, T., Schrems, G., Baeuerle, D., "Laser-Induced Particle Removal from Silicon Wafers." *Proceedings of SPIE - The International Society for Optical Engineering*, (2000), 4065, 249-259
- [23] <http://www.cmxr.com/Industrial/Handbook>
- [24] Dhamdhere, A.R., Malshe, A.P., Yedave, S.N., Schmidt, W.F., Brown, W.D., "Failure Mechanisms and Modeling in High Power Optical Device Packaging: Semiconductor Laser Diodes - A Case Study." *American Society of Mechanical Engineers, Electronic and Photonic Packaging, EPP*, (2001), 1, 193-200
- [25] Agarwal, R., Samson, S., Bhansali, S., "Fabrication of Vertical Mirrors using Plasma Etch and KOH:IPA Polishing." *Journal of Micromechanics and Microengineering* 17.1 (2007): 26-35.
- [26] Jiang, A.L.X., Ming, L.C., Gao, J.C.Y., Hwee, T.K., "Silicon Wafer Backside Thinning with Mechanical and Chemical Method for Better Mechanical Property." *2006 7th International Conference on Electronics Packaging Technology, ICEPT '06*, (2007)

- [27] Schönfelder, S., Bagdahn, J., Ebert, M., Petzold, M., Bock, K., Landesberger, C., "Investigations of Strength Properties of Ultra-Thin Silicon." Proceedings of the 6th International Conference on Thermal, Mechanical and Multi-Physics Simulation and Experiments in Micro-Electronics and Micro-Systems - EuroSimE (2005), 105-111
- [28] Shen, J., Liu, S., Yi, K., He, H., Shao, J., Fan, Z., "Subsurface Damage in Optical Substrates." Optik 116.6 (2005): 288-94.
- [29] Sibailly, O., Wagner, F., Richerzhagen, B., "Laser Micro-Machining in Microelectronic Industry by Water Jet Guided Laser." Proceedings of SPIE - The International Society for Optical Engineering, (2004), 5339, 258-264
- [30] Couty, P., Wagner, F., Hoffmann, P., "Laser Coupling with a Multimode Water-Jet Waveguide." Optical Engineering 44.6 (2005): 1-8.
- [31] Kautek, W., Krüger, J., "Femtosecond Pulse Laser Ablation of Metallic, Semiconducting, Ceramic and Biological Materials." Proc. SPIE 2207 (1994): 600-11.
- [32] Liu, X., Mourou, G., "Ultrashort Laser Pulses Tackle Precision Machining." Laser Focus World 33.8 (1997): 101-18.
- [33] Molian, P.A. "Ultrafast Pulsed Lasers for Manufacturing Applications with Special Reference to Diamond Machining." Proceedings of the 1997 Conference on Lasers and Electro-Optics, CLEO. Baltimore, MD, USA, (1997)
- [34] Banks, P.S., Stuart, B.C., Perry, M.D., Feit, M.D., Rubenchik, A.M., Armstrong, J.P., Nguyen, H., Roeske, F., Lee, R.S., Myers, B.R., Sefcik, J.A., "Femtosecond Laser Machining." Proceedings of the 1998 Conference on Lasers and Electro-Optics, CLEO. San Francisco, CA, USA, 3 May 1998 through 8 May 1998.
- [35] Pronko, P.P., Dutta, S.K., Squier, J., Rudd, J.V., Du, D., Mourou, G., "Thermophysical Effects in Laser Processing of Materials with Picosecond and Femtosecond Pulses." Journal of Applied Physics 78.10 (1995): 6233-40.
- [36] Chichkov, B.N., Momma, C., Nolte, S., Von Alvensleben, F., Tünnermann, A., "Femtosecond, Picosecond and Nanosecond Laser Ablation of Solids." Applied Physics A: Materials Science and Processing 63.2 (1997): 109-15.
- [37] Gamaly, E.G., Rode, A.V., Luther-Davies, D., "Ultrafast Ablation with High-Pulse-Rate Lasers. Part I: Theoretical Considerations." Journal of Applied Physics 85.8 I (1999): 4213-21.
- [38] Bonse, J., Baudach, S., Krüger, J., Kautek, W., Lenzner, M., "Femtosecond Laser Ablation of Silicon-Modification Thresholds and Morphology." Applied Physics A: Materials Science and Processing 74.1 (2002): 19-25.
- [39] Schäfer, C., Urbassek, H. M., Zhigilei, L. V., "Metal Ablation by Picosecond Laser Pulses: A Hybrid Simulation." Physical Review B - Condensed Matter and Materials Physics 66.11 (2002): 1154041-8.

- [40] Lorazo, P., Lewis, L. J., Meunier, M., "Short-Pulse Laser Ablation of Solids: From Phase Explosion to Fragmentation." *Physical Review Letters* 91.22 (2003).
- [41] Herziger, G., Kreutz, E. W., Wissenbach, K., "Fundamentals Of Laser Processing Of Materials." *Proceedings of SPIE - The International Society for Optical Engineering*, (1986), 668, 2-10
- [42] Liu, X., Du, D., Mourou, G., "Laser Ablation and Micromachining with Ultrashort Laser Pulses." *IEEE Journal of Quantum Electronics* 33.10 (1997): 1706-16.
- [43] Kononenko, T.V., Konov, V.I., Garnov, S.V., Danielius, R., Piskarskas, A., Tamoshauskas, G., Dausinger, F., "Comparative Study of the Ablation of Materials by Femtosecond and Pico-Or Nanosecond Laser Pulses." *Quantum Electronics* 29.8 (1999): 724-8.
- [44] Le Harzic, R., Huot, N., Audouard, E., Jonin, C., Laporte, P., Valette, S., Fraczkiwicz, A., Fortunier, R., "Comparisen of Heat-Affected Zones due to Nanosecond and Femtosecond Laser Pulses using Transmission Electronic Microscopy." *Applied Physics Letters* 80.21 (2002): 3886.
- [45] Lee, B.M., Baik, H.K., Seong, B.S., Munetoh, S., Motooka, T., "Molecular-Dynamics Analysis of the Nucleation and Crystallization Process of Si." *Physica B: Condensed Matter* 392.1-2 (2007): 266-71.
- [46] Bonse, J., Brzezinka, K.W., Meixner, A.J., "Modifying Single-Crystalline Silicon by Femtosecond Laser Pulses: An Analysis by Micro Raman Spectroscopy, Scanning Laser Microscopy and Atomic Force Microscopy." *Applied Surface Science* 221.1-4 (2004): 215-30.
- [47] Pronko, P. P., Dutta, S.K., Squier, J., Rudd, J.V., Du, D., Mourou, G., "Machining of Sub-Micron Holes using a Femtosecond Laser at 800 Nm." *Optics Communications* 114.1-2 (1995): 106-10.
- [48] Ermer, D.R., Papantonakis, M.R., Baltz-Knorr, M., Nakazawa, D., Haglund Jr., R.F., "Ablation of Dielectric Materials during Laser Irradiation Involving Strong Vibrational Coupling." *Applied Physics A: Materials Science and Processing* 70.6 (2000): 633-5.
- [49] Takeshima, M., "Auger Recombination in a Quasi-One-Dimensional-Structure Semiconductor." *Physical Review B* 31.2 (1985): 992-9.
- [50] Burakov, I.M., Bulgakova, N.M., Stoian, R., Rosenfeld, A., Hertel, I.V., "Theoretical Investigations of Material Modification using Temporally Shaped Femtosecond Laser Pulses." *Applied Physics A: Materials Science and Processing* 81.8 (2005): 1639-45.
- [51] Hirayama, Y., Obara, M., "Heat Effects of Metals Ablated with Femtosecond Laser Pulses." *Applied Surface Science* 197-198 (2002): 741-5.
- [52] Van Vechten, J.A., Tsu, R., Saris, F.W., Hoonhout, D., "Reasons to Believe Pulsed Laser Annealing of Si does Not Involve Simple Thermal Melting." *Physics Letters A* 74.6 (1979): 417-21.
- [53] Van Vechten, J.A., Tsu, R., Saris, F.W., "Nonthermal Pulsed Laser Annealing of Si, Plasma Annealing." *Physics Letters A* 74.6 (1979): 422-6.

- [54] Sokolowski-Tinten, K., Bialkowski, J., Cavalleri, A., Von Der Linde, D., Oparin, A., Meyer-Ter-Vehn, J., Anisimov, S.I., "Transient States of Matter during Short Pulse Laser Ablation." *Physical Review Letters* 81.1 (1998): 224-7.
- [55] Cavalleri, A., Sokolowski-Tinten, K., Bialkowski, J., Schreiner, M., Von Der Linde, D., "Femtosecond Melting and Ablation of Semiconductors Studied with Time of Flight Mass Spectroscopy." *Journal of Applied Physics* 85.6 (1999): 3301-9.
- [56] Izawa, Y., Izawa, Y., Setsuhara, Y., Hashida, M., Fujita, M., Sasaki, R., Nagai, H., Yoshida, M., "Ultrathin Amorphous Si Layer Formation by Femtosecond Laser Pulse Irradiation." *Applied Physics Letters* 90.4 (2007).
- [57] Agranat, M.B., Anisimov, S.I., Makshantsev, B.I., "The Anomalous Thermal Radiation from Metals Produced by Ultrashort Laser Pulses. I." *Applied Physics B Photophysics and Laser Chemistry* 47.3 (1988): 209-21.
- [58] Lu, Q., Mao, S.S., Mao, X., Russo, R.E., "Theory Analysis of Wavelength Dependence of Laser-Induced Phase Explosion of Silicon." *Journal of Applied Physics* 104.8 (2008).
- [59] Kaebernick, H., Bicieanu, D., Brandt, M., "Theoretical and Experimental Investigation of Pulsed Laser Cutting." *CIRP Annals - Manufacturing Technology* 48.1 (1999): 163-6.
- [60] Wang, X.Y., Riffe, D.M., Lee, Y.S., Downer, M.C., "Time-Resolved Electron-Temperature Measurement in a Highly Excited Gold Target using Femtosecond Thermionic Emission." *Physical Review B* 50.11 (1994): 8016-9.
- [61] Fann, W.S., Storz, R., Tom, H.W.K., Bokor, J., "Electron Thermalization in Gold." *Physical Review B* 46.20 (1992): 13592-5.
- [62] Preuss, S., Demchuk, A., Stuke, M., "Sub-Picosecond UV Laser Ablation of Metals." *Applied Physics A Materials Science & Processing* 61.1 (1995): 33-7.
- [63] Venkatakrisnan, K., Tan, B., Stanley, P., Sivakumar, N.R., "The Effect of Polarization on Ultrashort Pulsed Laser Ablation of Thin Metal Films." *Journal of Applied Physics* 92.3 (2002): 1604.
- [64] Venkatakrisnan, K., Tan, B., Stanley, P., Lim, L.E.N., Ngoi, B.K.A. "Femtosecond Pulsed Laser Direct Writing System." *Optical Engineering* 41.6 (2002): 1441-5.
- [65] Venkatakrisnan, K., Tan, B., "Thin Silicon Wafer Dicing with a Dual-Focused Laser Beam." *Journal of Micromechanics and Microengineering* 17.12 (2007): 2505-15.
- [66] Venkatakrisnan, K., Stanley, P., Sivakumar, N.R., Tan, B., Lim, L.E.N., "Effect of Scanning Resolution and Fluence Fluctuation on Femtosecond Laser Ablation of Thin Films." *Applied Physics A: Materials Science and Processing* 77.5 (2003): 655-8.
- [67] Nolte, S., Momma, C., Kamlage, G., Chichkov, B.N., Tuennermann, A., von Alvensleben, F., Welling, H., "Micromachining with Femtosecond Lasers." *Conference on Lasers and Electro-Optics Europe - Technical Digest*, (1998), 510-511

- [68] Chang, J.J., Warner, B. E., "Laser-Plasma Interaction during Visible-Laser Ablation of Methods." *Applied Physics Letters* 69.4 (1996): 473-5.
- [69] Yokotani, A., Matsuo, N., Kawahara, K., Kurogi, Y., Matsuo, N., Ninomiya, T., Sawada, H., Kurosawa, K. , "Development of Dicing Technique for Thin Semiconductor Substrates with Femtosecond Laser Ablation." *Proceedings of SPIE - The International Society for Optical Engineering*, (2002), 4637, 180-187
- [70] Kamata, M., Imahoko, T., Ozono, K., Obara, M.. "Materials Processing by use of a Ti: Sapphire Laser with Automatically-Adjustable Pulse Duration." *Applied Physics A: Materials Science and Processing* 79.7 (2004): 1679-85.
- [71] Bliss, D.E., Adams, D.P., Cameron, S.M., Luk, T.S., "Laser machining with ultrashort pulses: Effects of pulse-width, frequency and energy." *Materials Research Society Symposium - Proceedings* 546, (1999): 81-84
- [72] Tönshoff, H.K., Ostendorf, A., Körte, F., Serbin, J., Bauer, T., "Generation of Periodic Microstructures with Femtosecond Laser Pulses." *Second International Symposium on Laser Precision Microfabrication*. Singapore, (2001)
- [73] Qiao, C. H, Fan, C.Y., Wang, Y.J., Feng, X.X., Cheng, D.J., "Simulation Experiment of High Energy Laser Propagation in the Atmosphere." *Qiangjiguang Yu Lizishu/High Power Laser and Particle Beams* 20.11 (2008): 1777-82.
- [74] Herrmann, R.F.W., Gerlach, J., Campbell, E. E. B., "Ultrashort Pulse Laser Ablation of Silicon: An MD Simulation Study." *Applied Physics A: Materials Science and Processing* 66.1 (1998): 35-42.
- [75] Momma, C., Chichkov, B.N., Nolte, S., Von Alvensleben, F., Tünnermann, A., Welling, H., Wellegehausen, B., "Short-Pulse Laser Ablation of Solid Targets." *Optics Communications* 129.1-2 (1996): 134-42.
- [76] Ngoi, B. K. A., et al. "Effect of Energy Above Laser-Induced Damage Thresholds in the Micromachining of Silicon by Femtosecond Pulse Laser." *Optics and Lasers in Engineering* 35.6 (2001): 361-9.
- [77] Chien, C. Y., Gupta, M. C., "Pulse Width Effect in Ultrafast Laser Processing of Materials." *Applied Physics A: Materials Science and Processing* 81.6 (2005): 1257-63.
- [78] Ostendorf, A., Kamlage, G., Klug, U., Korte, F., Chichkov, B.N., "Femtosecond Versus Picosecond Laser Ablation." *Proceedings of SPIE - The International Society for Optical Engineering*, (2005), 5713, 1-8
- [79] Le Harzic, R., Kamlage, G., Klug, U., Korte, F., Chichkov, B.N., "Pulse Duration and Energy Density Influence on Laser Processing of Metals with Short and Ultra-Short Pulses." *Proceedings of SPIE - The International Society for Optical Engineering*, (2005), 5713, 115-122
- [80] Fujita, M., Izawa, Yu., Tokita, S., Izawa, Y., Yamanaka, C. , "Ultrafast Phase Transition of Si by Femtosecond Laser Pulse Irradiation." *Conference on Lasers and Electro-Optics Europe - Technical Digest*, (2007)

- [81] Korfiatis, D.P., Thoma, K. A, Vardaxoglou, J.C., "Conditions for Femtosecond Laser Melting of Silicon." *Journal of Physics D: Applied Physics* 40.21 (2007): 6803-8.
- [82] Venkatakrishnan, K., Tan, B., Ngol, B.K.A., "Submicron Holes in Copper Thin Film Directly Ablated using Femtosecond Pulsed Laser." *Optical Engineering* 40.12 (2001): 2892-3.
- [83] Jandeleit, J., Urbasch, G., Hoffmann, H.D., Treusch, H.-G., Kreutz, E.W., "Picosecond Laser Ablation of Thin Copper Films." *Applied Physics A: Materials Science and Processing* 63.2 (1997): 117-21.
- [84] Xu, S., Qiu, J., Jia, T., Li, C., Sun, H., Xu, Z., "Femtosecond Laser Ablation of Crystals SiO₂ and YAG." *Optics Communications* 274.1 (2007): 163-6.
- [85] Torrisi, L., Margarone, D., "Investigations on Pulsed Laser Ablation of Sn at 1064 Nm Wavelength." *Plasma Sources Science and Technology* 15.4 (2006): 635-41.
- [86] Yokotani, A., Kurogi, Y., Matsuo, N., Sawada, H., Ninomiya, T., Kawahara, K., Kurosawa, K., "Development of Dicing Technique for Thin Semiconductor Substrate using Temporally Shaped Femtosecond Laser." *Electrical Engineering in Japan (English translation of Denki Gakkai Ronbunshi)* 149.3 (2004): 43-8.
- [87] Venkatakrishnan, K., Sudani, N., Tan, B., "A High-Repetition-Rate Femtosecond Laser for Thin Silicon Wafer Dicing." *Journal of Micromechanics and Microengineering* 18.7 (2008).
- [88] Balchev, I.I., Minkovski, N.I., Kostadinov, I.K., Sabotinov, N.V., High-speed Precise Laser Cutting with Copper Bromide Laser, *Bulg. J. Phys.* 33 (2006) 39–47
- [89] Craciun, V., Bassim, N., Singh, R.K., Craciun, D., Hermann, J., Boulmer-Leborgne, C., "Laser-Induced Explosive Boiling during Nanosecond Laser Ablation of Silicon." *Applied Surface Science* 186.1-4 (2002): 288-92.
- [90] Bleiner, D., Gasser, p., "Structural Features of Laser Ablation Particulate from Si Target, as Revealed by Focused Ion Beam Technology." *Applied Physics A: Materials Science and Processing* 79.4-6 (2004): 1019-22.
- [91] Tan, B., Dalili, A., Venkatakrishnan, K., "High Repetition Rate Femtosecond Laser Nano-Machining of Thin Films." *Applied Physics A: Materials Science and Processing* (2008): 1-9.
- [92] Goater, A.D., Burt, J.P.H., Morris, D.J., Menachery, A., Rizvi, N.H., Matthews, D.R., Summers, H.D., "Laser Micromachining of Optical Biochips." *Proceedings of SPIE - The International Society for Optical Engineering*, (2007), 6459
- [93] Mayyas, M.A., Shiakolas, P.S., "Application of Thin Plate Splines for Surface Reverse Engineering and Compensation for Femtosecond Laser Micromachining." *Proceedings of the 20th IEEE International Symposium on Intelligent Control, ISIC '05 and the 13th Mediterranean Conference on Control and Automation*, (2005), 125-130
- [94] Zheng, H.Y., Zhou, W., Qian, H.X., Tan, T.T., Lim, G.C., "Polarisation-Independence of Femtosecond Laser Machining of Fused Silica." *Applied Surface Science* 236.1 (2004): 114-9.

- [95] Kamalu, John N., "Orientation Effects in the Three-Dimensional Laser Machining of Mild Steel." LIA (Laser Institute of America), (1992), 74, 231-237
- [96] Ameer-Beg, S., Perrie, W., Rathbone, S., Wright, J., Weaver, W., Champoux, H., "Femtosecond Laser Micro Structuring of Materials." Applied Surface Science 127-129 (1998): 875-80.
- [97] Campbell, E.E.B., Ashkenasi, D., Rosenfeld, A., "Ultra-Short-Pulse Laser Irradiation and Ablation of Dielectrics." Materials Science Forum 301 (1999): 123-44.
- [98] Borowiec, A., Haugen, H. K., "Femtosecond Laser Micromachining of Grooves in Indium Phosphide." Applied Physics A: Materials Science and Processing 79.3 (2004): 521-9.
- [99] Crawford, T.H.R., Borowiec, A., Haugen, H. K., "Femtosecond Laser Micromachining of Grooves in Silicon with 800 Nm Pulses." Applied Physics A: Materials Science and Processing 80.8 (2005): 1717-24.
- [100] Chong, D.Y.R., Lee, W.E., Lim, B.K., Pang, J.H.L., Low, T.H., "Mechanical Characterization in Failure Strength of Silicon Dice." Therm Phenom Electron Syst Proc Intersoc Conf, (2004), 2, 203-210, Las Vegas, NV
- [101] Sun, X. K., Xin, X.J., Pei. Z. J., "Finite Element Analysis of Die-Strength Testing Configurations for Thin Wafers." Journal of Electronic Packaging, Transactions of the ASME 127.2 (2005): 189-92.
- [102] Ilavarasan, P., Molian, P.A., "Modelling of Surface Roughness in Laser Cutting", Proceedings of fifth Int. FAIM conference, Germany, June (1995)
- [103] Barsch, N., Körber, K., Ostendorf, A., Tönshoff, K.H., "Ablation and Cutting of Planar Silicon Devices using Femtosecond Laser Pulses." Applied Physics A: Materials Science and Processing 77.2 (2003): 237-42.
- [104] Le Blanc, S.P., Sauerbrey, R., "Spectral, Temporal, and Spatial Characteristics of Plasma-Induced Spectral Blue Shifting and its Application to Femtosecond Pulse Measurement." Journal of the Optical Society of America B: Optical Physics 13.1 (1996): 72-88.
- [105] Mao, X.L., Chan, W.T., Shannon, M.A., Russo, R.E., "Plasma Shielding during Picosecond Laser Sampling of Solid Materials by Ablation in He Versus Ar Atmosphere." Journal of Applied Physics 74.8 (1993): 4915-22.
- [106] Shirk, M.D., and Molian, P.A., "A Review of Ultrashort Pulsed Laser Ablation of Materials." Journal of Laser Applications 10.1 (1998): 18-28.
- [107] Varel, H., Ashkenasi, D., Rosenfeld, A., Wähmer, M., Campbell, E.E.B., "Micromachining of Quartz with Ultrashort Laser Pulses." Applied Physics A: Materials Science and Processing 65.4-5 (1997): 367-73.

2013-31-122